

OAK RIDGE NATIONAL LABORATORY LIBRARIES



3 4456 0539366 9

TD

ORNL-TM-4347

cy.4

TD LIBRARY DEC 1973

CRYOGENIC DIELECTRICS AND SUPERCONDUCTING AND CRYOGENIC MATERIALS TECHNOLOGY FOR POWER TRANSMISSION

Annual Report — July 1, 1973

TD LIBRARY DEC 1973



OAK RIDGE NATIONAL LABORATORY

OPERATED BY UNION CARBIDE CORPORATION • FOR THE U.S. ATOMIC ENERGY COMMISSION

This report was prepared as an account of work sponsored by the United States Government. Neither the United States nor the United States Atomic Energy Commission, nor any of their employees, nor any of their contractors, subcontractors, or their employees, makes any warranty, express or implied, or assumes any legal liability or responsibility for the accuracy, completeness or usefulness of any information, apparatus, product or process disclosed, or represents that its use would not infringe privately owned rights.

Contract No. W-7405-eng-26

Activity No. 04-85-01

CRYOGENIC DIELECTRICS AND SUPERCONDUCTING
AND CRYOGENIC MATERIALS TECHNOLOGY
FOR POWER TRANSMISSION

Annual Report - July 1, 1973

Cryoelectrics Section
Engineering Sciences Group
Thermonuclear Division

NOVEMBER 1973

NOTICE This document contains information of a preliminary nature and was prepared primarily for internal use at the Oak Ridge National Laboratory. It is subject to revision or correction and therefore does not represent a final report.

OAK RIDGE NATIONAL LABORATORY
Oak Ridge, Tennessee 37830
operated by
UNION CARBIDE CORPORATION
for the
U.S. ATOMIC ENERGY COMMISSION

TABLE OF CONTENTS

	<u>Page</u>
I. ABSTRACT	1
II. PROGRAM ELEMENTS	3
A. Cryoelectric Program	5
Introduction	5
1. Experimental Equipment	6
a) 700 kV ac Power Supply and Test Area	6
b) 130 kV dc and 80 kV ac Test Facility	9
c) Intermediate and High Voltage Cryostats	12
d) Rogowski Electrodes	18
e) Partial Discharge Detection	20
2. Auxiliary Investigations	23
3. Exploratory Experiments	25
4. Future Activity	30
References to Sect. II.A	32
B. Superconducting Materials	33
1. Niobium-Rare Earth Dispersion Studies	33
2. Measurement of J_c and ΔH by ac Susceptibility	41
3. Construction of ac Loss Measuring Equipment	43
4. Concluding Remarks	43
References to Sect. II.B	48
C. Dispersion Hardening of Aluminum	49
Introduction	49
1. Residual Resistivity Ratio of Cominco Zone- Refined Aluminum	49
2. Alloy Preparation	51
3. Future Activity	51
References to Sect. II.C	54
APPENDIX A, Travel Report - Austria and Germany	55
APPENDIX B, A Note on J. Gerhold's and on R. J. Meat's Investigations on the Dielectric Breakdown of Helium at Very low Temperatures	69
APPENDIX C, Report on Biddle Technical School Partial Discharge Detection Course	87
APPENDIX D, Operation of ac Series Resonant Test Sets	93
APPENDIX E, Heat Transfer Down Vapor-Cooled Structures into Cryogenic Liquids	105

TABLE OF CONTENTS (cont.)

	<u>Page</u>
APPENDIX F, Pressure Withstand Calculations	115
APPENDIX G, Computational and Experimental Field Analysis for High Voltage Engineering	123
DISTRIBUTION LIST	151

I. ABSTRACT

The principal effort in the dielectric program during this reporting period, March 1 - June 20, has been to install the 700 kV series resonant transformer so that high voltage ac testing can be accomplished during the coming year. Provisions were made that this unit will share a test stand with the Haefely 600 kV dc power supply. Design and fabrication of a helium dewar with a 1000 kV bushing for use in this test stand has continued. The design of a cryostat for experiments with intermediate voltages was completed, and the assembling of this cryostat is underway. A small laboratory for exploratory experiments with voltages up to 130 kV dc and 80 kV ac has been set up. A Biddle partial discharge detector has been ordered. A Faraday cage has been located which can provide a low interference laboratory for low level discharge measurements. Auxiliary investigations have been continued which are necessary for the design, construction, and operation of our test equipment.

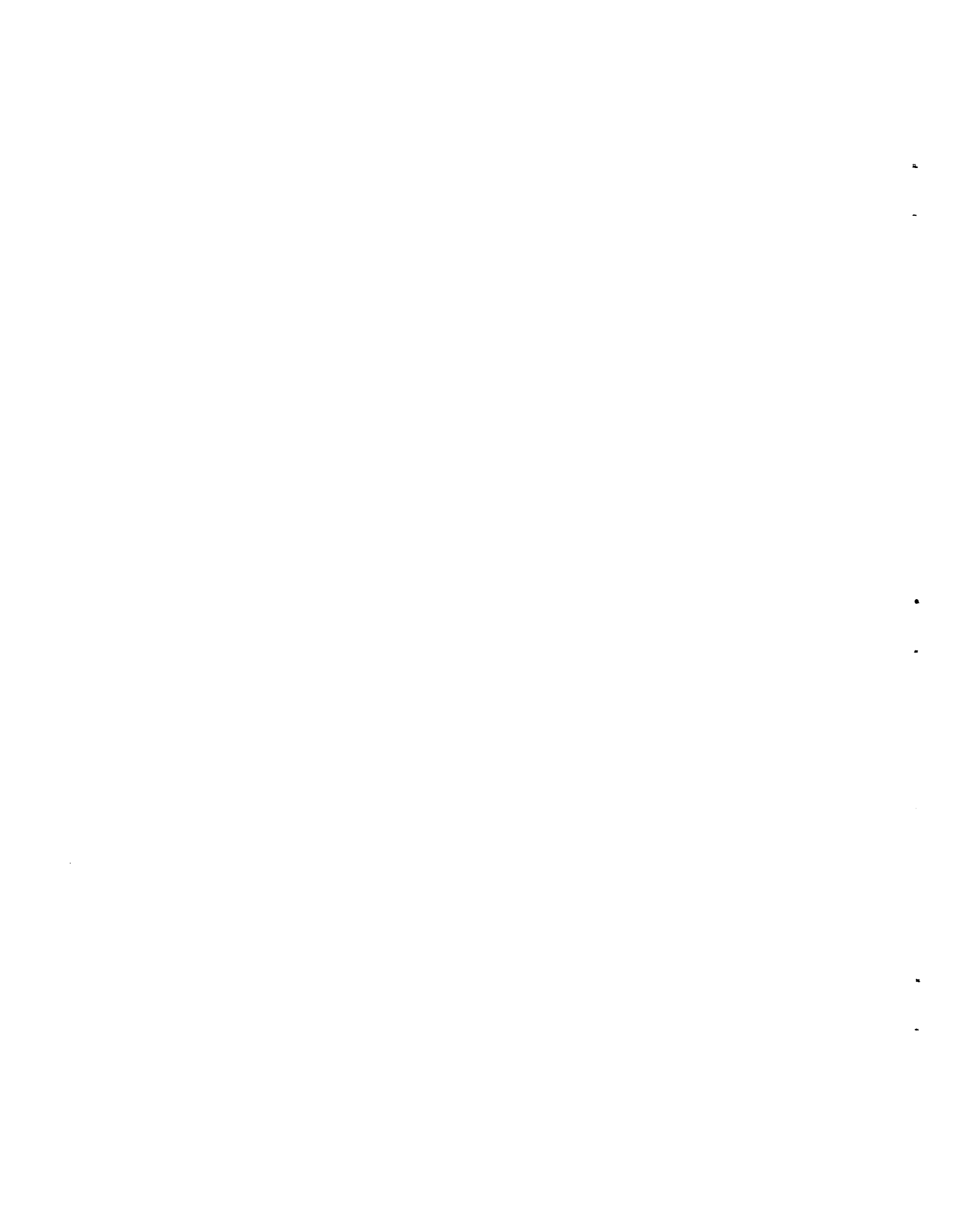
The superconducting materials study has continued with work in three main areas: 1) Niobium-rare earth dispersion studies, 2) measurement of critical current density, J_c , and surface shielding parameter, ΔH , in the dispersions, and 3) construction of ac loss measuring equipment.

The dispersion hardening of aluminum activity has concentrated on a study of the residual resistivity ratio of the high purity zone-refined aluminum from Cominco Products since the material barely reached 80% of the specified value of $13,000 \pm 1000$. Sensitivity of the residual resistivity of the material to handling and thermal history was explored and compared with previous materials obtained from Cominco which met the

same specification. The results which indicate a high sensitivity and a possibility of a maximum in the residual resistivity ratio as a function of annealing temperature do not clearly show why the two lots of material should differ. A set of alloy ingots was prepared to make specimens to study hardening characteristics vs electrical resistivity.

Funding for the two materials studies has not been included in the FY 1974 budget so they will be placed in a standby status. Since both programs now have candidate materials at least partially characterized, they can be reinitiated on relatively short notice should funding become available in the near future.

II. PROGRAM ELEMENTS



A. CRYOELECTRIC PROGRAM

Introduction

As indicated in the Semiannual Report - March 1, 1973, we acquired from Simplex Wire and Cable Company a cascaded test set for 700 kV ac manufactured by Hipotronics, Inc. consisting of two series resonant transformers rated 350 kV and 525 kVA each, with associate exciters, reactors, and a dual control console. We received the mentioned items at the end of March, and the installation in our laboratory was essentially completed by June 30. A safety fence has been erected in accordance with the safety rules for high voltage equipment. The fence also encloses the test stand which is arranged in such a way that either 700 kV ac or 600 kV dc power can be conveniently transmitted to the test object. A preliminary report on operation tests with the 700 kV cascaded resonance transformer set is given.

Progress has been made in the design and fabrication of the high voltage cryostat. The design of its vacuum bushing considers the peak voltage of the 700 kV ac test set, i.e., of about 1000 kV. The design of the bushing and the dewar of a cryostat for intermediate voltages was completed, its assembling is underway, and a precision device for spacing the electrodes was successfully tested.

A small laboratory for experiments with voltages up to 130 kV dc and 80 kV ac has been put into operation. Exploratory dielectric breakdown tests with liquid nitrogen have been performed there. Several "auxiliary investigations" which are necessary for the design, construction, and operation of our test equipment were made. We used a newly designed

"three-sphere clamp" for investigating the withstand voltage of cylindrical insulation layers. Another auxiliary activity was the approximate determination of the equipotential lines for the design of the high voltage cryostat by means of our conductive paper field plotting device. More accurate field calculations were made employing the finite element method.

Since partial discharges are of interest both for testing high voltage apparatus and for investigating pre-discharge phenomena in cryogenic insulation systems, we ordered a partial discharge detector from J. G. Biddle Company. Operation of this equipment may require low external noise level, and we were able to locate in the laboratory a well shielded, commercially built room (Faraday cage) of sufficient dimensions for performing tests with intermediate voltage.

1. Experimental Equipment

a) 700 kV ac Power Supply and Test Area

The 700 kV ac 1050 kVA power supply manufactured by Hipotronics, Inc. and acquired from Simplex Wire and Cable Company was received at the end of March. The specifications and general features of this series resonant power source were described in Appendix D of the previous report (ORNL-TM-4187). The essentials of the theory of operation of the supply are described in Appendix D of this report.

During this report period, the power supply has been installed in accordance with safety requirements, wiring and grounding have been completed, and a few preliminary tests have been run. The equipment is shown in place in Fig. A-1. The experimental area contains a test stand for mounting large bushings, dewars, and other pieces of experimental



PHOTO 1581-73

Figure A-1. 700 kV series resonant ac power supply.

equipment. It is placed to provide convenient access to both the 600 kV dc and 700 kV ac power supplies. The stand is 14 ft long and 11 ft wide, so that several experiments may be mounted at once if necessary.

The heavy transformers and reactors were placed with due regard for floor loading. Positioning of the units was also made with the idea of conserving space, maximizing experimental functions, and at the same time maintaining the required least stand-off distances of 8 ft from all surfaces that might reach 350 kV and 15 ft from possible 700 kV surfaces.

The supply consists of two systems each consisting of a regulator which supplies 60 Hz power to an exciter transformer, which in turn feeds into a 350 kV high voltage transformer that may be tuned with an associated variable inductor (or reactor). Each of the two systems may be operated independently as a 350 kV source. For 700 kV operations, the second system is floated as the output voltage of the first. For convenience, the three modes of operation are designated as follows:

- A mode - grounded system as 350 kV supply
- B mode - floated system as 350 kV supply
- C mode - both systems in cascade as 700 kV supply.

In order to comply with the various safety codes, several provisions had to be made in the high voltage area, a rectangular space roughly 25 ft x 45 ft with 40 ft head room. A 15 in. high concrete retaining wall was constructed around the area to contain the whole 5550 gallons of transformer oil in all of the units in case of ruptures. A drain will conduct any oil spillage to the exterior of the building. In case of fire, two fog nozzles were installed at positions adjacent to the high voltage area.

Most of the safety features, of course, are concerned with electrical hazards. An 8 ft high expanded metal fence was constructed around the retaining wall. A simplified floor plan of the layout is shown in Fig. A-2. A photograph of the high voltage area is shown in Fig. A-1. The fence is equipped with flashing red lights that are energized when the high voltage equipment is in operation. The gate into the high voltage area is equipped with an interlock such that anyone entering the area automatically shuts down the high voltage equipment. Ten portable grounding hooks have been fabricated, and a ten-step procedure for grounding the high voltage units has been established as part of the standard operating procedures.

Initial operation of the high voltage system on June 29 was only successful in the A mode. One of the digital voltmeters in the B mode control console was not operating correctly and has been returned for repairs. In addition, there seem to be some inconsistencies in the electronics system of the control units and these are presently under investigation. It is expected that these problems will be solved in the near future.

b) 130 kV dc and 80 kV ac Test Facility

Since it was necessary for the 700 kV test area to overlap part of the original fenced-in test area, the 130 kV test set had to be moved. A new 130 kV test facility was set up in a small room adjoining the main bay of the building. Figure A-3 shows a floor plan. The dimensions of the enclosed area are 9 1/2 ft by 7 ft, nearly identical to those of a shielded room which is available for high precision partial discharge measurements. This enclosure is described more fully in Sect. II.A1-e below.

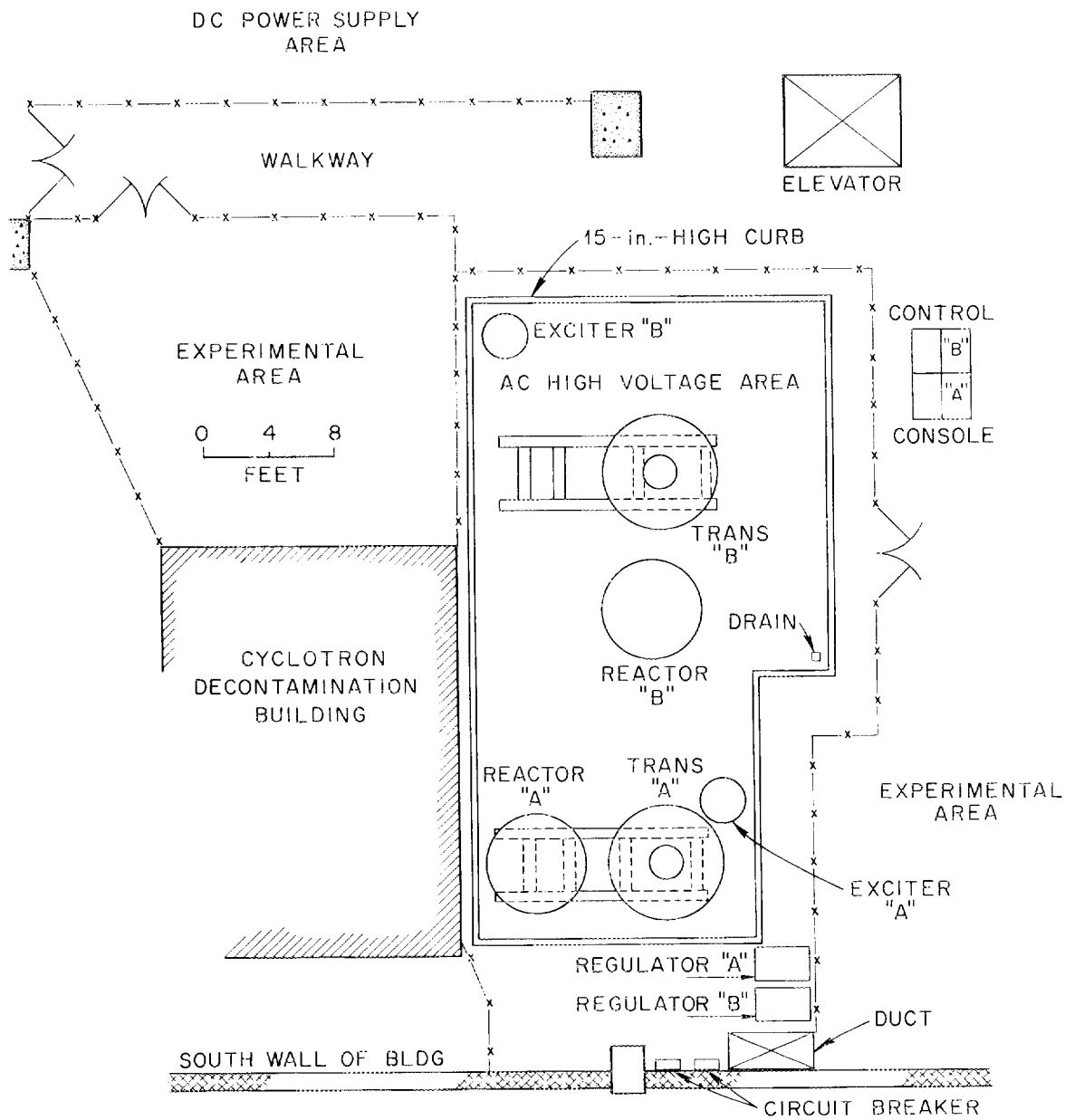


Figure A-2. Floor plan - high voltage area.

ORNL-DWG 73-9404

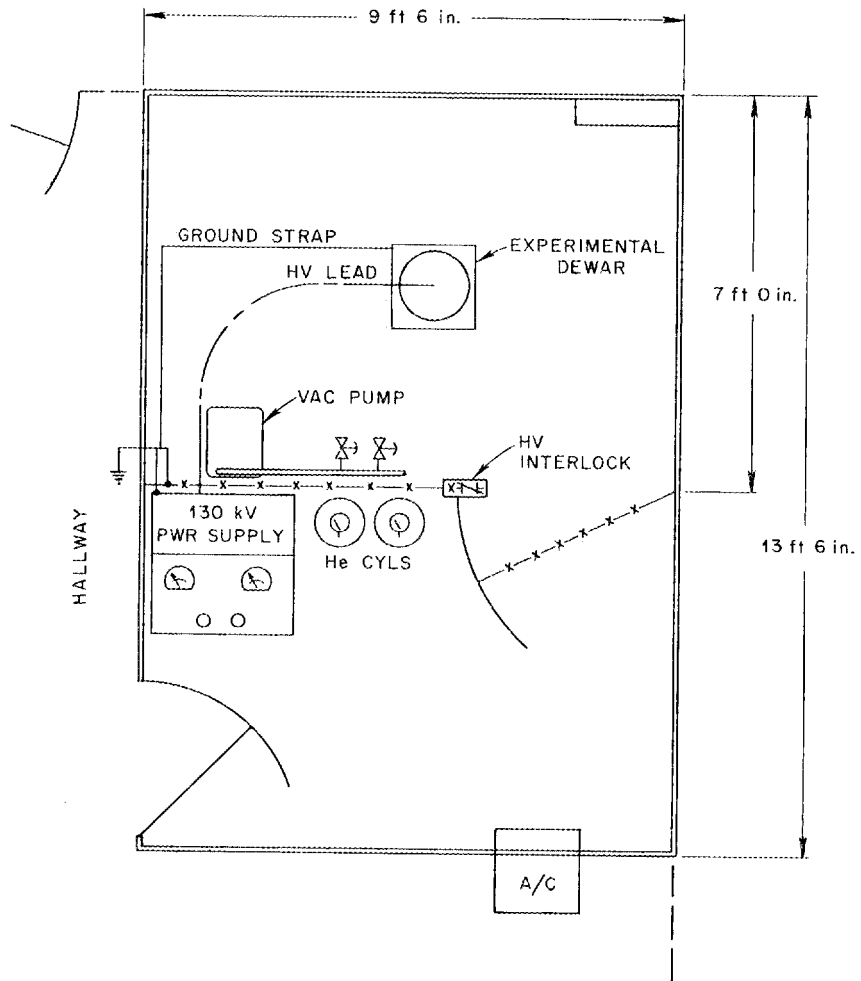


Figure A-3. Layout - Room 281.

In this way, we expect that most of the problems which might arise from working in such a confined space will be solved before the shielded room is actually used.

After the Beta Electric Company 130 kV, 50 mA supply was set up in this room, we observed that the supply was suffering internal breakdowns at sustained voltages above 100 kV. This was eventually traced to a set of high voltage filter capacitors which had been installed by a previous user. New capacitors and rectifier tubes were installed, and the high voltage tank drained, cleaned, and refilled with clean insulating oil. The supply is now operating perfectly at the full rated voltage. The peak-to-peak ripple of the supply was measured to be 2.6% at 50 kV and 2.9% at 120 kV, with a frequency of 120 Hz.

c) Intermediate and High Voltage Cryostats

Two cryostats are under construction for intermediate voltage and high voltage ranges. The intermediate voltage version is designed to fit into an existing 5 1/2 in. glass helium dewar. The high voltage vacuum bushing for use with the 600 kV dc and 700 kV ac supplies is 41 in. in diameter and requires construction of its own large stainless steel dewar with observation ports.

Figure A-4 is an assembly drawing of an intermediate voltage cryostat constructed according to the concepts outlined in our previous report for service with the 130 kV power supply. The maximum gradient sustainable in a vacuum gap, 100 kV/cm, will not be exceeded on the high voltage lead A until it reaches 200 kV with respect to the ground tube B, and the apparatus may be useful with one of the units of the 700 kV test set.

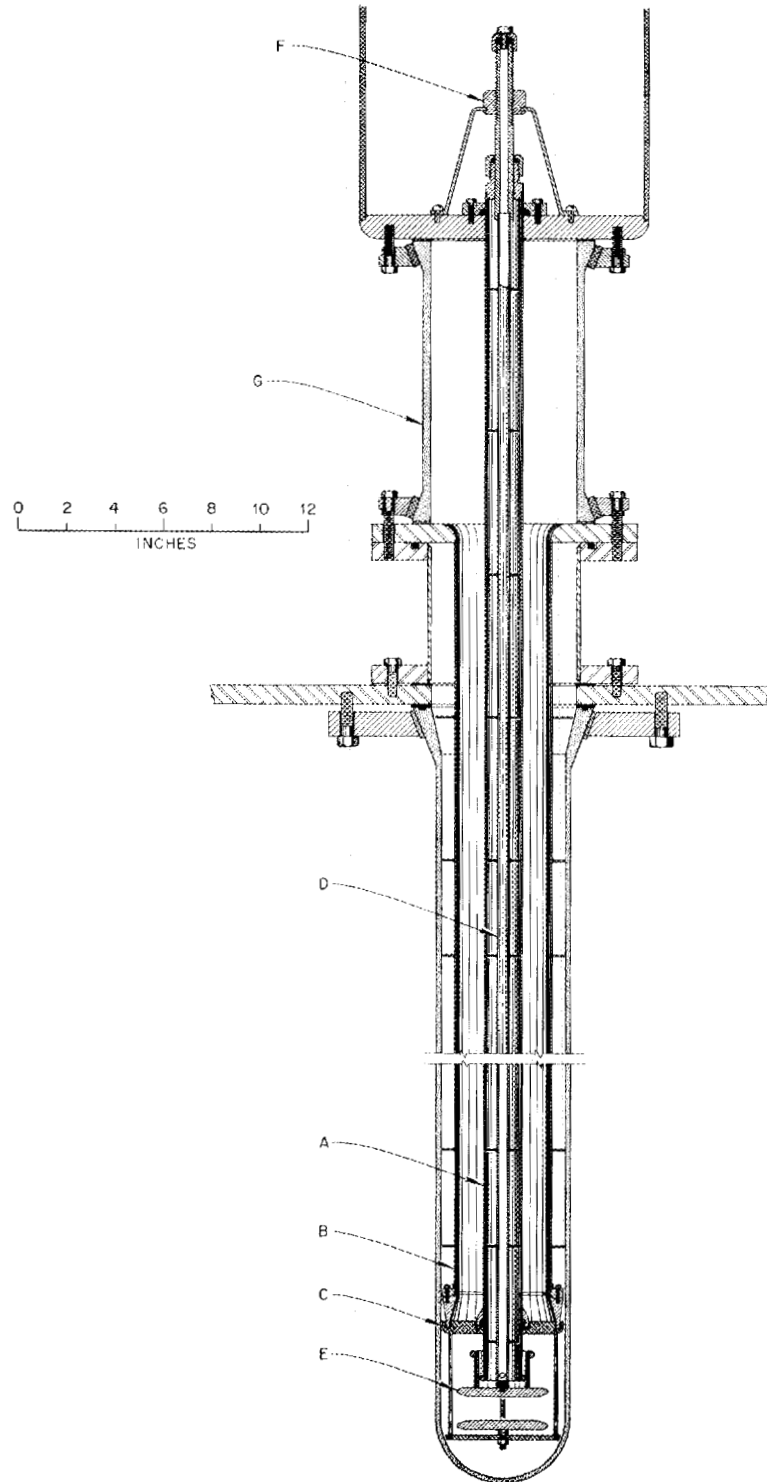


Figure A-4. Intermediate voltage cryostat.

The two tubes of the bushing are joined at the bottom in a vacuum-tight seal to an insulating disc C of G-10 fiberglass. As long as the liquid level is above this insulator, the vapor rising inside A and outside B will not be electrically stressed, and discharges in the low breakdown strength vapor will be avoided. The high voltage electrode E is mounted on tube D, which slides freely up and down inside A.

A screw mechanism for accurately positioning the electrode has been constructed and is shown in Fig. A-5. A precision of better than 0.0005 in. is possible with this device. It is shielded by a corona-free enclosure and insulated from ground by the 6 in. diameter, 12 in. high Pyrex pipe G. Tubes B and D are provided with heat exchange fins which intercept part of the conductive heat leak into the liquid and shunt it into the rising vapor. These fins also shield thermal radiation down the inside of A and down the space between B and the dewar wall. No provision was made for radiation shielding in the vacuum space between A and B because of the small estimated size of the resulting heat leak. The heat leak calculated for this apparatus by the procedures outlined in Appendix E is about 100 mW. All the parts of this apparatus have been received from the shops and are in the process of assembly.

The proposed design for the high voltage cryostat is shown in Fig. A-6. Items A through E are analogous to their counterparts in Fig. A-4. However, the scale of this cryostat is much larger to accommodate the high voltages to be applied from the 600 kV dc and 700 kV ac supplies. The high voltage tube A is 8 in. and the ground tube B is 40 in. in diameter. Because of the large diameter, radiation through the vacuum is appreciable, of the order of 15 W. The radiation baffles F intercept

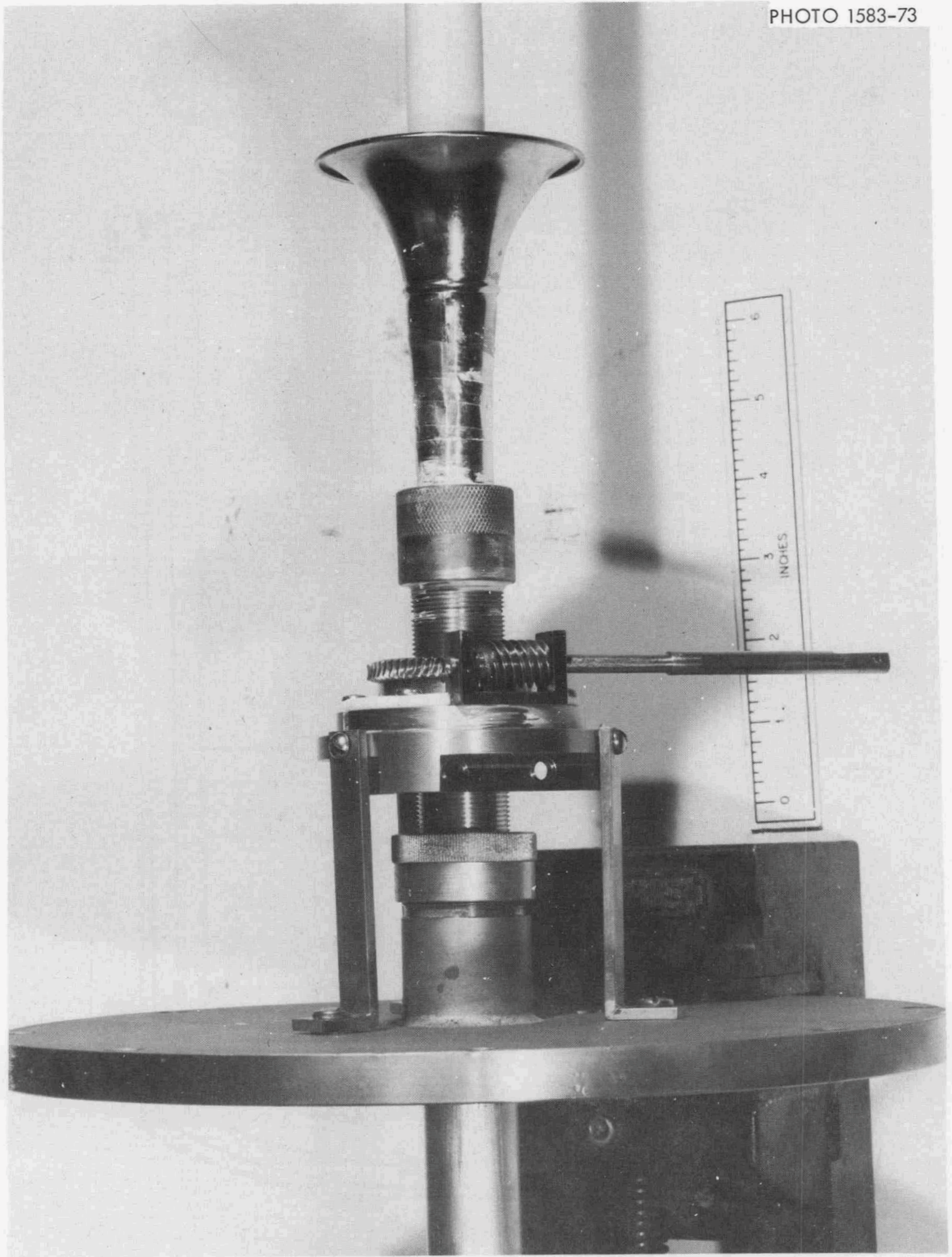


Figure A-5. Electrode positioning mechanism.

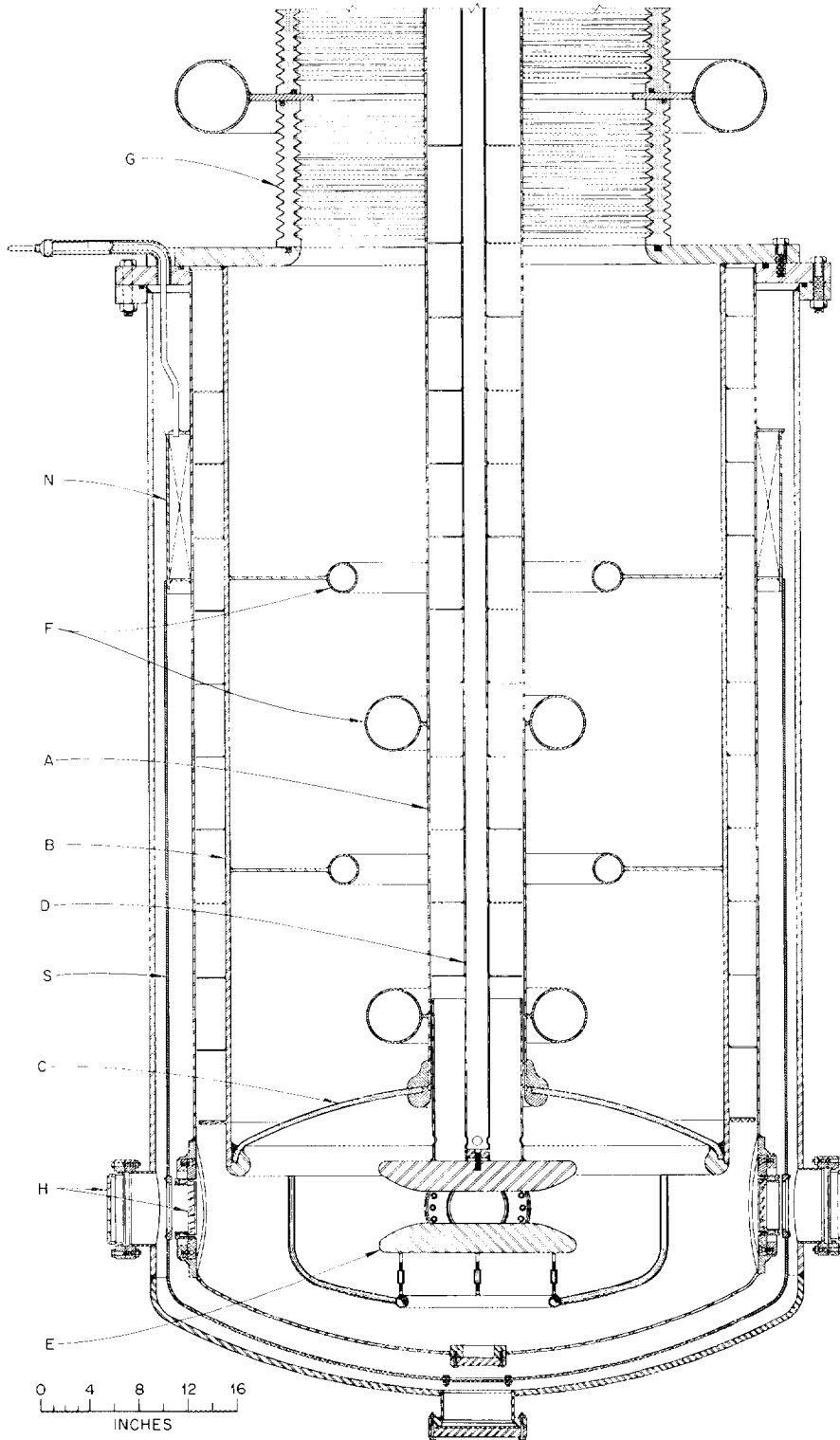


Figure A-6. High voltage cryostat.

this heat leak. In order to prevent high field gradients at their edges, these baffles are terminated by large toroids. These toroids were chosen from the several sizes available with the help of preliminary field plots (see Fig. A-10) and electrostatic field calculations described in Appendix G, Sect. III. The apparatus is designed to reach the peak voltage of the 700 kV ac test set on the high voltage tube A before the field anywhere in the bushing reaches the critical value of 100 kV/cm. The high voltage termination and electrode positioning mechanism will rest on a stack of large porcelain stand-off tubes which were obtained from a previous high voltage accelerator experiment.

Visual observations will be made through windows H, manufactured by the Ceramaseal Company. The 4 in. inner window on the helium chamber is quartz to minimize thermal contraction, while the 6 in. outer window is regular optical glass. Three windows will be installed at 90 degree intervals, with provision for a fourth if required.

The helium chamber will be further shielded by a copper shell S suspended in the vacuum space between the inner and outer tanks from the liquid nitrogen bath N. Superinsulation will also be attached to this shield.

It is the object of the program to carry out breakdown measurements in liquid helium at pressures up to 10 atm. The pressure withstand calculations for the internal parts of the bushing are given in Appendix F. Design of the low temperature insulator C presents a difficult problem, since this piece must withstand the combined forces of thermal contraction and the 10 atm pressure of the helium beneath it. The design under consideration is an inverted spherical dish laid up with fiberglass cloth

and epoxy. Some preliminary discussions have taken place with other groups at the laboratory with experience in construction of fiberglass reinforced epoxy structures.

The total heat leak into the helium is expected to be of the order of 3 or 4 W on the basis of calculations in Appendix E. This corresponds to a helium boil-off rate of about 5 or 6 liters per hour. Since the total capacity of the helium space is about 250 liters, there should be no difficulty in keeping the dewar cold for long periods of time without helium retransfer. Furthermore, if the liquid is overpressured slightly to suppress boiling, its large heat capacity will keep the temperature from rising appreciably while measurements are being performed.

Design drawings are complete for the inner and outer vacuum tanks and for the copper nitrogen shield, and construction of these items is in progress. Fabrication of the vacuum bushing will begin as soon as the design of the low temperature insulator is finalized. The drawings and calculations have been submitted to the ORNL Pressure Vessel Review Committee for approval.

d) Rogowski Electrodes

It is desirable to perform breakdown measurements between infinite plane electrodes because the electric field is then uniform and calculated simply by the ratio of voltage to gap. However, the electrodes must be finite, and if the edges are curved too sharply, the resulting field enhancement will make breakdowns more likely at the edges than in the central uniform field region. Maxwell originally showed that a contour of the form $X/S = X_0/S + 2/\pi \ln(Y/S)$ as depicted in Fig. A-7 will give the maximum field strength in the flat region inside the X_0 ,

ORNL-DWG 73-9407

$$\frac{x}{s} = \frac{x_0}{s} + \frac{2}{\pi} \ln \frac{y}{s}$$

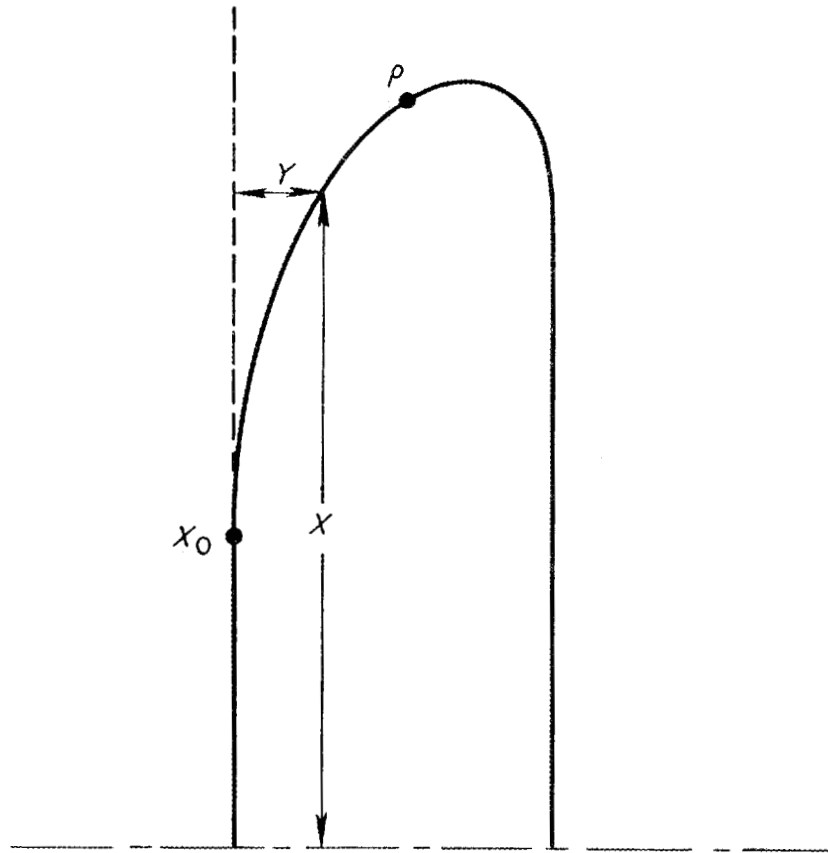


Figure A-7. Rogowski electrode contour.

as long as the gap is less than $2S$. Electrodes with such a contour were first used by Rogowski. The size of the electrode is determined by the value of $2S$ needed to stand off the maximum voltage to be used. Three sets of Rogowski electrodes have been constructed using tape-controlled machines for maximum voltages of 250 kV, 500 kV, and 1000 kV. The 1000 kV electrodes are roughly $1\frac{1}{4}$ in. in diameter, while the 500 kV and 250 kV sets are one-half and one-fourth this size. The finished electrodes are shown in Fig. A-8. One question to be considered is the influence of the grounded dewar wall on the field between the electrodes. In the 1000 kV cryostat, the radius of the inner wall is 23 in., giving a 16-in. clearance to the edges of the electrodes. Preliminary analog field plots indicate very little effect, and more exact finite element computer calculations which take account of the cylindrical geometry are underway.

e) Partial Discharge Detection

At some applied electric field below its ultimate breakdown strength, an insulation system usually exhibits small discharges which do not bridge the entire dielectric. These partial discharges can occur in small cavities or gas bubbles in the dielectric, near conductor-dielectric junctions, around small solid inclusions in the dielectric, or at surface asperities on conductors which cause local field enhancement. Since these discharges can be destructive to the insulation and are in any case a source of electrical loss, measurements of their magnitude and frequency are of great interest. We have purchased a balanced partial discharge detector from the J. G. Biddle Company. This instrument has the greatest sensitivity of any commercially available partial discharge detector and is capable of detecting discharges as small as 0.03 pC. Its design also

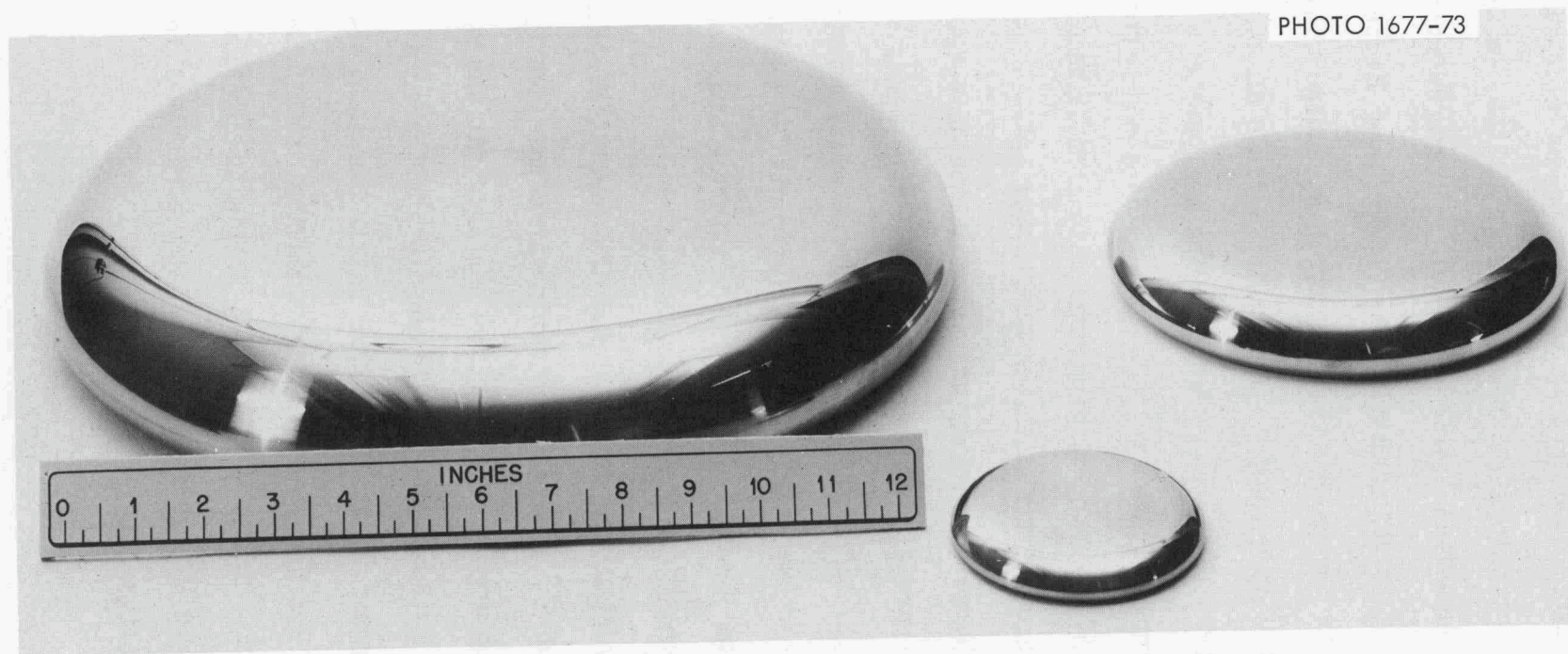


Figure A-8. Rogowski electrodes for 250 kV, 500 kV, and 1000 kV.

simplifies discharge detection in the presence of electrical interference. Further details are given in Appendix C. Since the circuit is essentially a high voltage capacitance bridge, it requires two identical samples. We expect to provide these by cutting the low voltage electrode into two equal halves. If the halves are well matched, charge should not build up preferentially on either side, and little field distortion should occur. The detector will also be used for checking the partial discharge level of our power supplies, high voltage connections, and bushings.

A feature of all partial discharge detectors is that they operate in a limited frequency band to reduce external noise. Hence, the pulse shape of a discharge is greatly distorted at the detector output. We plan to observe partial discharge pulses directly using a fast oscilloscope in order to obtain information about the rise time, amplitude, and duration of the discharges. We have selected a Tektronix 7904 mainframe with 0.8 nsec rise time preamplifiers and 0.5 nsec/div time base. This scope will also be useful in future impulse tests.

We may find that high-sensitivity partial discharge measurements will require that the apparatus be set up in a shielded Faraday cage. An existing enclosure is available for our use. It was manufactured in 1969 by Erik A. Lindgren and Associates, Inc. It has inside dimensions of 9 ft 9 in. square x 7 ft 7 in. high and is double-isolated with steel and copper shields. The guaranteed attenuation of this enclosure is 120 dB for 15 kHz - 10,000 MHz electric fields and 15 kHz magnetic fields, and 30-36 dB for 60 Hz magnetic fields. All electrical inputs and ventilation channels are thoroughly filtered.

2. Auxiliary Investigations

During this report period we realized that it is convenient to distinguish between our main experimental program and "auxiliary investigations." These auxiliary investigations are expected to provide numerical values for the design, fabrication, and operation of equipment for our main experimental program. Such investigations may concern the dielectric and the mechanical strength of design material, flashover performance in air and in vacuum, electric noise production outside the actual test specimen, casting of epoxy, the mechanical performance of various kinds of solid dielectrics under thermal stresses, and methods of achieving vacuum-tight cryogenic connections between assemblies. These investigations may be quite extensive and must at times be the principal focus of the activity. The air flashover experiments mentioned in our previous semi-annual report fall into this category.

During this report period a simple apparatus was constructed to perform auxiliary tests on insulation in concentric geometries (Fig. A-9). The three spheres formed the ground electrode and could be adjusted to fit tightly around the insulation. The whole apparatus was mounted in the flashover test stand and immersed in a 4 liter beaker of transformer oil. A short 3 in. sample insulated with seven layers of shrinkable PVC tubing successfully withstood the full 130 kV available with the supply, although above 100 kV surface flashovers often occurred between the high voltage electrode and grounded spheres. The sample was also immersed in liquid nitrogen repeatedly with no fracturing.

Further auxiliary investigations involved preliminary analog field plots for the high voltage cryostat. A photograph of a finished plot is

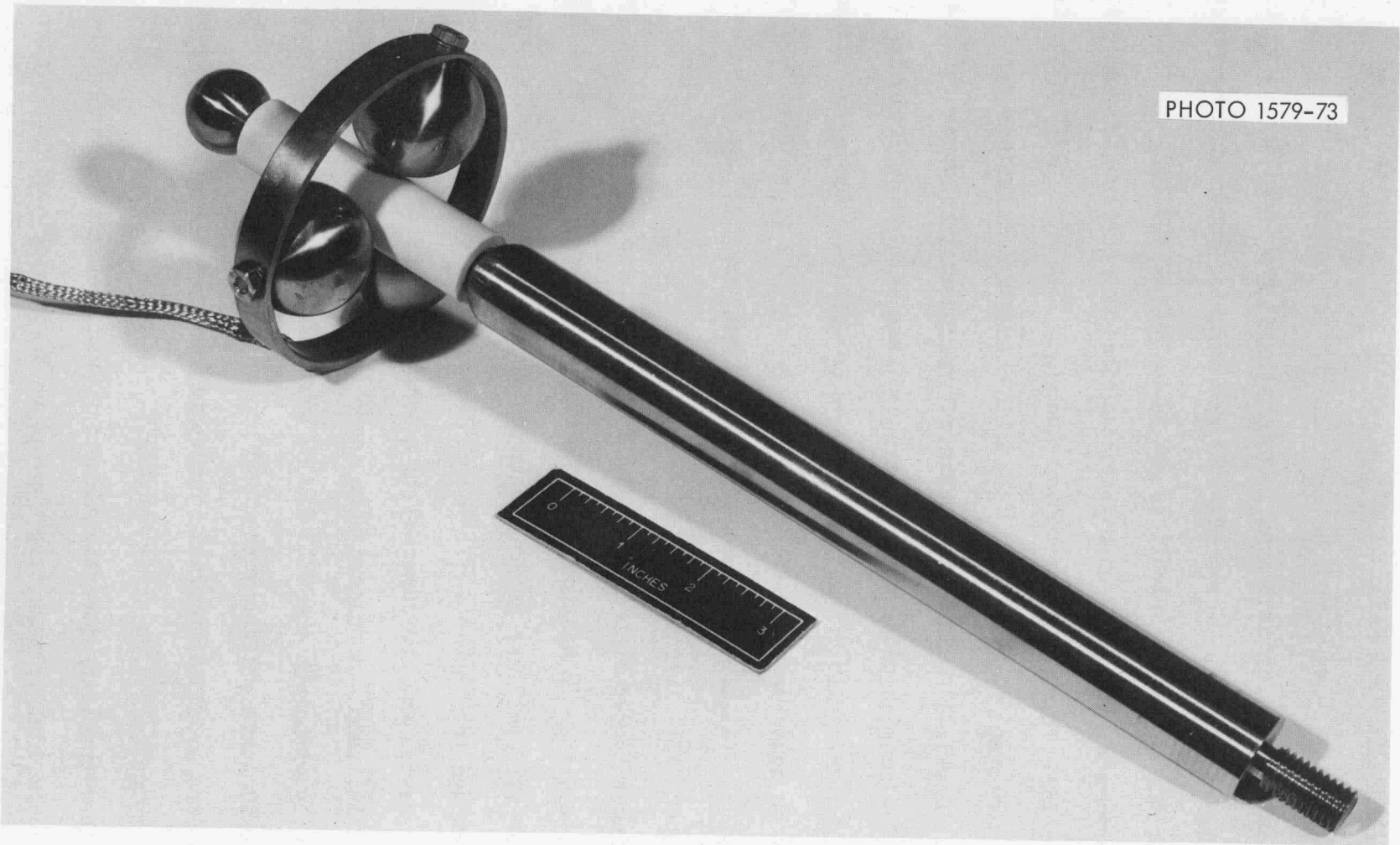


Figure A-9. Three-sphere concentric geometry assembly.

shown in Fig. A-10. Contours corresponding to the cross-sectional structure of the cryostat (cf. Fig. A-6) were painted on semiconducting paper with highly conductive silver paint, and the equipotential lines determined as discussed in Appendix G. The lines are labeled with their respective percentages of the total potential difference. These investigations allowed us to establish rough dimensions of the apparatus before going to more accurate finite element computer calculations as also discussed in Appendix G.

3. Exploratory Experiments

In our main experimental program we also include "exploratory experiments" which are related to the ultimate objectives of our program but which do not incorporate all the features which may eventually be desirable. The object of these experiments is to identify problems and establish experimental techniques rather than to provide final data.

The first exploratory tests attempted were breakdown measurements in liquid nitrogen. The air flashover test stand was modified for these experiments by replacing the 8-in. disc electrodes with a 2-in. diameter spherical steel high voltage electrode and a 4-in. diameter stainless steel ground plane. A foam-insulated box was built around the electrodes to hold liquid nitrogen. The high voltage electrode was positioned by means of a screw mechanism and monitored by a dial gauge similar to the one shown in Figs. A-5 and A-11. After cooling the electrodes to nitrogen temperature, the zero position was determined by measuring the resistance between the electrodes with an ohmmeter. The high voltage electrode was then backed off to the desired gap. Ten to 20 breakdowns were made at gaps of 0.010 in., 0.020 in., and 0.030 in. Owing to the large amount

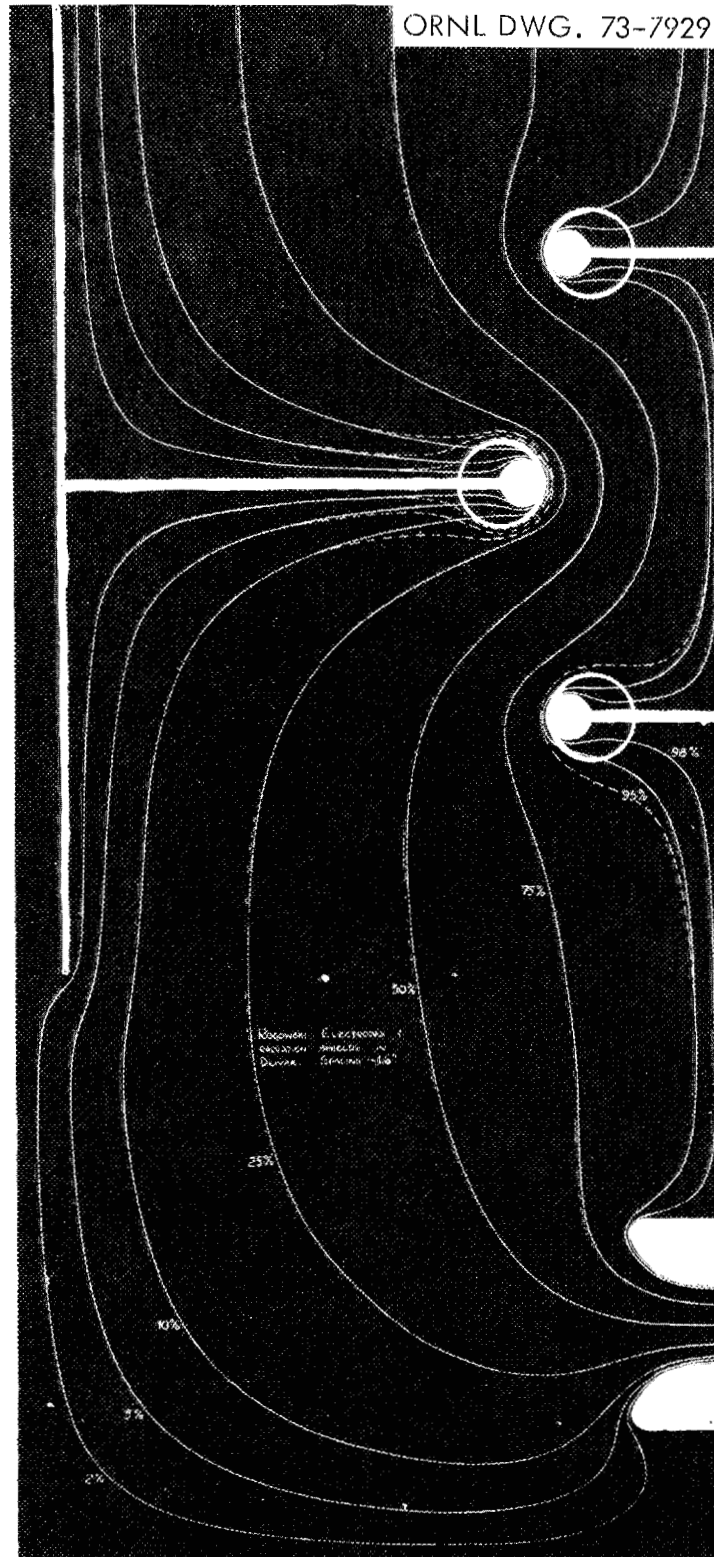


Figure A-10. Analog plot of radiation shields for vacuum bushing. Rogowski electrodes at bottom.

PHOTO 1592-73

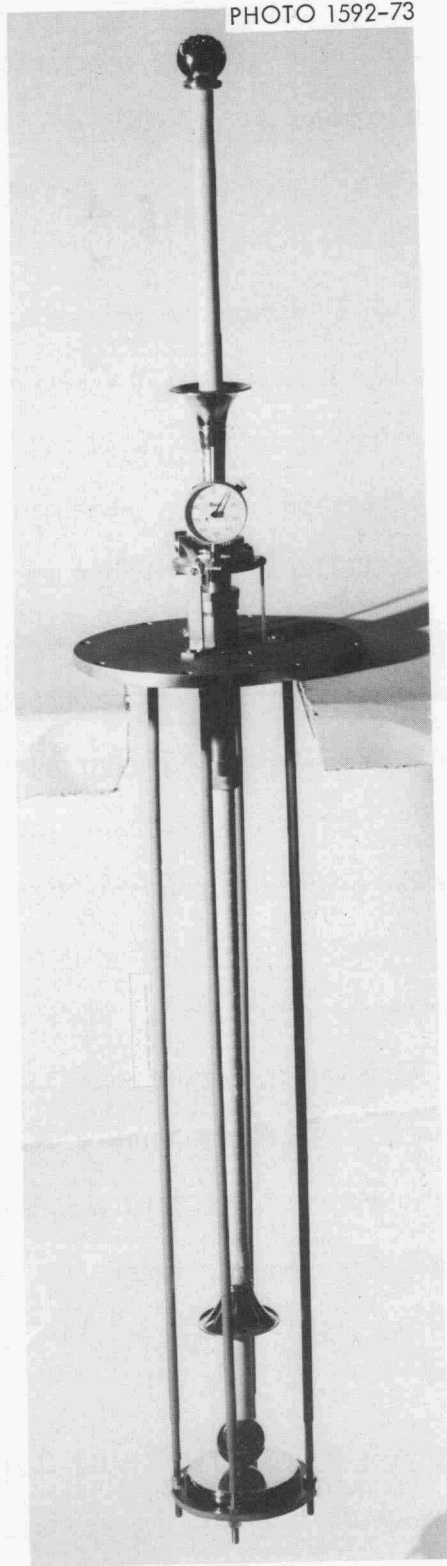


Figure A-11. Exploratory helium cryostat sphere-plane electrode assembly.

of frozen air and moisture contamination in this arrangement, the breakdown fields showed wide scatter, ranging from about 525 kV/cm to 600 kV/cm. Published values of ac breakdown at similar spacings for liquid nitrogen at 1 atm are 452 kV/cm (50 Hz ac peak)¹ and 696 kV/cm (60 Hz ac peak),² bracketing our values.

We believe that the wide scatter in our results was due to an insulating contamination layer which built up on the electrodes within a few hours. This was indicated by the large resistance measured between the touching electrodes after this time. Hence, the field in the gap was affected by these additional dielectric layers in an unpredictable way.

To prevent the entrance of contaminants, we decided to construct a sealed bushing which could be mounted in a glass dewar. Information obtained in the previously mentioned auxiliary tests was used in the design of this bushing. The first version tested was insulated with six layers of PVC shrinkable tubing on a 3/8 in. center electrode, to give a total diameter of 3/4 in. and a length of 48 in. Figures A-11 and 12 show the complete cryostat. The insulation was covered with a grounded single layer of 0.002 in. thick aluminum tape wound between the two stress cones. Hence, as long as the liquid level is kept above the lower cone, no breakdown can occur in the unstressed vapor. The dial gauge directly measures the travel of the high voltage electrode. Figure A-5 shows a close-up of the screw mechanism which positions the electrode, as described in Sect. II.A2-c.

One trial run has at present been made with this apparatus. In spite of the successful electrical and cryogenic auxiliary tests on a short insulation sample, the 4-ft bushing cracked during cooldown. More

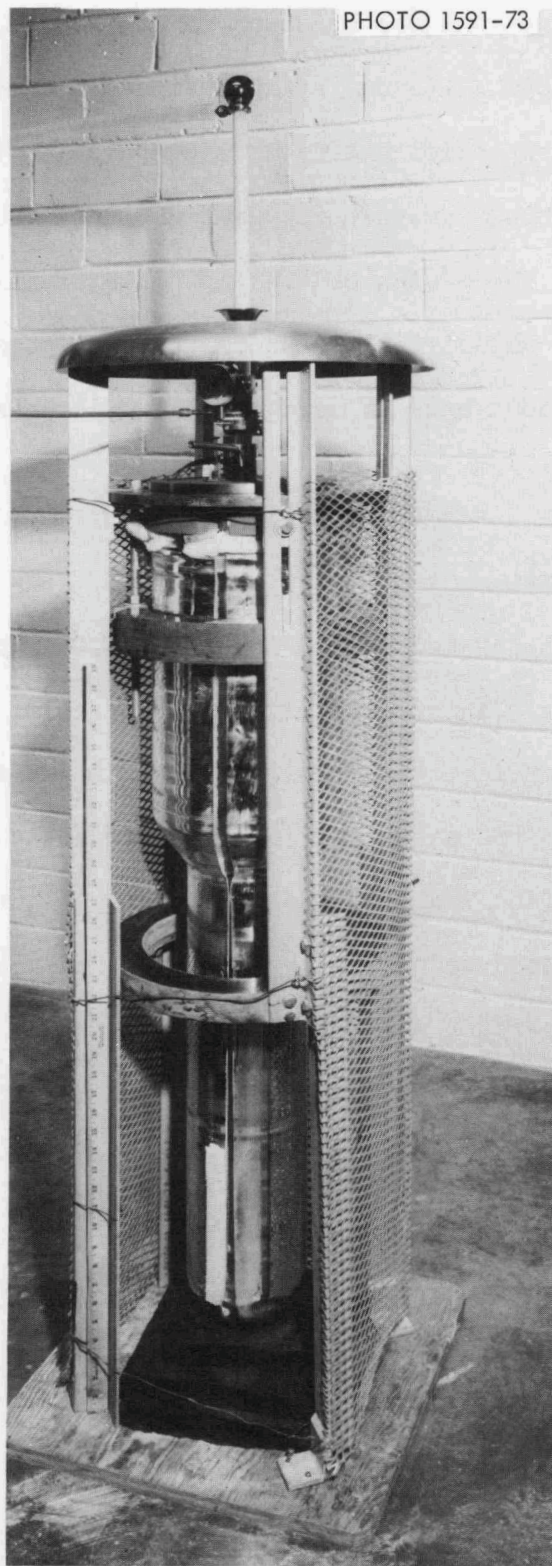


Figure A-12. Exploratory helium cryostat with dewars.

auxiliary investigations are underway on other types of insulation. At present Stycast 2850 FT (blue) epoxy is the most attractive candidate, having a thermal expansion coefficient comparable with most metals. However, the PVC bushing remained vacuum-tight during cooldown, which demonstrates that the design of the top plate of this cryostat was satisfactory. We expect that it should soon be possible to obtain exploratory breakdown data in cryogenic liquids under conditions of low contamination.

4. Future Activity

The change in funding level between FY 1973 and FY 1974 will require a reduction in our planned activity during FY 1974. Accordingly, we have chosen to defer consideration of impulse testing until a later date. Should the results of the ac and dc breakdown tests and the partial discharge investigations indicate that impulse tests at relatively low voltage levels should be undertaken, then we could build a one-stage 600 kV impulse generator using the capacitors which we have on hand and the Haefely power supply.

During FY 1974 appreciable additional work on equipment, auxiliary investigations, and exploratory experiments will be necessary. However, we expect that the focus of activity should shift over to main program experiments with intermediate and high dc and ac voltages as the year progresses. Specific tasks to be accomplished in the various areas are the following:

Equipment

1. Construct an improved preliminary bushing.

2. Complete assembly of intermediate voltage cryostat.
3. Final checkout of 700 kV ac test set operation.
4. Temperature and pressure measurement and control equipment.
5. Receive and set up partial discharge detection equipment.
6. Activate shielded room.
7. Construct high voltage cryostat.

Auxiliary Investigations

1. Find suitable insulation material for preliminary bushing.
2. Make high voltage flashover and partial discharge tests on room temperature bushings and insulator columns for high voltage cryostat.
3. Develop a low temperature insulator for high voltage cryostat.

Exploratory Experiments

1. Liquid helium and liquid nitrogen breakdown experiments using preliminary bushing.
2. Confirm Gerhold and Meats' measurements using intermediate voltage cryostat.
3. Exploratory tests with high voltage cryostat.

Main Program Experiments

1. Breakdown of cryogenic liquids; breakdown and flashover of cryogenic solid insulators--intermediate voltages.
2. Breakdown of cryogenic liquids; breakdown and flashover of cryogenic solid insulators--high voltage.

REFERENCES TO SECT. II.A

1. P. H. Burnier, J. L. Moreau, and J. P. Lehmann in Advances in Cryogenic Engineering, Vol. 15 (1970) p. 76.
2. K. Mathes, IEEE Trans. Elec. Insul. EI-2, 24 (1967).

B. SUPERCONDUCTING MATERIALS

We report a continuation of the work discussed in the March 1 semiannual report on the study of the influence of material variables on ac losses in superconductors. This work may be classified into three main areas: 1) niobium-rare earth dispersion studies, 2) measurement of critical current density, J_c , and surface shielding parameter, ΔH , in the dispersions, and 3) construction of ac loss measuring equipment.

1. Niobium-Rare Earth Dispersion Studies

In the March 1 report we showed that additions of insoluble yttrium particles to heavily cold-worked (92% reduction in area) niobium markedly increased the hysteresis of dc magnetization curves. As a measure of this hysteresis (and "fluxoid pinning"), we chose to use B_R , the remanent magnetization in zero applied field. We found that Y increased the B_R of pure Nb from about 2.0 kG to a maximum of 3.15 kG for the Nb-1.0 at/o Y alloy. We now report the results of annealing treatments on these Nb-Y alloys. The cold-worked samples were annealed for one hour at 600, 800, 1000, and 1500°C respectively. The samples annealed at 600 and 800°C were sealed into quartz capsules at a pressure of 10^{-7} torr and heated in muffle furnaces. The samples annealed at 1000 and 1500°C were heated in tantalum element resistance vacuum furnaces in dynamic vacuum of better than 5×10^{-6} torr at temperature. Superconducting-normal transition temperatures (T_c) were measured on all samples by the inductive method. After an initial decrease in T_c for the cold-worked Nb-Y alloys on annealing at 600°C (from 9.37 ± 0.08 K to 9.29 ± 0.02 K), the T_c 's remained constant with annealing temperature. The pure niobium, however, showed a steady

decrease with annealing temperature from 9.27 ± 0.08 K for the as-cold worked sample to 9.19 ± 0.01 K for the sample annealed at 1500°C . The drop in T_c for the Nb-Y alloys on annealing at 600°C and higher temperatures must be related to the decrease in dislocation density, i.e., resistivity. The continued decrease in T_c in pure Nb is presumably due to pick-up of oxygen. Therefore, the use of Y in Nb serves as a "getter" for oxygen and allows the Nb matrix to remain pure even after annealing at 1500°C in moderately good vacua ("hard" vacuum $< 10^{-8}$ torr in required to eliminate oxygen contamination in Nb). This also implies that Y dispersions will help to maintain a high H_{c1} in Nb.

The results of dc magnetization measurements, as values of B_R , are presented versus atomic percent Y for the various annealing temperatures in Fig. B-1. The B_R values for the samples annealed at 600 and 800°C follow the same general pattern as the cold-worked results with some dependence on Y content and a maximum in B_R at 1.0 a/o Y. The pure Nb actually shows a higher B_R for these heat treated samples than the as-cold worked condition. This is consistent with previous work of others¹ and reflect the "sharpening" of the dislocation cell walls, with a decreased dislocation density in the cell centers and an increased dislocation density in the cell walls, which has been found to increase fluxoid pinning. After the alloys have been heated to sufficiently high temperatures for recrystallization to occur (between 800°C and 1000°C for Nb and the Nb-Y dispersions), the values of B_R show very little dependence on Y content. That is, the data for 1000°C anneals and, more pronounced, the data for 1500°C anneals show little change in B_R from the 0.1 a/o to the 2.0 a/o Y samples after a dramatic increase from pure Nb. This point is also

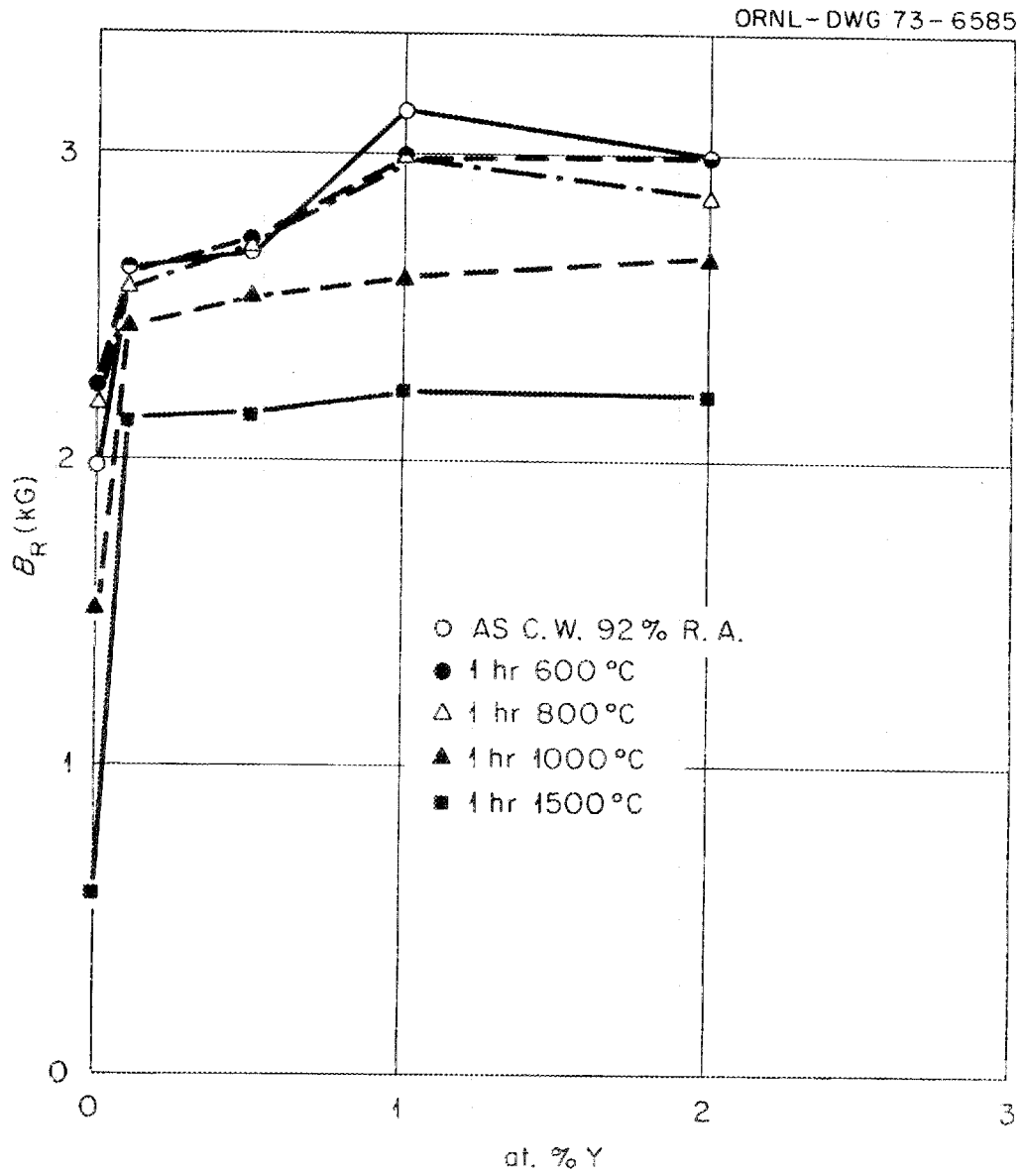


Figure B-1. B_R , remanent magnetization vs atomic percent yttrium for various annealing treatments.

illustrated by plotting B_R versus annealing temperature for pure Nb and the various Nb-Y dispersions in Fig. B-2. In the following paragraphs we shall present a tentative explanation of this behavior aided by the results of optical metallography and transmission electron microscopy.

Transmission electron microscopy was carried out on 1/8 in. diameter discs spark-machined from the specimen rods, jet-polished, and electrolytically thinned. The thin foils were observed in a Hitachi electron microscope at an operating voltage of 200 kV. With the exception of the presence of Y particles, the microstructures of the cold-worked samples of pure Nb and the Nb-Y dispersions appeared identical. The structures, illustrated in Figs. B-3a and B-3b for pure Nb and Nb-0.1 a/o Y, respectively, consisted of the "cell structure" with dense dislocation walls surrounding volumes with a lower dislocation density. Measurement of the average cell diameter was carried out for pure Nb, Nb-0.1 a/o Y, and Nb-2.0 a/o Y. The results are listed in the Table below. The error was taken as \pm twice the standard deviation. Thus, with experimental error, the cell size for pure Nb and the dispersions is the same. It was difficult to retain the Y particles in the foils during polishing for the higher Y-content alloys but particles were retained in the Nb-0.1 a/o Y dispersion. These roughly spherical particles had an average diameter of $0.50 \pm 0.10 \mu\text{m}$. For the Nb-0.1 a/o Y alloy, with $0.5 \mu\text{m}$ particles, one can calculate the average distance between particles knowing the volume fraction and volume per particle. It comes to $3.3 \mu\text{m}$ so that on average we have $1/2 \mu\text{m}$ particles $3-4 \mu\text{m}$ apart. This is consistent with the optical metallography. Since the dislocation structures are similar, one must conclude that the increases in B_R due to Y additions are due to

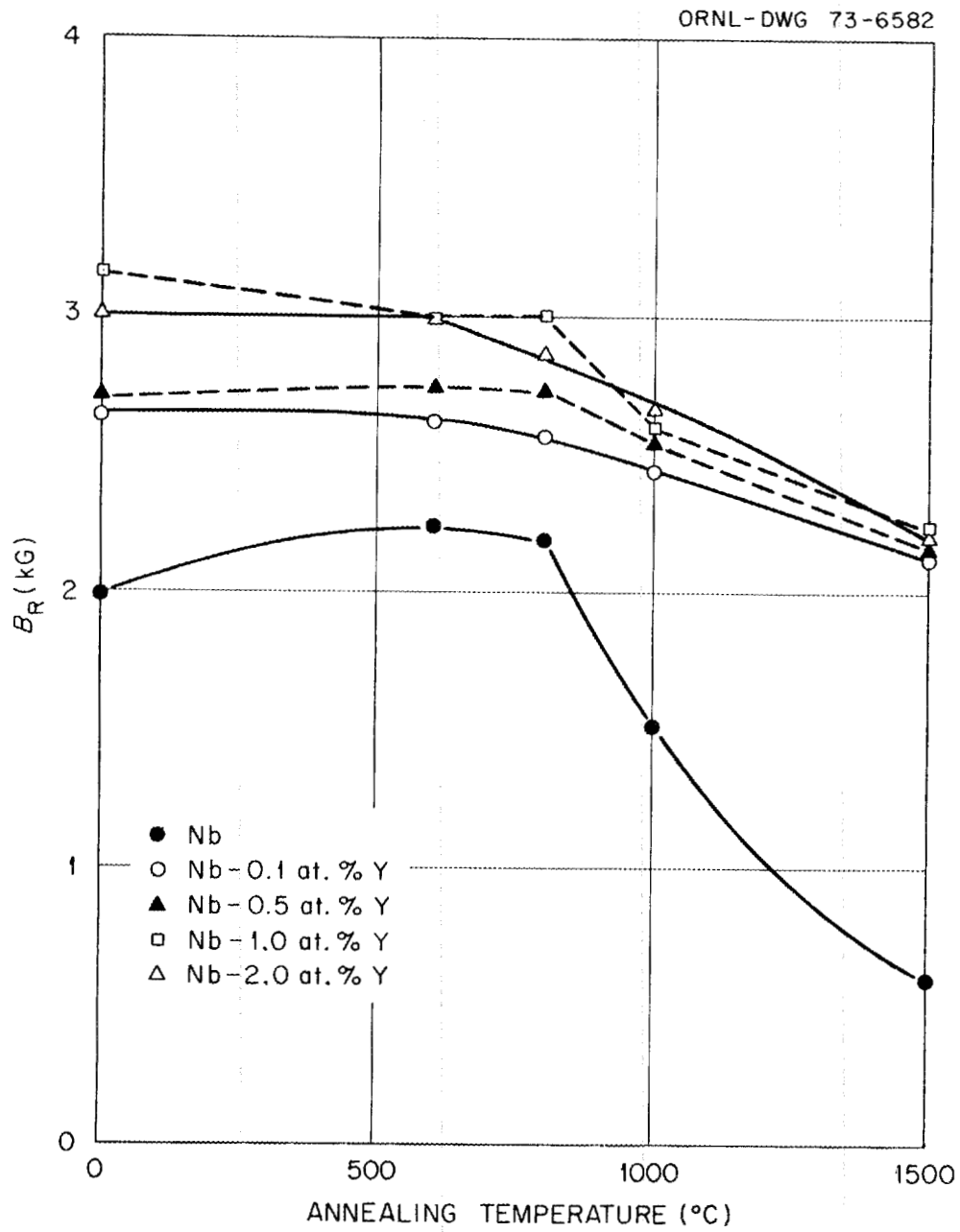


Figure B-2. B_R , remanent magnetization vs annealing temperature (one hour anneals) for pure Nb and Nb-Y dispersions.

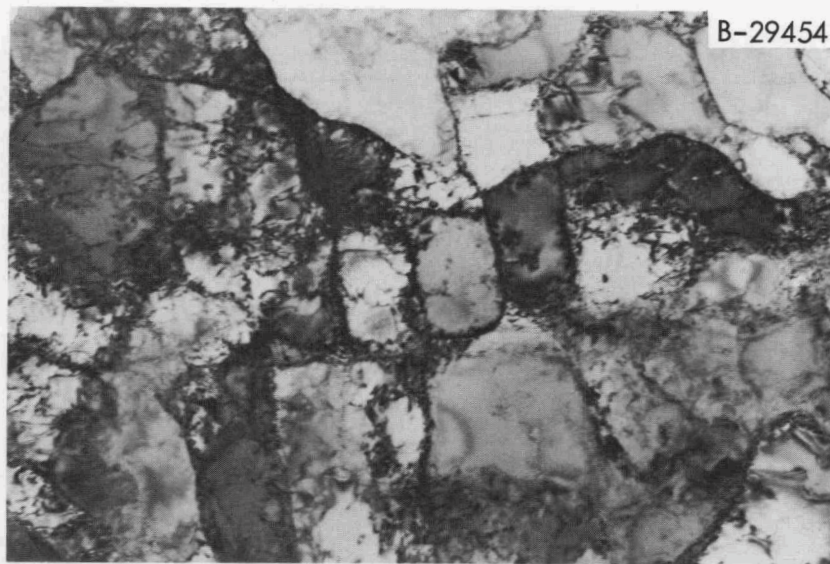


Figure B-3a. Transmission electron micrograph of pure Nb cold-worked 92% reduction in area. Magnification 30,000x.

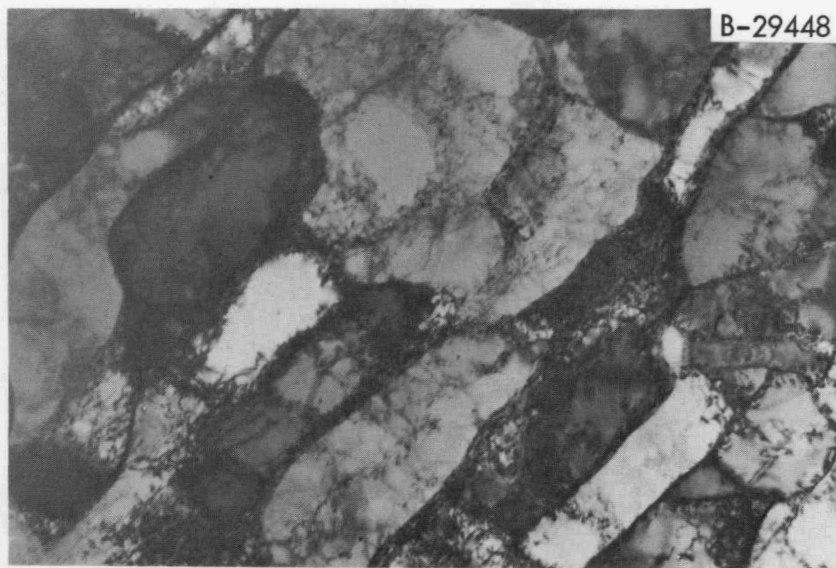


Figure B-3b. Transmission electron micrograph of Nb-0.1 at. % Y cold-worked 92% reduction in area. Magnification 30,000x.

fluxoid pinning by the Y particles themselves. Pinning in the samples annealed below 1000°C is then due to both the dislocation structure and the Y particles.

Table

Alloy	Average Cell Size
Pure Nb	$0.41 \pm 0.14 \mu\text{m}$
Nb-0.1 a/o Y	$0.39 \pm 0.18 \mu\text{m}$
Nb-2.0 a/o Y	$0.45 \pm 0.08 \mu\text{m}$

We find optical metallography provides the best aid in understanding the B_R results for the 1000°C and 1500°C heat treatments. The most obvious difference between pure Nb and Nb-Y dispersions annealed at 1500°C , aside from the presence of Y particles, is the difference in recrystallized grain size. The average grain diameter for pure Nb annealed at 1500°C was $210 \pm 60 \mu\text{m}$ ($\pm 2\sigma$) while for Nb-0.1 a/o Y and Nb-2.0 a/o Y it was $38 \pm 9 \mu\text{m}$ and $40 \pm 4 \mu\text{m}$ respectively. These microstructures are illustrated in the micrographs in Fig. B-4a and B-4b. Thus, the grain sizes of the Y-containing samples are about five times smaller than for pure Nb annealed at 1500°C . Grain size difference alone cannot account for the difference in B_R , however. By chance, the pure Nb samples annealed at 1000°C had the same recrystallized grain size ($39 \pm 9 \mu\text{m}$) as the Nb-Y samples annealed at 1500°C , but a much lower value of B_R as seen in Fig. B-2. Also, the Y particles, per se, must not be a major contribution to B_R since there is little difference between the 0.1 and 2.0 a/o Y samples as illustrated

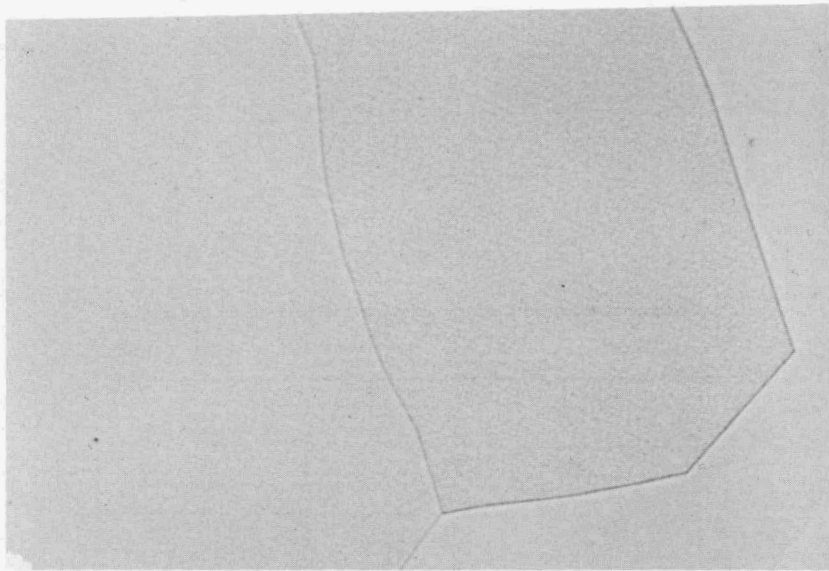


Figure B-4a. Optical micrograph of pure Nb annealed one hour at 1500°C. Magnification 500x.

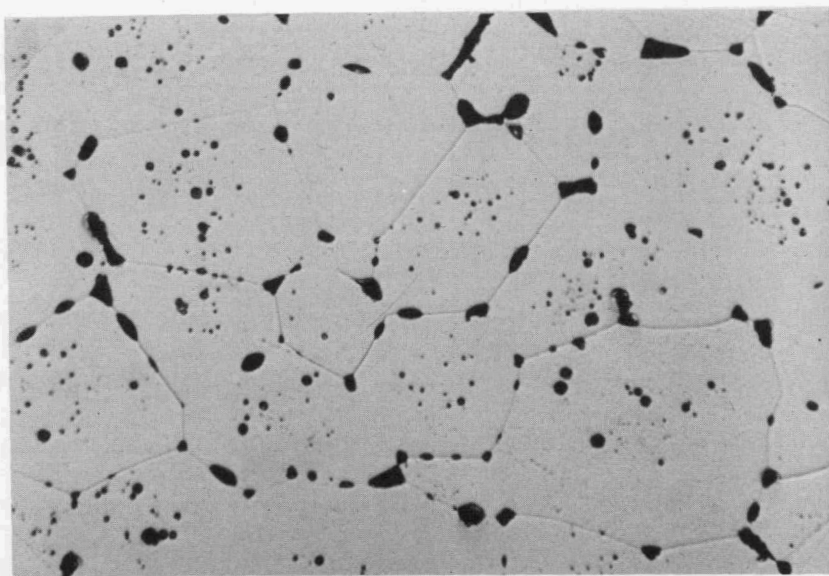


Figure B-4b. Optical micrograph of Nb-2.0 at. % Y annealed one hour at 1500°C. Magnification 500x.

most clearly in Fig. B-1. Our tentative conclusion is that the high angle grain boundaries are chiefly responsible for flux pinning and the Y particles not only inhibit grain growth, thus providing a fine grain size, but increase the pinning effectiveness of the grain boundaries by coating them with a "film" of Y.

In summary, yttrium additions increase the magnetic hysteresis of Nb and maintain its high T_c on annealing by acting as a getter for oxygen. The insensitivity to Y content of B_R of recrystallized samples would simplify production for any large-scale application of these materials.

We have prepared Nb-Gd dispersions with 0.1 a/o Gd, 0.5 a/o Gd, and 1.0 a/o Gd. As our previous work predicted,² we found no advantage in the ferromagnetic Gd particles as flux pinning sites over paramagnetic Y. We have carried out dc magnetization on Nb-Gd samples as cold-worked and annealed at 600°C with values for B_R similar, but slightly lower, than the corresponding Nb-Y dispersions.

2. Measurement of J_c and ΔH by ac Susceptibility

The two material parameters which determine ac losses in superconductors above H_{c1} are J_c , the critical current density, and ΔH , the surface shielding parameter.³ We have included ΔH in a recent re-examination⁴ of the Bean harmonic analysis method⁵ for extracting J_c from ac susceptibility measurements. Our technique provides a check on whether the assumptions of the model are met in a given experiment. We have applied this technique to the Nb and Nb-Y samples and have found agreement with the model, so that we have obtained values of J_c and ΔH . J_c results vs applied field for the pure Nb and Nb-2.0 a/o Y samples annealed at 1500°C are presented in Fig. B-5. The much higher J_c values for the Nb-2.0 a/o Y sample are

ORNL-DWG 73-6584

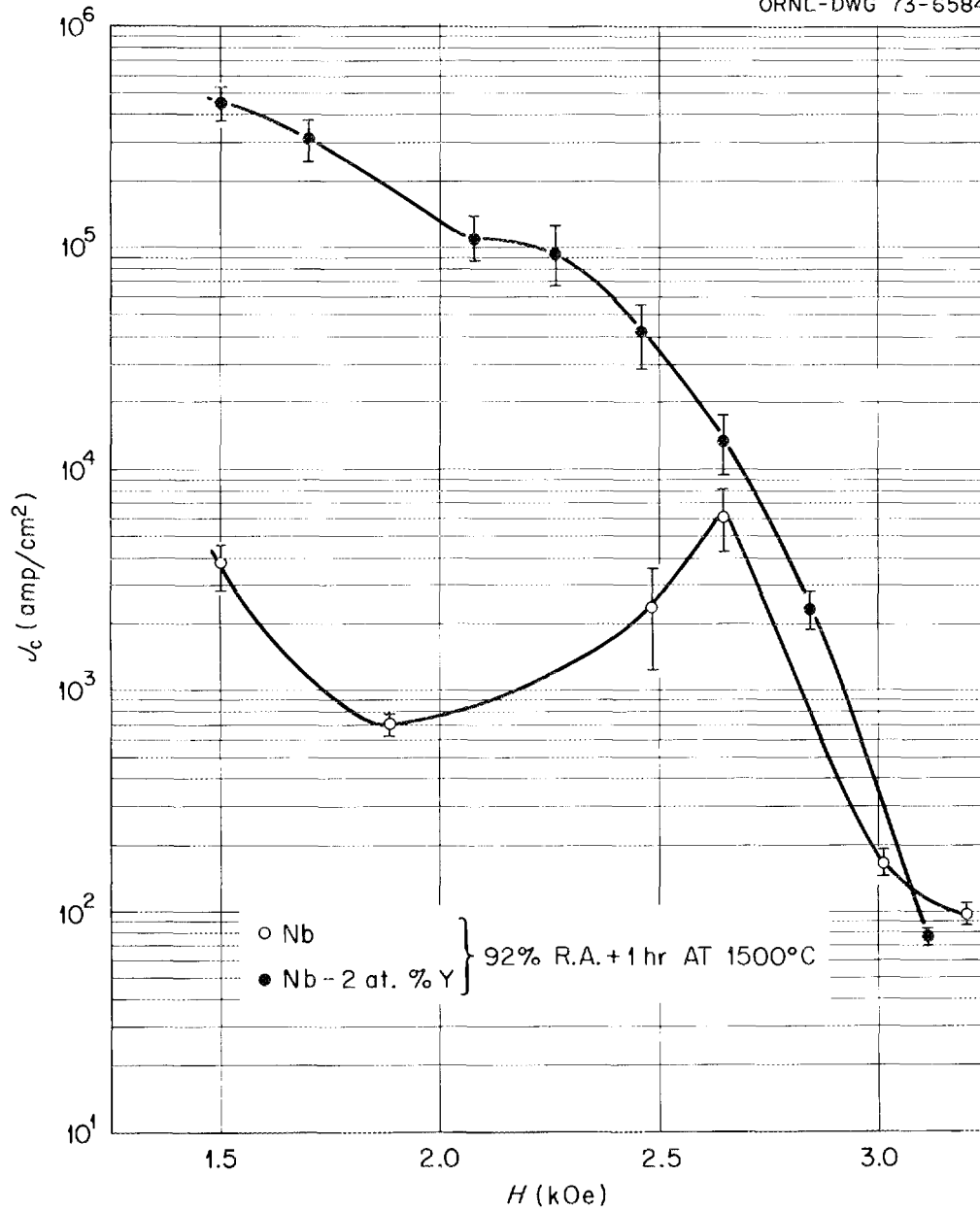


Figure B-5 Critical current density, J_c , vs applied field H for pure Nb and Nb-2.0 at. % Y samples annealed one hour at 1500°C.

consistent with the above differences in B_R values. A peak effect is noted in the pure Nb. As expected from the B_R results, J_c vs H curves for the other Nb-Y alloys were similar to that for Nb-2.0 a/o Y but have not been plotted in Fig. B-5 for clarity. ΔH values for the above samples are plotted vs applied field in Fig. B-6. Here we see the pure Nb has a larger ΔH than the Nb-2.0 a/o Y sample. Again, the other Nb-Y samples had ΔH values which superimpose on those of Nb-2.0 a/o Y within experimental error.

We now have the ability to measure and therefore separate the relative importance of J_c and ΔH on ac losses. We can then compare the ac losses calculated from these measurements by theoretical models with the ac losses we shall measure directly with our wattmeter technique.

3. Construction of ac Loss Measuring Equipment

All of the required equipment for measuring ac losses by the electronic wattmeter technique has now been assembled. This includes: the wattmeter which was obtained from the electronics group at Brookhaven National Laboratory, an ac power supply consisting of a transformer and variac to enable us to apply up to 50 A to our ac magnet, the superconducting solenoid (coil constant = 135 Oe/A) to provide the ac magnetic field, and the support assembly. A photograph of this equipment is given in Fig. B-7. Preliminary calibration checks on the wattmeter have been run, and the ac loss apparatus should soon be operational.

4. Concluding Remarks

At present, the program on superconducting materials for power transmission will not be funded in FY 1974. Should funding become

ORNL-DWG 73-6583

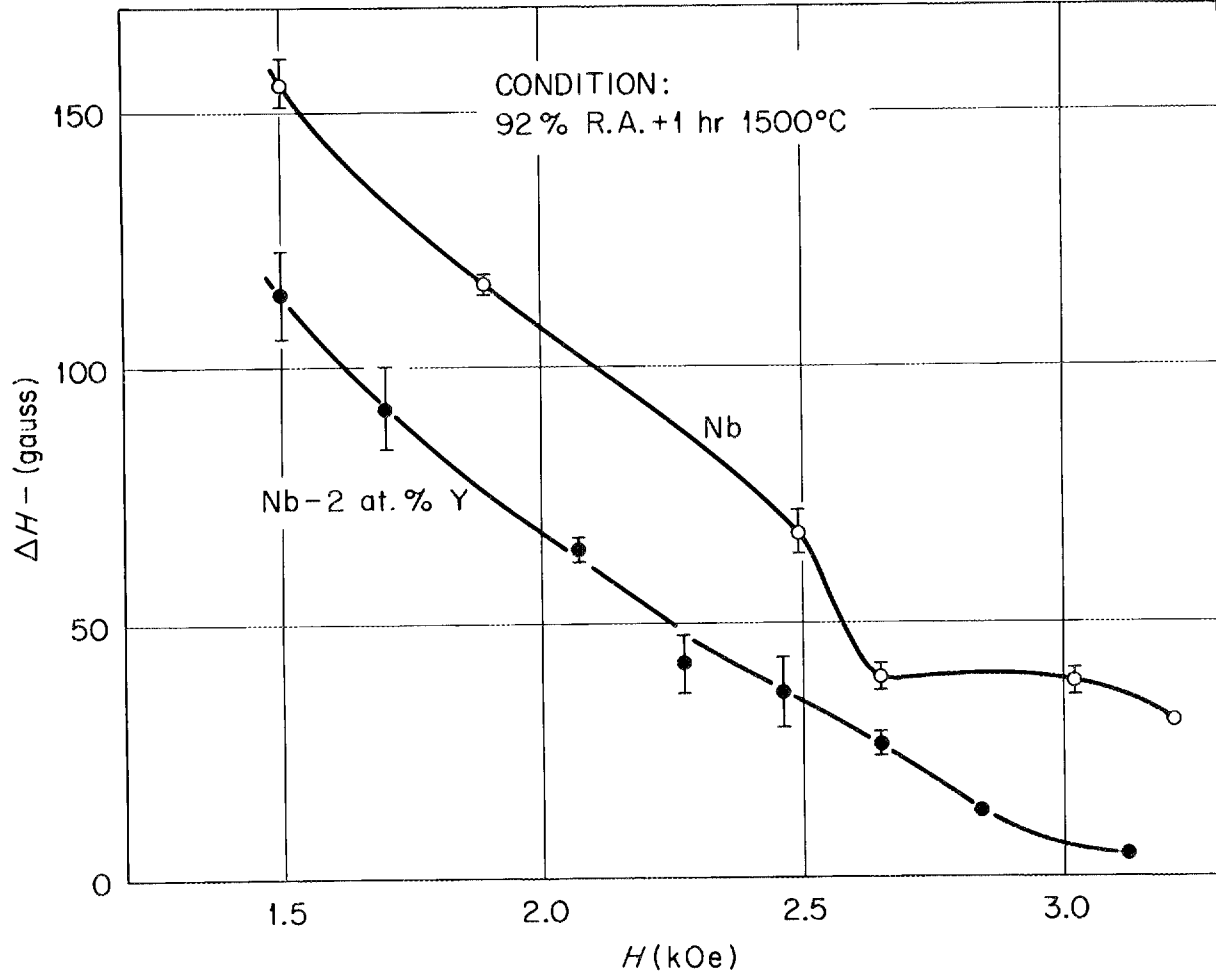


Figure B-6. Surface shielding parameter, ΔH , vs applied field H for pure Nb and Nb-2.0 at. % Y samples annealed one hour at 1500°C.

45

Y-120055



Figure B-7a. Superconducting solenoid and support assembly for ac loss measurement apparatus.

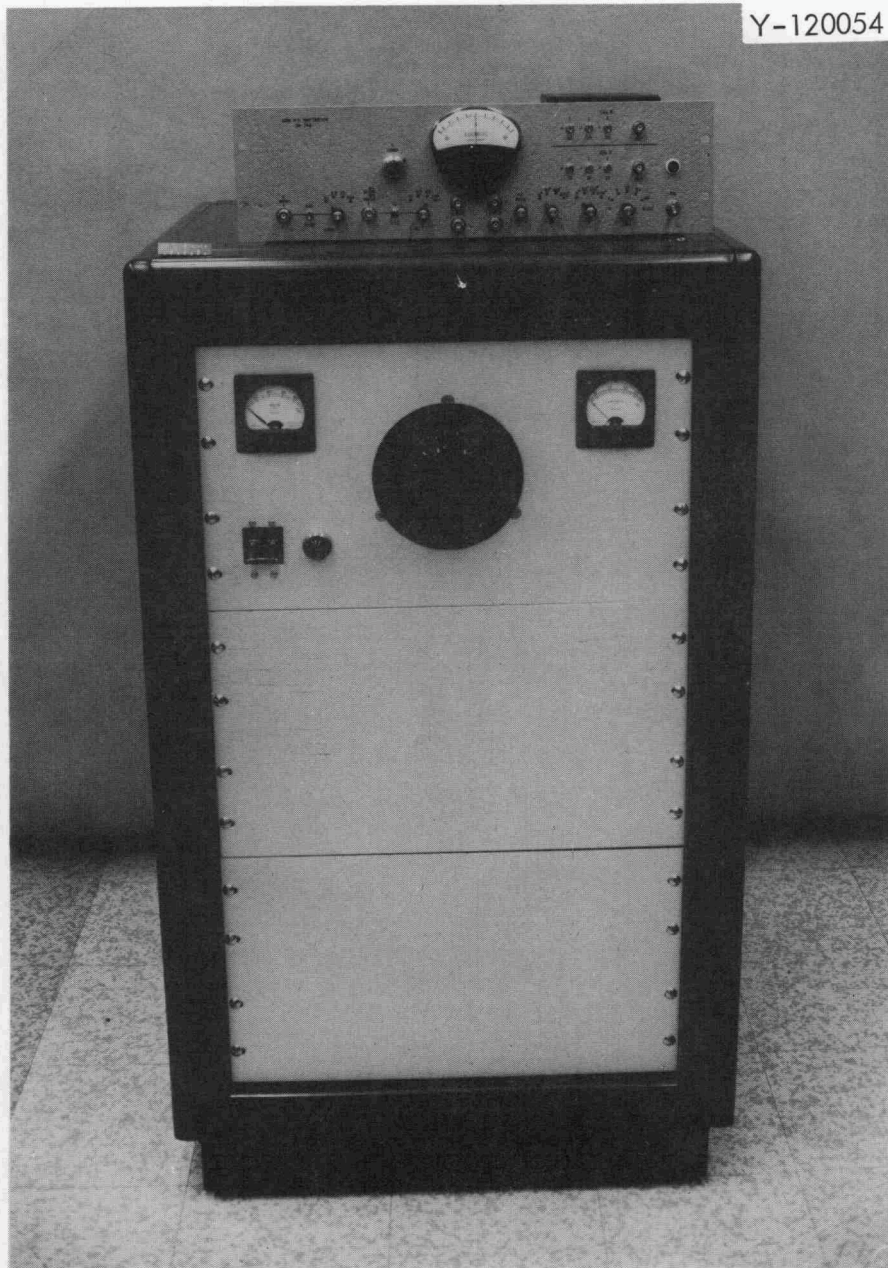


Figure B-7b. Wattmeter and ac magnet power supply for ac loss measurement apparatus.

available we are now in a position to make an important contribution to understanding the relative importance of material variables on ac losses in superconductors at fields above H_{c1} . We will have a rather unique set of experimental tools available for studying bulk flux pinning, surface effects, and their influence on ac losses, particularly at fields above H_{c1} --the field region of interest for high T_c materials. The Nb-Y alloys studied these last 8 months as "model" materials may be practical materials if a conductor based on Nb is desired.

REFERENCES TO SECT. II.B

1. Eg. A. V. Narlikar and D. Dew-Hughes, *Phys. Stat. Sol.* 6, 383 (1964);
J. Mater. Sci. 1, 317 (1966).
2. C. C. Koch and G. R. Love, *J. Appl. Phys.* 40, 3582 (1969).
3. S. L. Wipf, Proc. 1968 Summer Study on Superconducting Devices
and Accelerators, BNL-50155, Brookhaven National Laboratory, 1968,
p. 511.
4. D. M. Kroeger, C. C. Koch, and W. A. Coghlan, *J. Appl. Phys.* 44,
2391 (1973).
5. C. P. Bean, *Rev. Mod. Phys.* 36, 31 (1964).

C. DISPERSION HARDENING OF ALUMINUM

Introduction

Work during this reporting period has been in two areas:

1) characterizing the residual resistivity ratio (RRR) of two batches of Cominco zone-refined aluminum and 2) producing zone leveled alloys of gold in aluminum. The results of the first activity shows very great sensitivity of the RRR to supplier's quality control since two batches supplied to identical specifications have RRR's differing by a factor of three. This work has also suggested a possible maximum in RRR dependent upon annealing conditions. The second activity has resulted in a stock of alloys from which samples can be made to study the precipitation hardening behavior of minute quantities of gold added to very high purity aluminum manipulation of the impurity dispersions by means of heat treatment. The objective to "map out" the yield strength/RRR relationships for various dispersion states in the aluminum gold alloy system will, however, await further funding.

1. Residual Resistivity Ratio of Cominco Zone-Refined Aluminum

Zone-refined aluminum, specified to have a residual resistivity ratio ($RRR = \rho_{300K} / \rho_{4K}$) equal to $13,000 \pm 1000$, was purchased from Cominco Products, Inc., and used to prepare the alloys discussed below in Sect. 2. Our RRR measurements, obtained by means of a four point dc probe technique, on this aluminum, henceforth known as batch II material, are summarized in the following Table. At best the RRR is about 30% lower than that specified by Cominco. The Table also illustrates how sensitive the RRR is to handling and thermal history of the aluminum.

Table. Residual Resistivity Ratio of Batch II Cominco Aluminum

Condition or Heat Treatment			RRR
Temperature (°C)	Time (hr)	Remarks	
610	1	Furnace Cooled	9772 ± 5%
610	72	Furnace Cooled	10,450 ± 5%
525	1	Furnace Cooled	10,300 ± 5%
610	1	Quenched into Ice- Brine Solution	2800 ± 1.5%
		As-Received	6165 ± 3%

All specimens were machined by centerless grinding from the as-received Cominco ingot section.

We had previously (in 1971) made a similar purchase of zone-refined aluminum (RRR = 13,000) from Cominco for another program. Reserve specimens from that lot of aluminum, now identified as batch I stock, were tested and compared with batch II material. The as-received, as-machined sample from batch I had a RRR of 13,400--about twice that of batch II. Furthermore, heat treated specimens from ~~batch~~ I reached a RRR of 30,000--about three times higher than batch II. We conclude that our handling and testing procedures are not the source of the low RRR of batch II material. These results may suggest, however, the need for better quality control on the part of the supplier.

Recently, Carapella, Bess, and Leseur¹ reported that high purity copper exhibited a RRR maximum as a function of increasing annealing temperature. We sought to establish whether similar behavior was followed

in aluminum. Batch I Cominco aluminum was melted, cast, and swaged to 0.1 in. diameter rod. Resistivity specimens were prepared from the swaged rod. One hour anneals were carried out on these specimens in air at temperatures between 400 and 610°C. The results are plotted in the following Figure and do suggest the possibility of a RRR maximum in aluminum. We interpret the increase in RRR in the range 400 to 525°C as due to recrystallization and grain growth, processes which cause the elimination of dislocations (introduced during swaging) and grain boundary area. The cause of the decrease in RRR at higher temperatures is not definitely known yet. An annealing temperature of 525°C appears to produce the highest RRR for swaged, zone-refined aluminum.

2. Alloy Preparation

During this reporting period, three alloys containing nominally 0.2, 0.1, and 0.05 wt % gold in zone-refined aluminum were prepared. Suitable quantities of the 1.1 wt % master alloy made previously,² were mixed with zone-refined Cominco aluminum by induction melting in ultrahigh purity graphite boats under a vacuum of better than 10^{-5} torr. After zone-leveling, the alloys were directionally solidified and diffusion annealed in the solid state at 610°C for two weeks. Two finger-shaped ingots, approximately 5 in. long and 1 in. in diameter, of each composition were produced. These ingots are the starting stock for a study of the dispersion hardening characteristics and electrical resistivity of high purity precipitable aluminum base alloys.

3. Future Activity

Since funding is not available for the coming year, this program will not be active. The alloy stock will, however, be held until such

ORNL-DWG 73-7978

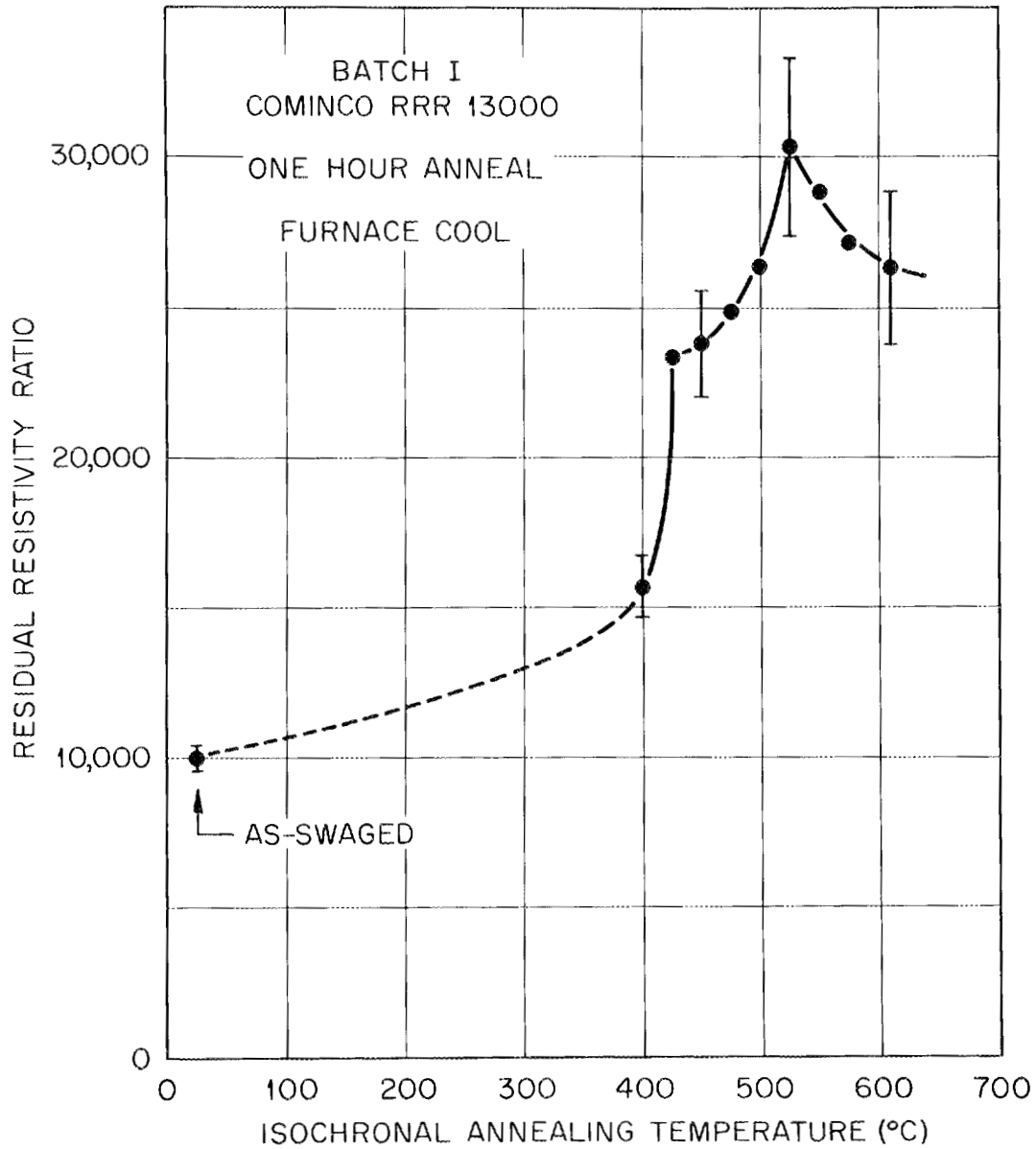


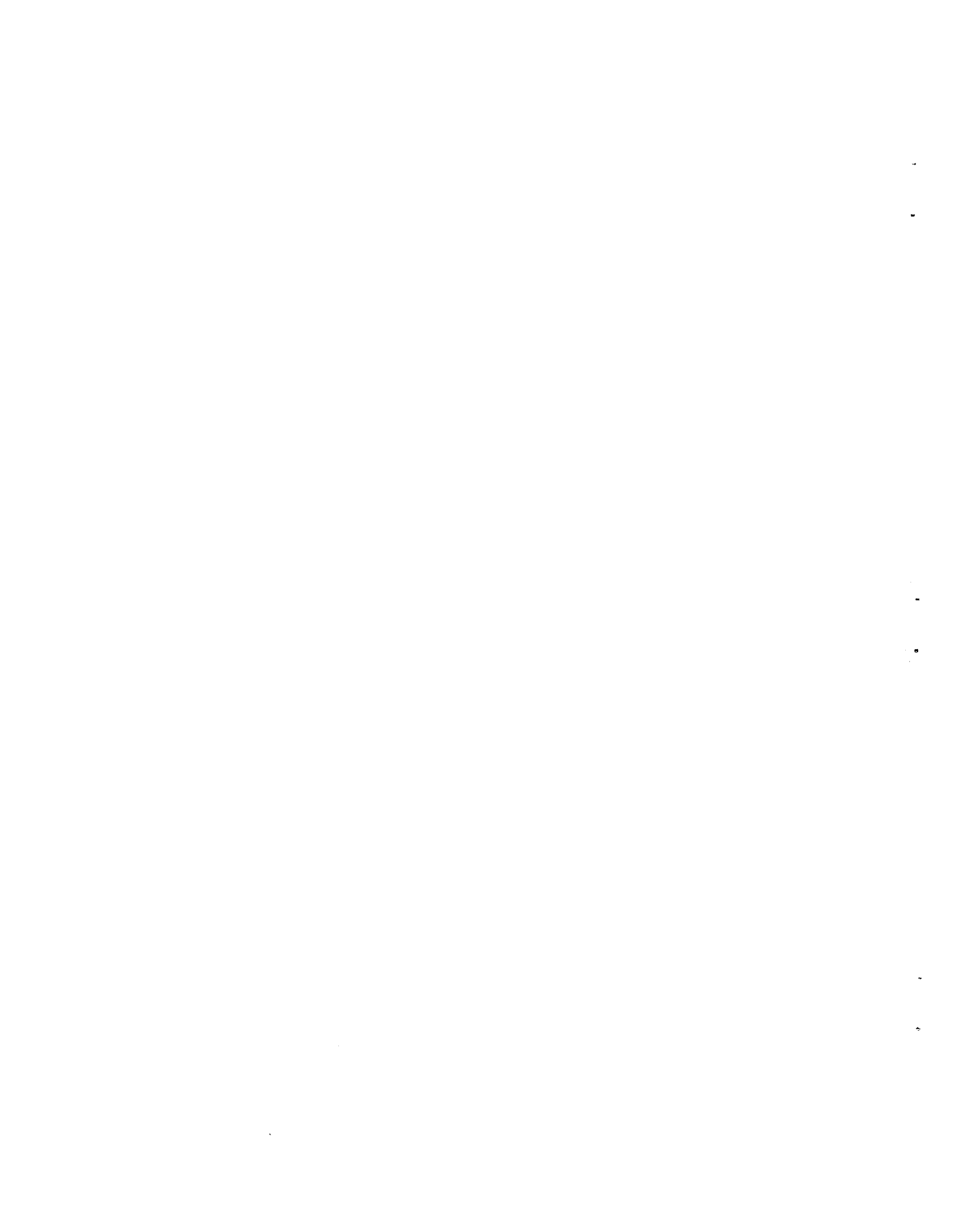
Figure. Residual resistivity ratio vs isochronal annealing temperature for batch I as-swaged Cominco zone-refined aluminum.

time that funds are available to continue toward the goal of discovering methods for improving the mechanical yield strength of very high conductivity aluminum while preserving the high residual resistance ratio needed for its use as a normal metal component in a superconductor composite. Additional tasks of interest which should be explored are the RRR maximum and the quality control needed to ensure reproducible production of very high purity aluminum and the alloys made from it.

REFERENCES TO SECT. II.C

1. S. C. Carapella, Jr., M. L. Bess, and D. R. Leseur, *J. Metals*
(January, 1973) p. 30.
2. Cryogenic Dielectrics and Superconducting and Cryogenic Materials
Technology for Power Transmission, Semiannual Report - March 1, 1973,
ORNL-IM-4187 (May, 1973).

APPENDIX A



TRAVEL REPORT - AUSTRIA AND GERMANY

W. F. Gauster

From February 8 through March 23, 1973, I made a trip to Austria because of my activities as an Honorary Professor of Cryoelectric Power Engineering at the University of Technology in Vienna and as a member of the Austrian Academy of Sciences. I used this opportunity to visit the Universities of Technology in Graz and Munich in order to discuss matters of interest for the Cryogenic Dielectrics and Superconducting and Cryogenic Materials Technology for Power Transmission program of ORNL.

I. GRAZ, UNIVERSITY OF TECHNOLOGY

A. HIGH VOLTAGE INSTITUTE (Versuchs-und Forschungsanstalt für Hochspannungstechnik, Graz, "VAH") (February 20-23, 1973)

I had discussions with Alfred Leschanz, Professor at the University of Technology and Director, VAH, and with two of his co-workers, Gerhard Praxl and Werner Horak. The Austrian Institute of Electrical Engineers (Österreichischer Verband der Elektrotechnik) has a very active section for high voltage engineering which keeps in close contact with similar organizations in the world.¹ There are three large high voltage laboratories in Austria: the VAH,² the Elektrotechnische Versuchsanstalt in Vienna, and the high voltage laboratory of the Elin-Union, Ltd. in Weiz.

In the following, I present a short description of the VAH. Located in the main bay of that laboratory is the high voltage transformer cascade.

It consists of three transformers which can produce either 1.2 MV in single-phase, series connection or 0.4 MV in three-phase connection. The cascade is energized by a three-machine set (one dc motor with a three-phase synchronous generator for 16 2/3 up to 60 Hz and a single-phase synchronous generator for 16 2/3 up to 150 Hz). At 50 Hz, 5-minute operation with 1235 kVA is possible.

The dc high voltage source is a six-step Greinacher-cascade which is operated with 500 Hz and produces 1500 kV, 10 mA dc with a ripple of less than 1% at full load. This voltage source can be used for energizing a single circuit impulse generator. Another 3.25 MV impulse generator is movable and can be used for outdoor tests.

Corona-free connections can be made to a central electrode, to a compensated voltage divider (system Zaengl), to a sphere gap with a sphere diameter of 2 m, and to a vacuum-tight tank with a high voltage bushing for tests in oil, in compressed gases, and in vacuum.

Much care has been taken in screening the high voltage bay. Seventy-five decibels can be reached with frequencies from 0.1 MHz up to the frequencies of television bands. This is achieved by providing a Faraday cage made of welded iron sheets, 1 mm thick. Special contact bands are arranged around the metal gate wings. Below the bottom of the Faraday cage, a network of copper bands (5.5 m mesh width) has been provided. These measures are necessary to protect the outside from electromagnetic disturbances and, vice versa, the inside from outside disturbances which is especially important when pre-breakdown experiments are being made.

In another bay a current impulse facility is located. The total stored energy of four capacitor banks is 100 kJ. With parallel connection

of the four banks, the current impulse is 170 kA, with a crest voltage of 50 kV; with series-parallel connection, 140 kA/100 kV and with series connection, 95 kA/200 kV.

The research and test program of VAM is very comprehensive. Besides the facilities for usual high voltage and high current tests and for various types of pre-breakdown tests, the mentioned special test facility for high voltage tests in oil, compressed gases, and vacuum is available. Especially important for the development of high voltage dc power transmission are test facilities for simulating unusual environmental conditions (temperature, humidity, rain, and various types of contamination). Finally, special movable dc isolation test equipment is available for testing the stator windings of large generators on site. For this purpose, ac tests with 50 to 60 Hz are not convenient because of the very high capacities against ground. Loss angle tests can be made with low frequencies. Other tests can be performed with special corona detectors.

The University of Technology, Graz, has a comprehensive study program for high voltage engineering. A curriculum of three courses is offered:

High Voltage Engineering I: Test and experimental techniques for high voltage ac, dc, impulse voltages and currents, and switching voltages.

High Voltage Engineering II: Demand upon insulating systems in normal operation and under special circumstances; electrostatic and dynamic field calculations; theories of electric strength; and the most important insulating materials and insulating systems.

High Voltage Engineering III: Origin and means of withstanding external and internal over-voltages in electrical energy distribution systems.

Up to the present, detailed lecture notes have been issued only for the first course in high voltage engineering, and I bought one copy of this detailed pamphlet (typewritten, 260 pages).

B. INSTITUTE FOR LOW TEMPERATURE RESEARCH (Anstalt für Tieftemperaturforschung, "ATF")

Furthermore, I visited with my old friend Dr. Peter Klaudy, Professor of Electrical Engineering at the University of Technology, Graz, and Director of the Institute for Low Temperature Research (which is only in loose connection with the University of Technology and is sponsored partly by various governmental agencies and partly by industry). For many years, Klaudy has been working on homopolar machines³ and on superconducting power lines,⁴ and he can rightly be called a "pioneer" in these two fields.

Concerning homopolar machines, a recent invention of Prof. Klaudy is his "liquid metal roll contact" which, in his opinion, will solve the brush problem. Klaudy showed me a working model and explained it to me in great detail. During a visit by Eric Forsyth of Brookhaven National Laboratory (which Klaudy greatly enjoyed), the same model was demonstrated and is mentioned in Forsyth's travel report.⁵ Recently, Klaudy published a detailed paper on this subject.⁶

For superconducting cables, Klaudy employs flexible corrugated metal tubes developed by the German cable company "Kabelmetall, Hannover." He tries to get sufficient means for testing in regular power operation a superconducting single-phase cable for 60 kV, 50 m long (manufactured in cooperation with AEG, Austria; Kabelmetall, Hannover; and Linde, Munich) at the electric power plant in Voitsberg, Styria.⁷

Concerning his idea to use an arrangement with a hard superconductor (preferably Nb_3Sn) as a very fast acting circuit breaker⁸ (switching time a few milliseconds, i.e. almost one order of magnitude smaller than one period of 50 or 60 cycles), Prof. Klaudy thinks that such a switch (which

reacts when a large dI/dt occurs and which does not have to "wait" until a large current is reached) could be successfully operated with cables for large transmission power; however, he feels that such a design would be too expensive.

I was mostly interested in the work of Klaudy's co-worker Jürg Gerhold, who finished his Ph.D. thesis on the dielectric breakdown strength of liquid helium in 1972. I bought a copy of that thesis (329 pages, 91 figures), and when I started to study it carefully, I was impressed by this expertly performed work. This thesis contains many interesting details which are not mentioned in Gerhold's publication in *Cryogenics*.⁹ Furthermore, I noticed that Gerhold's experimental equipment and methods are in many respects similar to those of R. J. Meats of Central Electricity Research Laboratories, Leatherhead, Surrey, England,¹⁰ and it is interesting to compare Gerhold's and Meats' results (see Appendix B).

II. MUNICH, TECHNICAL UNIVERSITY

On March 21-23, 1973, I visited the High Voltage Institute of the Technical University in Munich. Director of this institute is Professor of Electrical Engineering Hans Prinz. His institute is internationally well known and several of his former students and co-workers are holding leading positions in various high voltage institutes.¹¹ Prof. Prinz was chairman of the International Symposium on High Voltage Technology, the Technical University, Munich, March 9-14, 1972. This conference was sponsored by the Verband Deutscher Elektrotechniker ("VDE") with the cooperation of the IEEE Power Engineering Society, and Prof. Prinz was kind enough to present our laboratory a copy of the proceedings.

Prof. Prinz also presented me the yearly reports of his institute for 1970, 1971, and 1972; a description of the high voltage experiments which are part of the curriculum of the Technical University, Munich, in that field (employing prefabricated, standardized modules manufactured by Messwandler-Bau, Bamberg); and a collection of his recent papers¹² which deal in a most interesting way with the history of high voltage engineering, starting with very early experiments with "friction electricity," leading up to the most recent developments (e.g., laser triggered high voltage sparks).

Prof. Prinz introduced me to the Deputy Director of his institute, Dr. J. Wiesinger, who is well known for his extensive investigations on lightning protection. Three of his co-workers presented me copies of their doctors theses and discussed their work with me.

- A. HANS STEINBIGLER: "Anfangsfeldstärken und Ausnützungsfactoren rotationssymmetrischer Elektroden Anordnungen in Luft" ("Onset Field Strength and Efficiency Factors of Rotational Symmetrical Electrode Arrangements in Air")

The efficiency factor η (after Schwaiger¹³) is the reciprocal value of the gradient factor g , as mainly used in the USA literature. It is determined by the electrostatic field configuration without considering space charge. Various mathematical methods for finding field configurations are discussed, and the author claims that the method of image point and line charges is most convenient. He presents an ALGOL program for this method of successive approximations. Numerical results are shown for various electrode arrangements (rod and sphere gaps, conical electrodes and tori). In order to predict the onset field strength of a certain electrode arrangement, it is necessary to introduce a criterion for the

electrical breakdown in air which considers the field configuration in the space between the electrodes. Steinbigler used the Schumann integral condition.¹⁴ An extensive series of carefully performed experiments shows a very good agreement between theory and experiment.

B. PAUL WEISS: "Rotationssymmetrische Zweistoffdielektrika"
("Rotational Symmetrical Two-Dielectrics Systems")

A paper covering the main results of the thesis has been presented at the International Symposium on High Voltage Technology, 1972.¹⁵

The mathematical method used for the determination of the electric field configuration is similar to that employed by Steinbigler and becomes--of course -- more complicated when two-dielectric systems are considered. Various electrode and dielectric arrangements have been investigated and show a good agreement between theory and experiment.

The most interesting result of Weiss' work is the observation and clear description of the "Einbettungs-Effekt" ("Embedding Effect"). When an electrode is embedded in dielectrics and the angle α between the electrode and the dielectric boundary is greater than 90° , the electric field strength at the boundary becomes infinite. In a similar way, when $\alpha < 90^\circ$, the field strength at the boundary is zero and, finally, for an angle $\alpha = 90^\circ$ the field strength at the boundary has a finite value. Various experiments verify clearly the existence of the "embedding effect."^{*}

* Concerning the theses by Steinbigler and by Weiss, Compare Appendix G, Sect. II.

- C. FRIEDRICH HEILBRONNER: "Durchzündverhalten und Spannungsaufbau mehrstufiger Stossgeneratoren" ("Firing Performance and Voltage Shape of Multistage Impulse Generators")

To analyze the firing performance and to find the voltage-time functions of the various stages of large impulse generators is a very difficult task. Until a few years ago, it was believed that a good agreement between theory and experiment could not be expected.¹⁶ However, very recently, sufficient information about the sparking process became available and, presently, a refined image converter technique allows determination of the exact firing moments without disturbing the firing process. Heilbronner succeeded in simplifying the extremely complicated system of equivalent circuits to such an extent that he could write tractable computer programs. He investigated the performance of a five-stage impulse generator for 1 MV and of a 12-stage generator for 3 MV, and it seems to be the first time that a very good agreement between theoretical prediction and experimental verification has been achieved.¹⁷

During my visit, Dr. Heilbronner informed me also about an international cooperation in the field of the physics of spark discharges with very high voltages.¹⁸ At the Les Renardières Laboratory of the Electricité de France, a working group with the following participants has been organized: CEGB (United Kingdom), CESI (Italy), EDF (France), and the Universities of Braunschweig (Germany), Munich (Germany), Padova (Italy), and Stuttgart (Germany). Breakdown phenomena of 5 m and 10 m rod-plane gaps in air with positive switching pulses have been investigated. Voltage, current, and field (at 13 points) at the plane and the current through the rod were measured. Two single converter cameras, one image intensifier camera, two still cameras, and two photomultipliers were simultaneously

employed to measure the light output from the gap. It was possible to determine the leader length and velocity of the discharge, the charge injected into the gap, and the time dependence of the field at the plane.¹⁹

Finally, I discussed with Prof. Prinz various special problems in connection with our working program at ORNL. Prof. Prinz gave me a copy of a paper which deals with a movable SF₆ insulated impulse generator²⁰ and another paper on the subject of high voltage discharges in high vacuum.²¹ Both publications are not easily available here.

I am very grateful to Messrs. Leschanz, Klaudy, and Prinz and their co-workers who did their best to convey to me so much information.

REFERENCES TO APPENDIX A

1. "Der derzeitige Stand der Hochspannungsforschung und Vorschläge für deren künftigen Gestaltung in Österreich," Österr. Verb. f. Elektrotechn., Sektion Hochspannungstechnik, Wien (May, 1972).
2. A. Leschanz and G. Oberdorfer, E.u.M. 85, 527-532 (December, 1968).
3. P. Klaudy, "Einige neuere Untersuchungen an Flüssigkeitskontakten," 2nd International Symposium on Electrical Contact Phenomena, Graz, Austria (May, 1964), followed by other publications.
4. P. Klaudy, "Some Remarks on Cryogenic Cables," Advances in Cryogenic Engineering, Vol. 11 (1965) pp. 684-693, followed by other publications.
5. E. B. Forsyth, Travel Report, September 24 to October 12, 1972, BNL (October 20, 1972).
6. P. Klaudy, "Ein neuer Flüssigkeitsrollkontakt und seine mögliche Verwendung im Hochleistungselektromaschinenbau," E.u.M. 89, No. 11, 439-445 (November, 1972).
7. P. Klaudy, "Über tiefstgekühlte, besonders supraleitende Kabel," E.u.M. 89, No. 3, 93-110 (March, 1972).
8. P. Klaudy "Überlastungsschutz supraleitender Starkstromgeräte," E.u.M. 85, No. 3, 89-98 (March, 1968) and Reference 6.
9. J. Gerhold, "Dielectric Breakdown of Helium at Low Temperatures," Cryogenic 12, 370-376 (October, 1972).
10. R. J. Meats, "Pressurised-Helium Breakdown at Very Low Temperatures," Proc. IEE 119, No. 6, 760-766 (June, 1972).
11. Alfred Fischer, "Hochspannungslaboratorien im In-und Ausland," ETZ-A 90, 656-662 (1969).

12. H. Prinz, Bull. Schweiz. E.V. 61, 8-18 (1970); 62, 97-109 (1971); and 63, 1-13 (1972).
13. A. Schwaiger, Elektrische Festigkeitslehre, Springer, Berlin, 1925.
14. W. O. Schumann, Elektrische Durchbruchsfeldstärke von Gasen, Springer, Berlin, 1923, p. 171.
15. P. Weiss, Proceedings International Symposium on High Voltage Technology, Technical University, Munich (March 9-14, 1972) pp. 73-80.
16. IEC Tech. Comm. No. 42, Proposed Amendments to Publication 60 (1962): High Voltage Test Techniques. Test Procedures. 42WG2 (Secr.) 69:5 (May, 1969) p. 11.
17. F. W. Heilbronner, Paper 71 TP 121-PWR, IEEE Winter Power Meeting, New York (January 31 - February 5, 1971) and ETZ-A 92, 372-376 (1971).
18. H. Heilbronner, ETZ-A 92, 603 (1971).
19. CIGRE, 1972 Session (August 28 - September 6), Paper 33-15 [Electra, No. 23 (July, 1972)].
20. K. Brändlin, K. Feser, and H. Sutter, Bull. Schweiz. E.V. 64, No. 3, 113-119 (February, 1973).
21. Ewald Bauer, Techn. Mitt. AEG-TELEFUNKEN 62, No. 7, 323-327 (1972).

.

.

.

.

.

.

APPENDIX B



A NOTE ON J. GERHOLD'S AND ON R. J. MEATS' INVESTIGATIONS
OF THE DIELECTRIC BREAKDOWN OF HELIUM
AT VERY LOW TEMPERATURES

W. F. Gauster

At the ERC Conference on Dielectric Properties at Cryogenic Temperatures (April 13, 1973), I presented a report on J. Gerhold's^{1,2} and on R. J. Meats'³ recent investigations on the dielectric breakdown of helium at very low temperatures. Due to the limitation of the available time, the report was very short, and it was not possible to compare in detail the goals, the methods, and the results of these investigations. Also, this appendix does by no means try to present a systematic and thorough study, but I will mention in a somewhat more comprehensive way a few highlights of Gerhold's and Meats' investigations, and I will point out several details which seem to be of special interest for further investigations with similar goals. J. Gerhold ("G") and also R. J. Meats ("M") mention the ranges of their investigations by indicating limits for the pressure p and the temperature T . This is shown in Fig. 1. Both authors cover practically important ranges for gaseous and liquid low temperature helium, however, G extends the range with respect to T , whereas M's investigations include a higher pressure range.

Table 1 compares the G and M experimental programs with respect to a few important points. G uses one metal cryostat with 5 in. working diameter; M uses for lower pressures a 10 in., for higher pressures a 5 1/2 in. dewar. G designed an electrode control mechanism for adjusting the upper high voltage electrode to the desired gap distance d without

TABLE 1

	Gerhold	Meats
Voltage (kV) \leq	40 dc and ac	65 dc
Electrode Shapes	Spherical (VDE, r = 2.5 cm) Point-plane Cylinder-plane	Rogowski (d = 6 cm) ---- ----
Electrode Surfaces	Technically clean Rough Oxide layer	Technically clean ---- ----
Electrode Material	Nb Stainless steel Cu leaded and unleaded	Nb Brass ----
Helium	Technically clean Contaminated	Technically clean ----

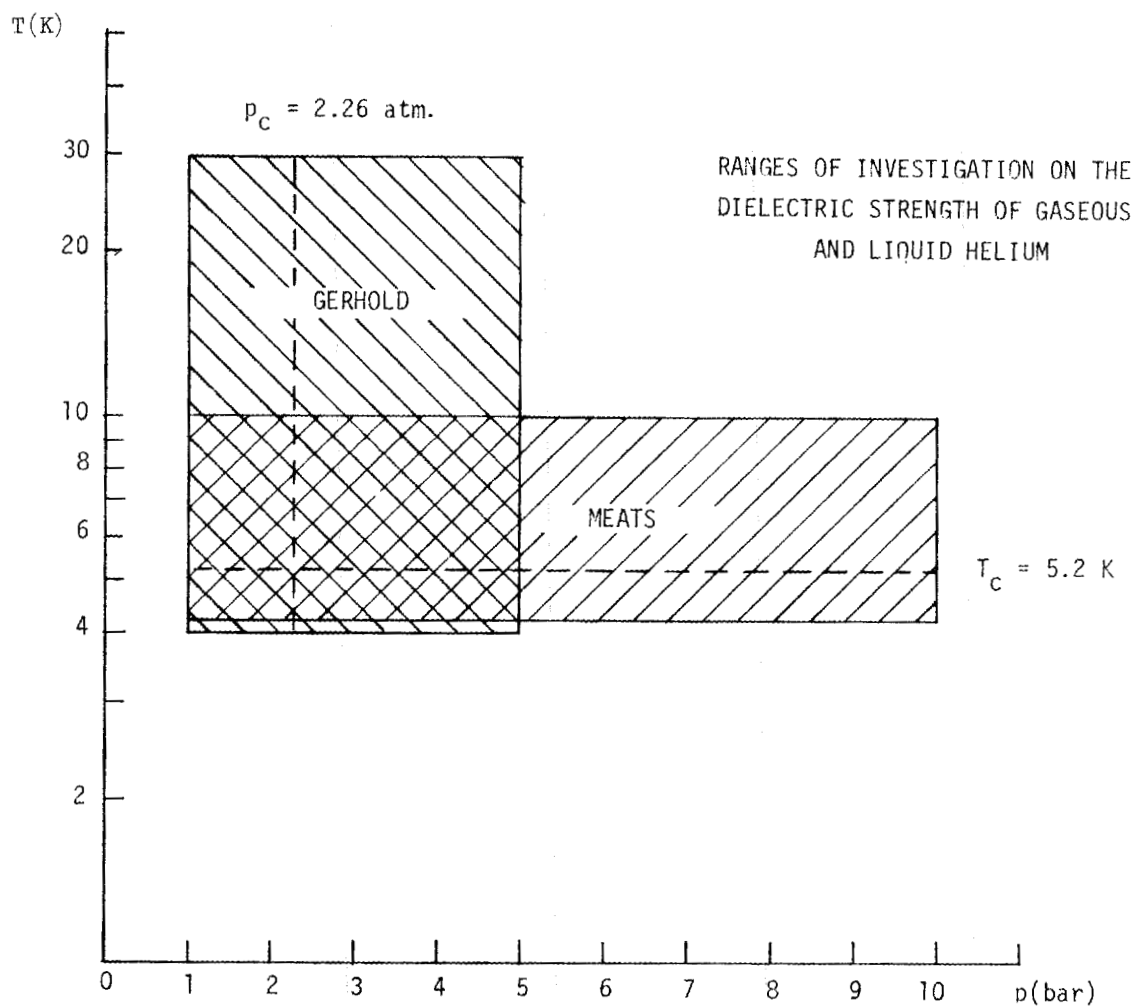


Figure 1. Ranges of investigations on the dielectric strength of gaseous and liquid helium.

the necessity of removing the electrodes from the interior of the cryostat. G claims that d could be measured with an accuracy of 0.01 mm. In M's dewars, the electrodes were supported in Perspex mountings with brass tie-rods without a mechanism for changing the electrode distance from outside the dewar. The change of a fixed gap distance during cooling from room temperature to 4.2 K was about 0.5% and was supposed to be less than the estimated maximum error of 1% in setting the gap (which were subsequently checked optically in a glass-wall cryostat).

Both, G and M, applied the test voltage at a rate of rise of a few 100 v/sec, which seems not to be critical. Furthermore, both authors used series resistances at the high voltage side. M employed a 10 M Ω current limiting resistor; G compared tests with 4 M Ω and with 50 k Ω series resistances and found after breakdowns minor differences in the electrode pittings.

M's 10 in. dewar designed for lower pressure was used for measuring the breakdown strength of cold gaseous helium with the electrodes arranged just above the liquid helium level. In order to achieve uniform temperature distribution, the electrodes were surrounded by a copper-mesh cylinder. A copper leg attached to the mesh made contact with the liquid helium. The temperature was measured with calibrated carbon-resistance thermometers. With this arrangement, the temperature of the gas between the electrodes was easily brought to the desired value by pumping, and during a series of measurements the typical change of temperature was only about 15 mK.

M's other cryostat contained a stainless steel pressure vessel of 14 cm internal diameter which was in contact with the helium of the cryostat by means of a copper leg. Furthermore, a tube was leading

from the pressure vessel to a high pressure helium gas system. In order to achieve uniform temperature distribution around the electrodes, the inner wall of the pressure vessel was lined with a copper sleeve around the Rogowski electrodes.

G used a special continuous flow cryostat⁴ (built by Leybold-Heraeus) with a spiral soldered copper pipe surrounding the electrode arrangement. With this design, the temperature could be kept constant with a tolerance of less than $\pm 1\%$ at any value between 4 and 30 K. The helium temperature was measured by calibrated carbon resistors and (for temperatures above 7 K) with calibrated platinum wire thermometers.

Carefully made electric breakdown experiments with gaseous low temperature helium by both experimenters show very little scattering and are well reproducible. M gives a very clear description of the breakdown phenomena in cold helium gas. The results obtained with gaps of 0.5, 1.0, and 2.5 mm and temperatures of 5.2, 5.8, 6.0, and 7.1 K are illustrated by Fig. 5 of Ref. 3. M distinguishes three distinct modes of electric breakdown:

1. with helium densities up to about 15 kg/m^3 , Paschen's law is obeyed and Townsend mechanisms is obviously decisive;
2. between 15 and about 60 kg/m^3 , deviation from Paschen's law and behavior similar to that of other compressed gases can be observed;
3. for densities above the critical density of 67 kg/m^3 , the increase of the dielectric strength is unexpectedly strong with an even more rapid rise for densities beyond 100 kg/m^3 .

Figure 6 of Ref. 3 represents a Paschen plot for gap widths of 0.5, 1.0, 1.5, 2.5, and 3 mm. In this way, M shows very nicely that with increasing gap widths the deviations from the common Paschen curve occur

at higher breakdown voltages (i.e., corresponding to larger values of the product of density and gap width). G's results with cold gaseous helium are similar to that of M.

M and also G emphasize that the breakdown phenomena in boiling (i.e., saturated) liquid helium are similar to those in the corresponding gas states (since the breakdown of gas bubbles is dominant). M points out that the frequently used expression for saturated liquid helium $V_s = k d^n$ with $0.9 \leq n \leq 1.0$ seems to have no theoretical backing. Of practical importance is that the value of $n = 0.5$ which has been derived from Fallou et al.⁵ experiments with $d = 10$ mm ("square law") is not in agreement with these and other experiments.

Furthermore, M investigated carefully the high density liquid helium breakdown with 50 mm diameter Rogowski electrodes (made of brass), with $d = 1$ mm and temperatures of 4.3, 4.5, 4.6, 4.73, and 5.02 K (see Ref. 3, Fig. 9). Based partly on Krasucki's⁶ reasonings, M develops a diagram presenting the breakdown voltage as a function of the square root of the "total bubble pressure." He obtains in very good agreement with his experimental data two straight line segments, one for the regime below, the other above the critical pressure p_c , the slope of the first segment being twice that of the second segment. G too is interested in the physics of the breakdown phenomena of non-saturated liquid helium, and he devotes a detailed section of his paper to a newly developed breakdown hypothesis.⁷

In his thesis,¹ G discusses in detail the statistical evaluation of his experiments. Like several other observers, he found skewed distributions and used for plotting the assumptions of gaussian distribution of

the logarithm of the breakdown voltage values. Figure 2 (identical to Fig. 55 of Ref. 1) shows an example for breakdown in non-boiling helium at 4.2 K and 1 atm, with technically clean stainless steel spherical electrodes with gap widths of 0.1, 0.2, 0.5 mm. Besides the mean value, the upper and lower field strength values for cumulative frequencies of 95 and 5%, respectively, can be easily determined. The resulting curves are shown in Ref. 2, Fig. 4. This kind of statistical evaluation can be simplified by using tables for plotting the cumulative probability values for gaussian distributions⁸ (see Table 2 of this appendix for the evaluation of up to 15 test values).

Of appreciable practical interest are G's observations on the influence of the material and the condition of the surface of the electrodes. In addition to results reported in Ref. 2, G's dissertation (Ref. 1) contains several interesting observations of that kind, and I would like to show in the following a few highlights. The first example concerns the difference of the electrical breakdown performance of the "technically clean" and of very carefully polished electrodes. The previously mentioned Fig. 4 of Ref. 2 applies to technically clean stainless steel surfaces. Figure 3 of this appendix (Fig. 61 of Ref. 1) represents the breakdown field strength as a function of the gap width for carefully polished stainless steel electrodes. The latter values are much smaller, for instance the 5% probability value is around one-third(!) of the corresponding value obtained with technically clean surfaces. Furthermore, the statistical scattering is appreciably reduced.

Another example is G's observations with copper electrodes. He compares technically clean surfaces with surfaces with oxide layers

TABLE 2

k	N														
	1	2	3	4	5	6	7	8	9	10	11	12	13	14	15
1	50.0	28.6	19.9	15.2	12.3	10.2	8.85	7.78	6.81	6.18	5.59	5.15	4.75	4.46	4.09
2		71.4	50.0	38.2	30.8	26.1	22.4	19.8	17.6	15.9	14.5	13.1	12.3	11.3	10.6
3			80.1	61.8	50.0	42.1	36.3	31.9	28.4	25.5	23.3	21.5	19.8	18.4	17.1
4				84.9	69.2	57.9	50.0	44.0	39.4	35.2	32.3	29.5	27.4	25.5	23.9
5					87.7	73.9	63.7	56.0	50.0	45.2	41.3	37.8	34.8	32.3	30.2
6						89.8	77.6	68.1	60.6	54.8	50.0	46.0	42.5	39.4	36.7
7							91.15	80.2	71.6	64.8	58.7	54.0	50.0	46.4	43.3
8								92.22	82.4	74.5	67.7	62.2	57.5	53.6	50.0
9									93.19	84.1	76.7	70.5	65.2	60.6	56.7
10										93.82	85.5	78.5	72.6	67.7	63.3
11											94.41	86.9	80.2	74.5	69.8
12												94.85	87.7	81.6	76.1
13													95.25	88.7	82.9
14														95.54	89.4
15															95.91

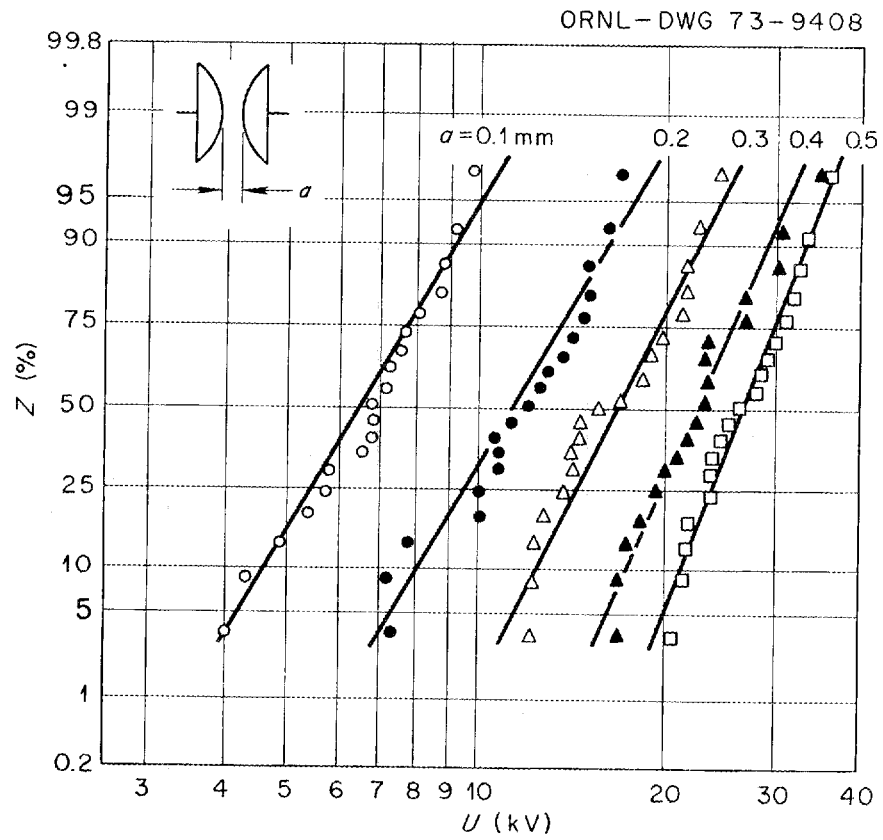


Figure 2. Breakdown voltages in liquid helium at 4.2 K and 1 atm with technically clean stainless steel electrodes.

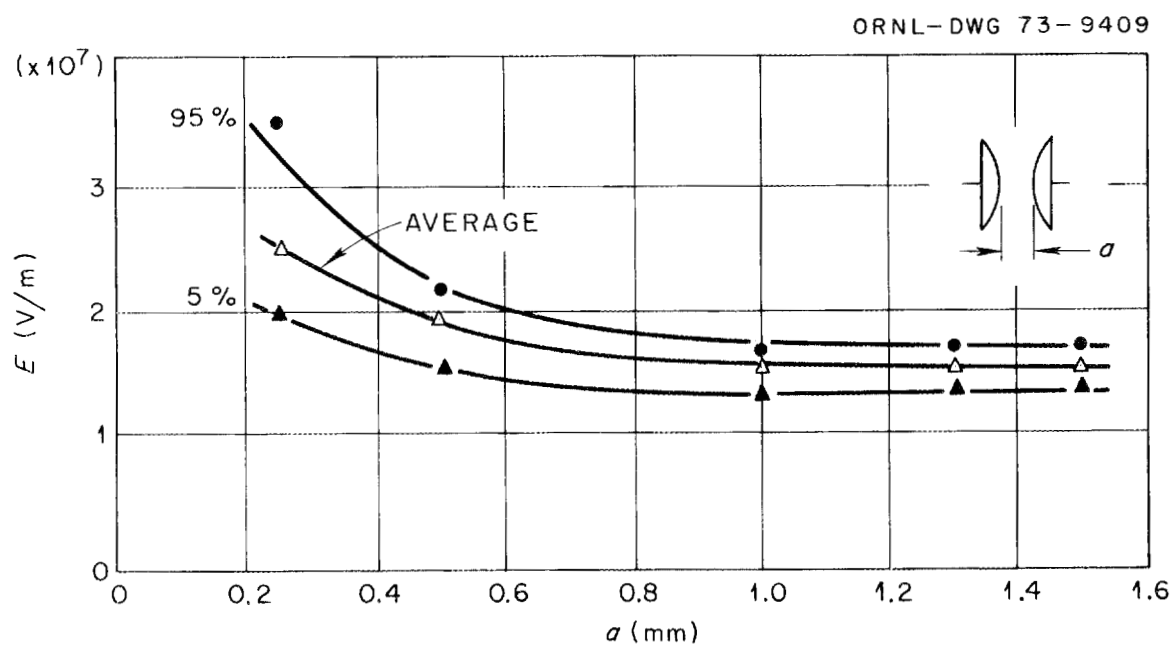


Figure 3. Breakdown voltages in liquid helium at 4.2 K and 1 atm with polished stainless steel electrodes.

produced by exposing the electrodes for a few days to humid air. Figures 4 and 5 of this appendix (corresponding to Figs. 65 and 66 of Ref. 1) are self-explanatory.

Furthermore, G investigated the influence of various types of contaminations of the liquid helium. He found contamination by frozen oil vapor (e.g., due to diffusion from vacuum pumps or oil-sealed gasometers) especially dangerous. It is interesting to observe the change in the scattering patterns (Fig. 6 of this appendix, corresponding to Fig. 75 of Ref. 1). In contrast to uncontaminated helium, the cumulative probability plot of the individual test points shows clearly "jumps" between the observed breakdown voltages.

In conclusion, it can be stated that Gerhold's and Meats' publications are valuable contributions to the experimental work on the dielectric breakdown of helium at very low temperatures. They are expertly and carefully performed, and several results are of general importance. However, the range of test voltages and, therefore, that of the gap distances is relatively small. Meats restricts himself to dc tests; Gerhold presents, besides dc measurements, only a few results obtained with ac. Neither of the two authors published observations with impulse voltage. These few remarks might be sufficient to show that it is very desirable to extend the work of Gerhold and of Meats to more extended regimes and to various other experimental conditions of practical importance.

The author acknowledges valuable discussions with H. M. Long.

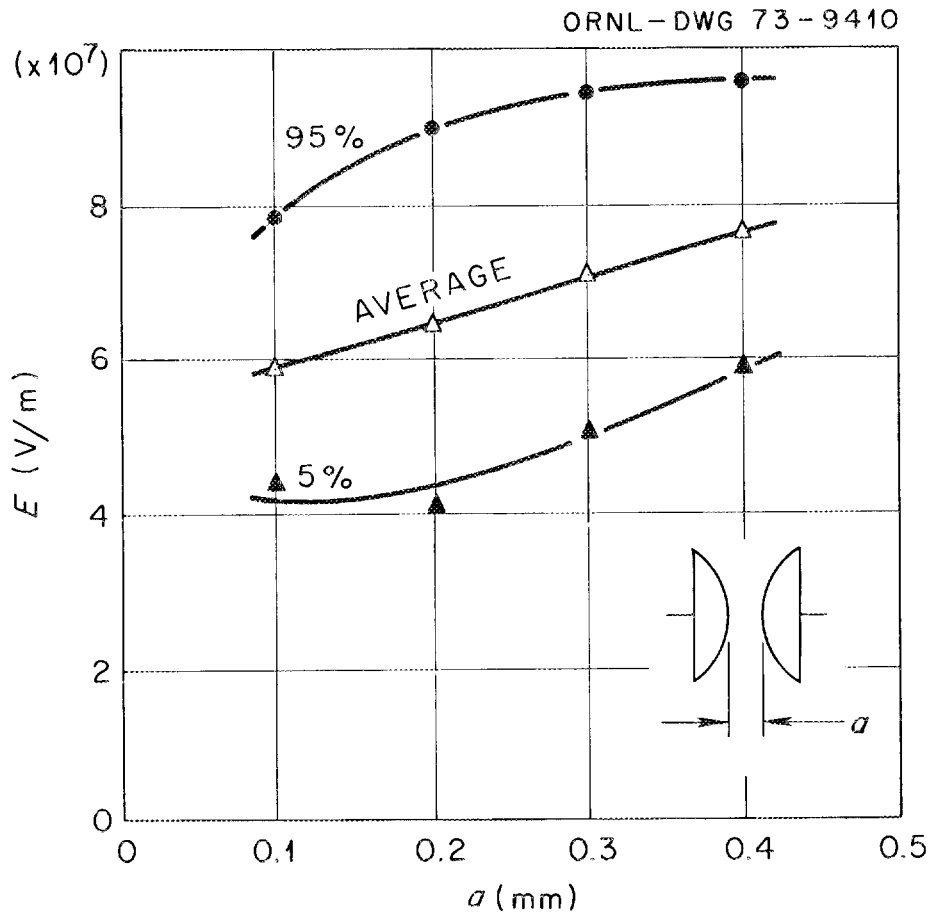


Figure 4 Breakdown voltages in liquid helium at 4.2 K and 1 atm with technically clean copper electrodes.

ORNL-DWG 73-9411

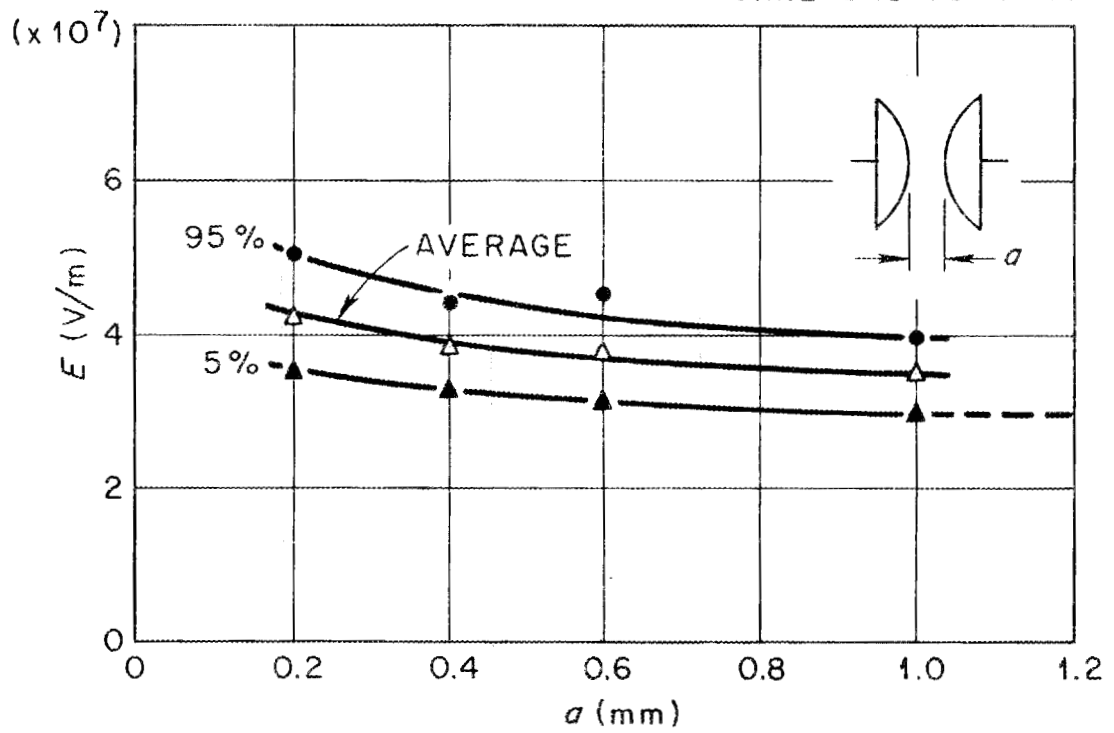


Figure 5. Breakdown voltages in liquid helium at 4.2 K and 1 atm with oxidized copper electrodes.

ORNL-DWG 73-9412

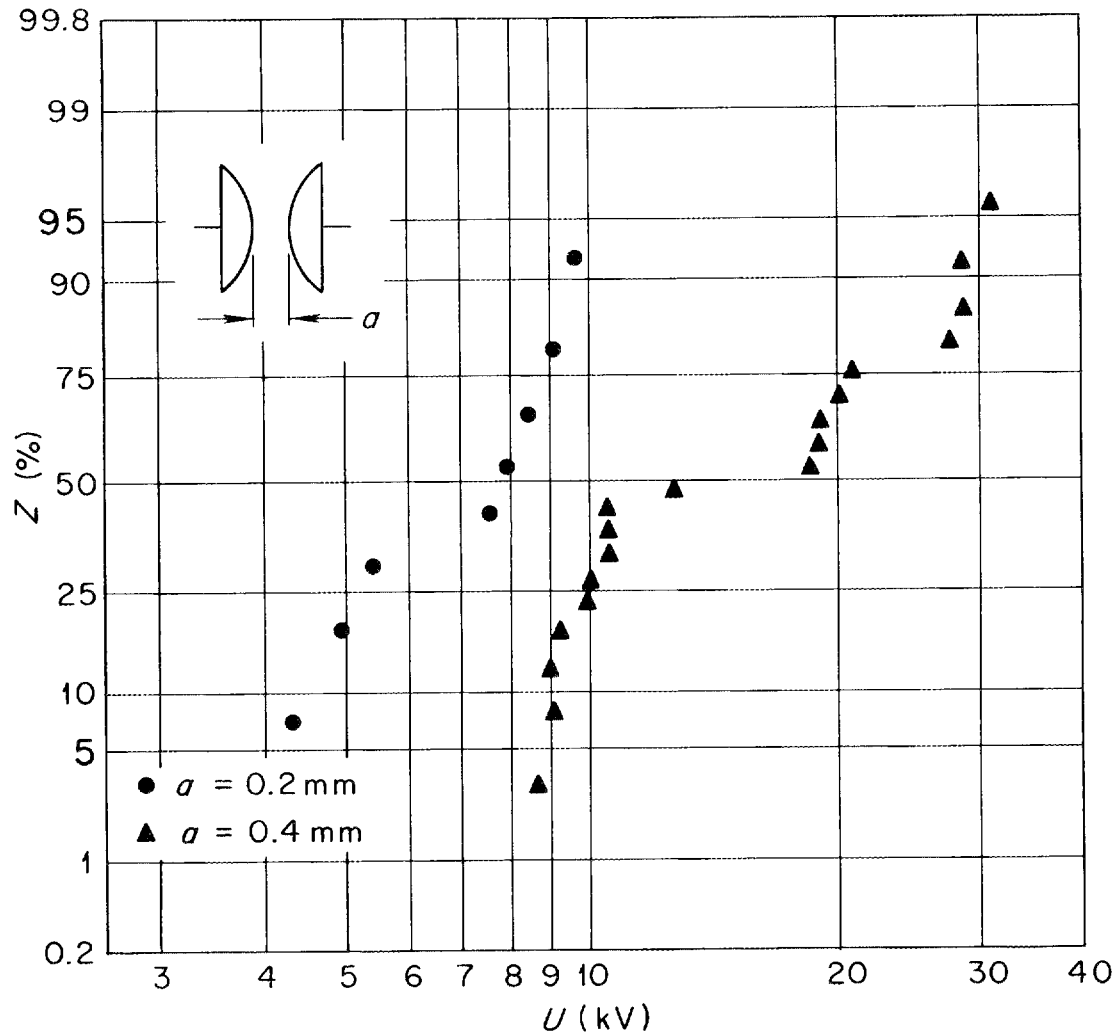
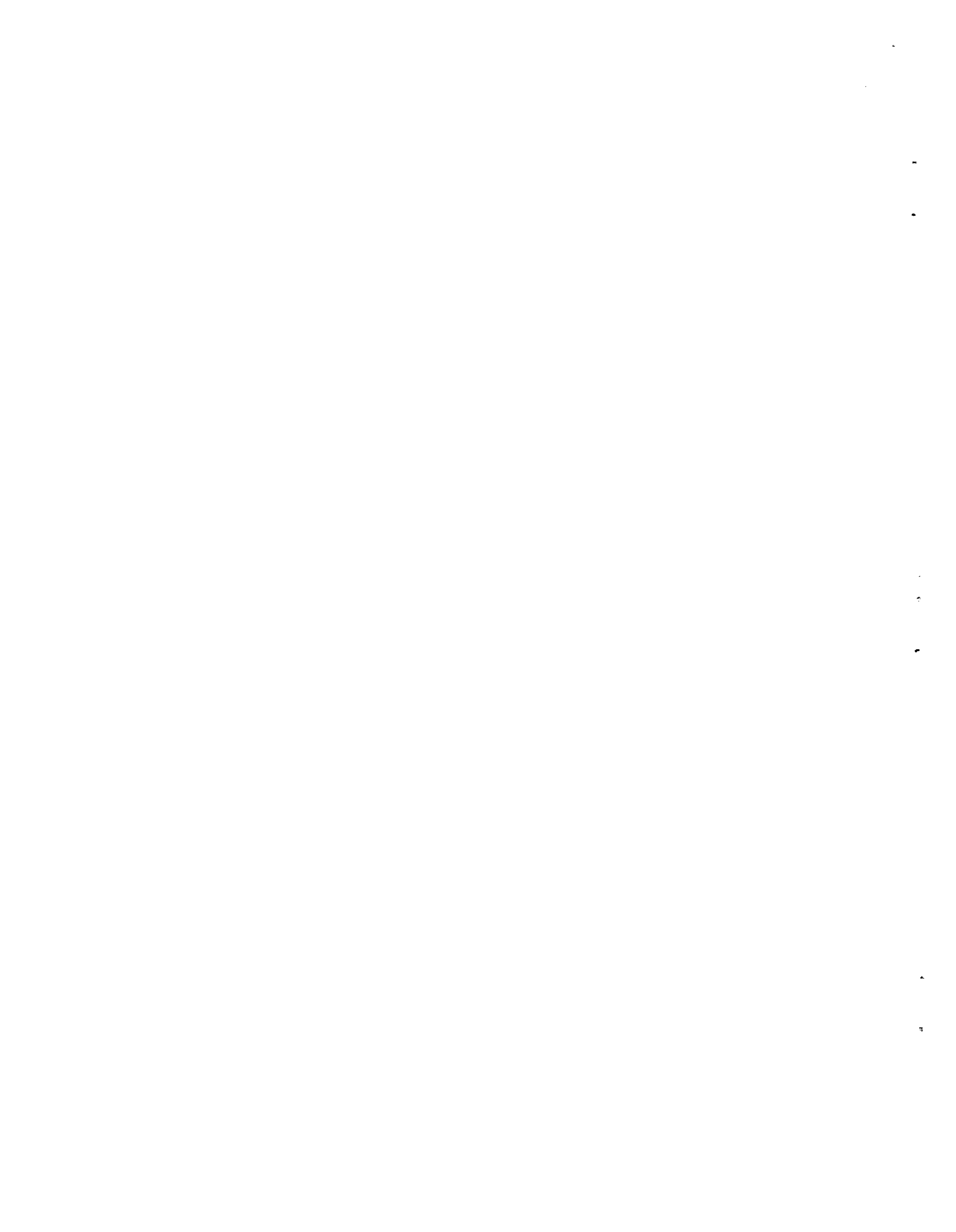


Figure 6. Breakdown voltages in liquid helium at 4.2 K and 1 atm with technically clean stainless steel electrodes. Helium with oil contamination.

REFERENCES TO APPENDIX B

1. J. Gerhold, "Durchschalgsfestigkeit von Helium bei tiefen Temperaturen," dissertation for Doktorat der Technischen Wissenschaften, University of Technology, Graz, Austria, 1972 (329 pages and 92 figures).
2. J. Gerhold, "Dielectric Breakdown at Low Temperatures," *Cryogenics* 12, 370-376 (October, 1972).
3. R. J. Meats, "Pressurised-Helium Breakdown at Very Low Temperatures," *Proc. IEE* 119, 760-766 (June, 1972).
4. G. Klipping, D. Vetterkind, and G. Waltentowitz, *Cryogenics* 5, 76 (1965); and G. Klipping, *Kältechnik* 13 (1961).
5. B. Fallou, J. Galand, J. Bobo, and A. Dubois, IIR, *Comm. Bull. IIF*, Conference on Low Temperature and Electric Power, London (1969) pp. 201-208.
6. Z. Krasucki, *Proc. Roy. Soc.* 294A, 393-404 (1966).
7. Ref. 2, pp. 374-375.
8. H. J. Henning and R. Wartmann, *Mitt. bl. f. Math. Stat.* 9 (1951).



APPENDIX C



REPORT ON BIDDLE TECHNICAL SCHOOL PARTIAL DISCHARGE DETECTION COURSE

S. W. Schwenterly

During the week of March 19-23, I attended a course at James G. Biddle Company in Plymouth Meeting, Pennsylvania, on the theory and practice of partial discharge measurement. Biddle designs and manufactures a large line of high voltage test equipment, and its technical staff contains individuals who are qualified in all areas of high voltage measurement. The main lecturer was E. B. Curdts, retired Director of Engineering of the company and Head of the Biddle Technical School. Most of the 16 participants in the course represented various electrical equipment manufacturing companies and were interested in routine partial discharge tests of insulation in production items such as cables, connectors, and transformers. An extra benefit of the course was the opportunity for discussions with these individuals.

The course consisted of four all-day and one half-day lecture sessions, with the final afternoon being left free for participants to gain experience in operating the equipment themselves. Topics covered included mechanisms of partial discharge, techniques of partial discharge measurement, factors governing system sensitivity and system calibration, methods of overcoming external electrical interference, identification of characteristic partial discharge signals, and design considerations in controlling partial discharge. After returning, I presented a seminar on this material for the Cryoelectric Group.

A major motivation for taking this course was to consider the various methods of partial discharge detection in order to choose the proper

instrumentation for our program. As a result of these considerations, we have chosen a balanced partial discharge detector manufactured by Biddle. A photograph of the front panel of this instrument is shown on the following page. The wiring diagram printed on the panel shows that it is basically a high voltage capacitance bridge. When the two arms are properly balanced, partial discharge pulses occurring in either specimen are amplified by the detector and displayed on the external oscilloscope and panel meter. However, external electrical interference or partial discharges affect both arms equally and are rejected. This system was chosen because of the following advantages:

1. It has the highest sensitivity of any commercially available partial discharge detector. The minimum detectable discharge is less than 0.03 pC for sample capacitances below 10^{-3} pF.
2. It inherently rejects external noise. Rejection ratios of 10,000 to 1 are possible with small samples.
3. Expensive corona-free high voltage coupling capacitors are not required.
4. Measurements at test voltage frequencies different from normal power frequency may be made.

The following disadvantages exist:

1. Specimens which must be grounded on one side cannot be tested in the balanced mode.
2. Two matched specimens are required.

If grounded specimens must be tested, a coupling capacitor must be obtained, and the system is operated as a standard "straight" partial discharge detector by grounding one leg of the bridge. Since this results in a drop in sensitivity and the loss of external noise rejection, we shall

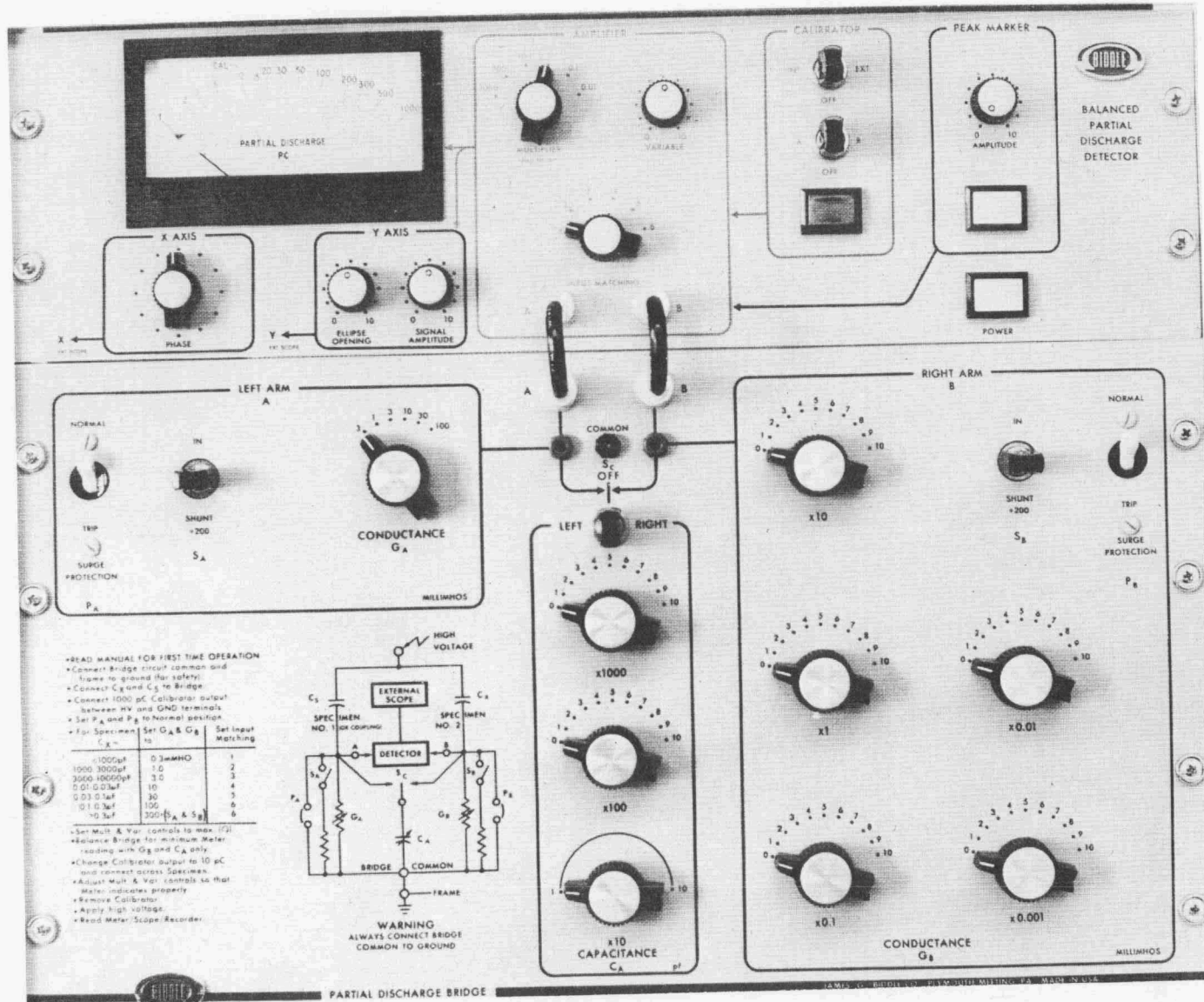


Figure. J. G. Biddle Company partial discharge detector.

try to avoid grounded specimens. We expect to deal with Item 2 by the use of a split ground electrode as previously discussed.

An order has been placed for this equipment, and delivery is expected in early August.

APPENDIX D



OPERATION OF AC SERIES RESONANT TEST SETS

W. F. Gauster

The information we received from Hipotronics included two drawings, "Simplified Schematics for 7350/700/525/105 SR," (reproduced as Figs. 3 and 5 of this appendix), without any explanation concerning the operation of this test equipment. In the following, I will discuss the basic principles.

1. Figure 1 shows a series resonant circuit driven by the excitation voltage V_e . With the usual designations,

$$\hat{I} = \frac{\hat{V}_e}{R + j \left(\omega L - \frac{1}{\omega C} \right)}. \quad (1)$$

The resonance condition is

$$\omega L = \frac{1}{\omega C} \quad (2)$$

and, therefore,

$$I_{\max} = \frac{V_e}{R}. \quad (3)$$

The "output voltage" is

$$\hat{V} = \hat{I} \left(-\frac{j}{\omega C} \right). \quad (4)$$

It assumes, in the case of resonance, the value

$$V_{\max} = \frac{I_{\max}}{\omega C} = \frac{V_e}{R \omega C} = V_e \frac{\omega L}{R}. \quad (5)$$

ORNL-DWG 73-9413

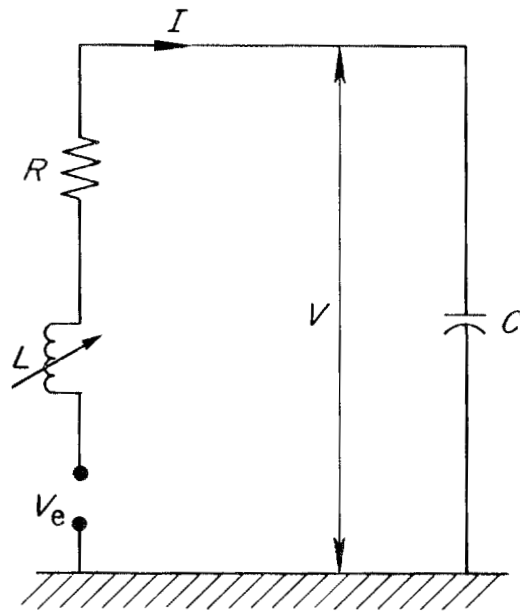


Figure 1. Series resonant circuit with variable inductor.

With the usual designation

$$\frac{\omega L}{R} = Q, \quad (6)$$

the relation

$$V_{\max} = QV_e \quad (7)$$

is obtained.

2. Hipotronics indicates that one ac series resonant test unit can be tuned in the range

$$0.0006 \mu\text{F} \leq C \leq 0.0114 \mu\text{F}. \quad (8)$$

From Eq. (2) follows for the inductance at resonance (with $\omega = 2\pi f = 120\pi = 377$)

$$11,700 \text{ H} \geq L \geq 615 \text{ H}. \quad (9)$$

The values are extremely high and, therefore, it is not possible to use a test arrangement as shown in Fig. 1. It is necessary to arrange the variable inductor on the low voltage side of a transformer which is shown in Fig. 2.

3. The turn ratio of the transformer is $n:1$. Since we assume an ideal transformer (for designations see Fig. 2),

$$V_s = \frac{1}{n} V_p \quad \text{and} \quad I_s = n I_p. \quad (10)$$

For the secondary circuit, the relation

$$\hat{V}_s = (R_s + j\omega L_s) \hat{I}_s \quad (11)$$

is valid.

ORNL-DWG 73-9414

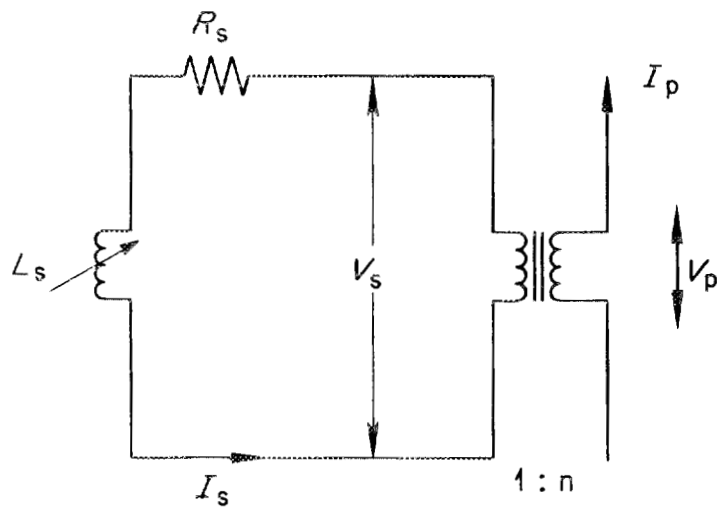


Figure 2. Transformer coupled variable inductor.

Combining Eqs. (10) and (11), we obtain

$$\hat{V}_p = n^2(R_s + j\omega L_s) \hat{I}_p = (R' + j\omega L') \hat{I}_p \quad (12)$$

with

$$R' + j\omega L' = n^2(R_s + j\omega L_s) . \quad (13)$$

That means the variable inductor at the secondary side of the high voltage transformer acts like an impedance on the primary side which is n^2 as large. By assuming an appropriate value of n , we can find a convenient range of values for the impedance of the inductor at the secondary side of the transformer which satisfies the tuning condition.

4. Figure 3 (reproduced from a Hipotronics drawing) represents a simplified schematic for one ac series resonant unit. It shows the high voltage transformer and the variable inductor as described in the previous section. The exciter voltage can be regulated by means of the 40 kVA regulator which is arranged at the secondary side of the exciter transformer. In order to measure the current, a calibrated resistor is provided between the low voltage terminal of that transformer and ground. The high voltage output of the entire unit is measured by means of a capacitive voltage divider. The connections to the "real" ground and to the somewhat higher potential of the low voltage terminal of the exciter transformer are shown in Fig. 3.

5. When two ac resonant series units are switched in series, voltages and currents can be calculated using an equivalent circuit shown in Fig. 4. The equivalent impedances $(R' + j\omega L')$ are n^2 times the actual impedances $(R + j\omega L)$ as explained by Eq. (13). Similar to Sect. 1, we obtain

ORNL-DWG 73-9415

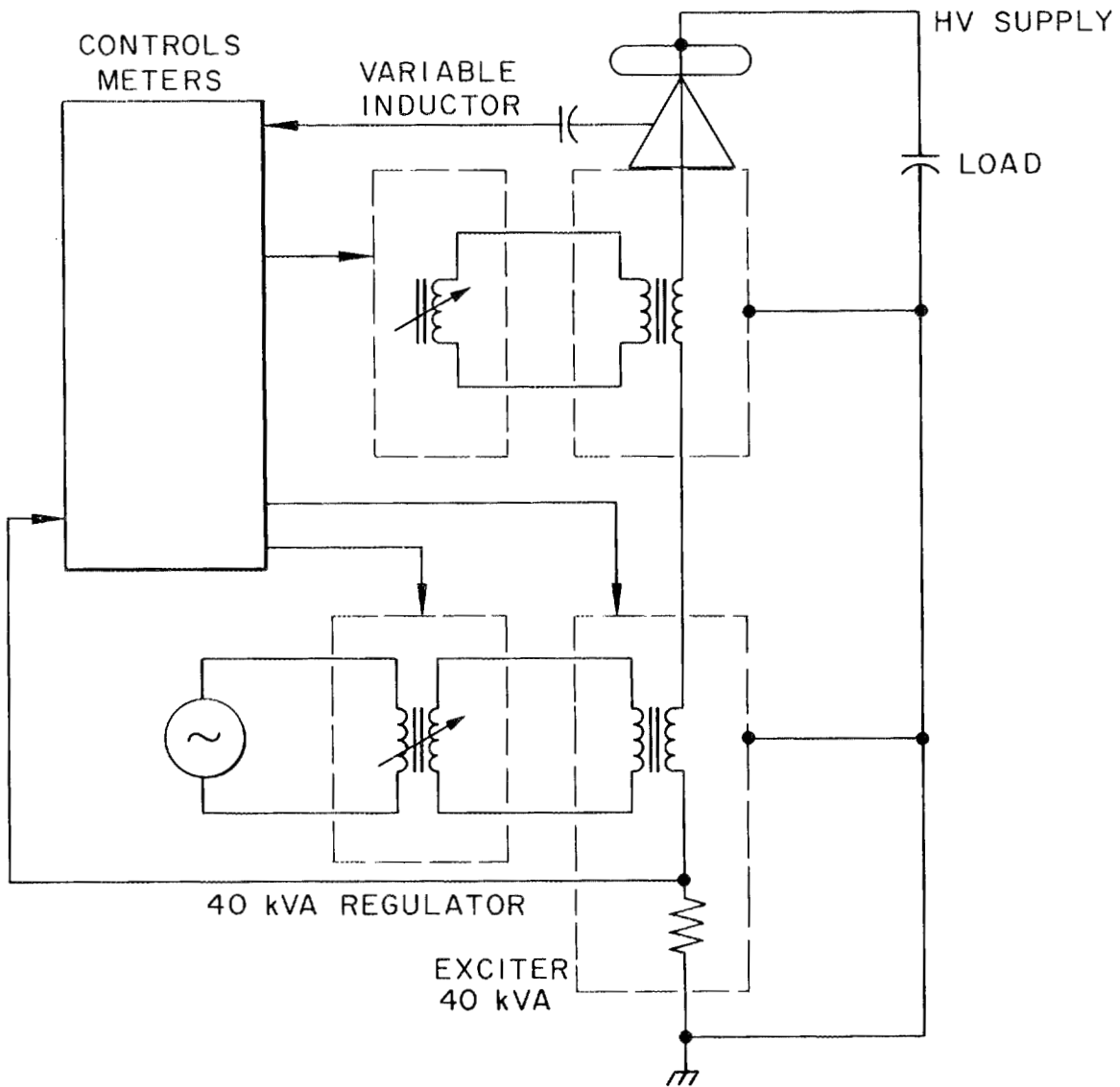


Figure 3. Simplified schematic units operated separately.

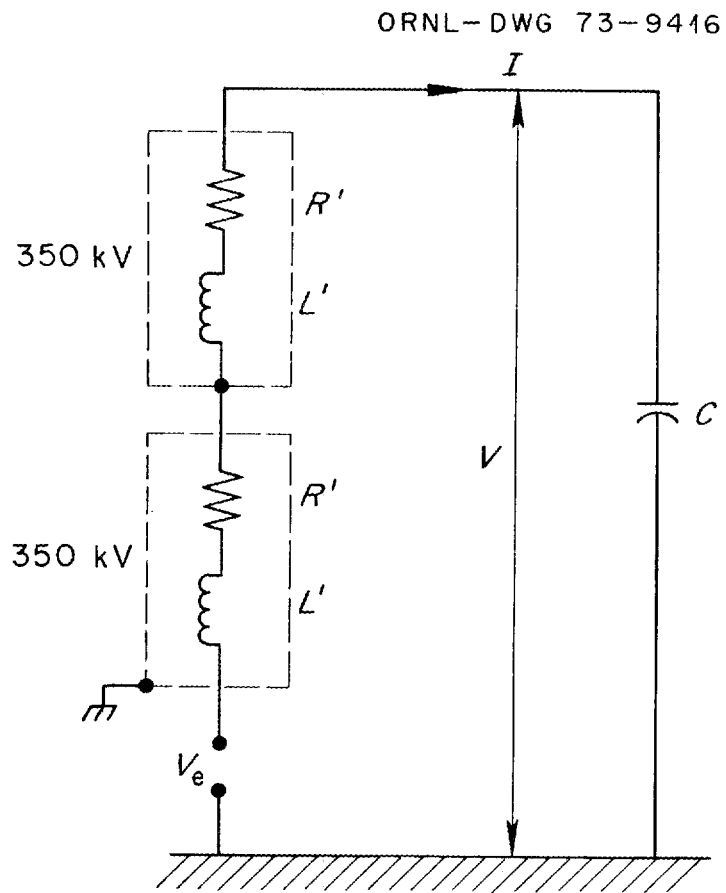


Figure 4. Equivalent circuit for series resonant units operated in cascade.

$$\hat{I} = \frac{\hat{V}_e}{2R' + j\left(2\omega L' - \frac{1}{\omega C}\right)} \quad (14)$$

$$I_{\max} = \frac{V_e}{2R'} \quad (15)$$

with the resonance condition

$$2\omega L' = \frac{1}{\omega C}. \quad (16)$$

Therefore, for series connections of two equal units with the previously considered value of L' , the range of capacities for which the resonant transformer can be tuned is determined by

$$0.0003 \mu\text{F} \leq C \leq 0.0057 \mu\text{F} \quad (17)$$

instead of Eq. (8). Furthermore,

$$V_{\max} = \frac{I_{\max}}{\omega C} = \frac{V_e}{2R'\omega C} = V_e \frac{\omega L'}{R'} = QV_e, \quad (18)$$

i.e., the Q factor is the same as that of one single unit and the maximum voltage output V_{\max} is again the input voltage V_e times the Q factor. Therefore, in order to produce an output voltage of 700 kV instead of the output voltage of 350 kV of a single unit, it is necessary to provide a maximum exciter voltage twice as high as for a single unit. If the two high voltage transformers are each designed for 350 kV, no damage will occur when the two units are switched in cascade, i.e., when one transformer tank is connected to the high voltage terminal of the other tank and appropriate insulation to ground is provided. This operation of

resonant series test sets with two units in series is in contrast to the operation of a test transformer with the winding ratio $2n$.

6. Figure 5 (reproduced from a Hipotronics drawing) represents a simplified schematic of two 350 kV units operated in cascade. Instead of a 40 kVA exciter and regulator as shown in Fig. 3, a 80 kVA exciter and regulator must be provided. From the master control unit, the two variable inductors can be operated. An ampere-meter is connected to the calibrated current resistor; the output voltage of the first high voltage transformer is measured by means of a capacitive voltage divider. A separate 700 kV voltage divider (not shown on Fig. 5) is provided for measuring the total voltage. Hipotronics reports that the capacity of this voltage divider is sufficiently large to provide the minimum capacity for resonance tuning.

ORNL-DWG 73-9417

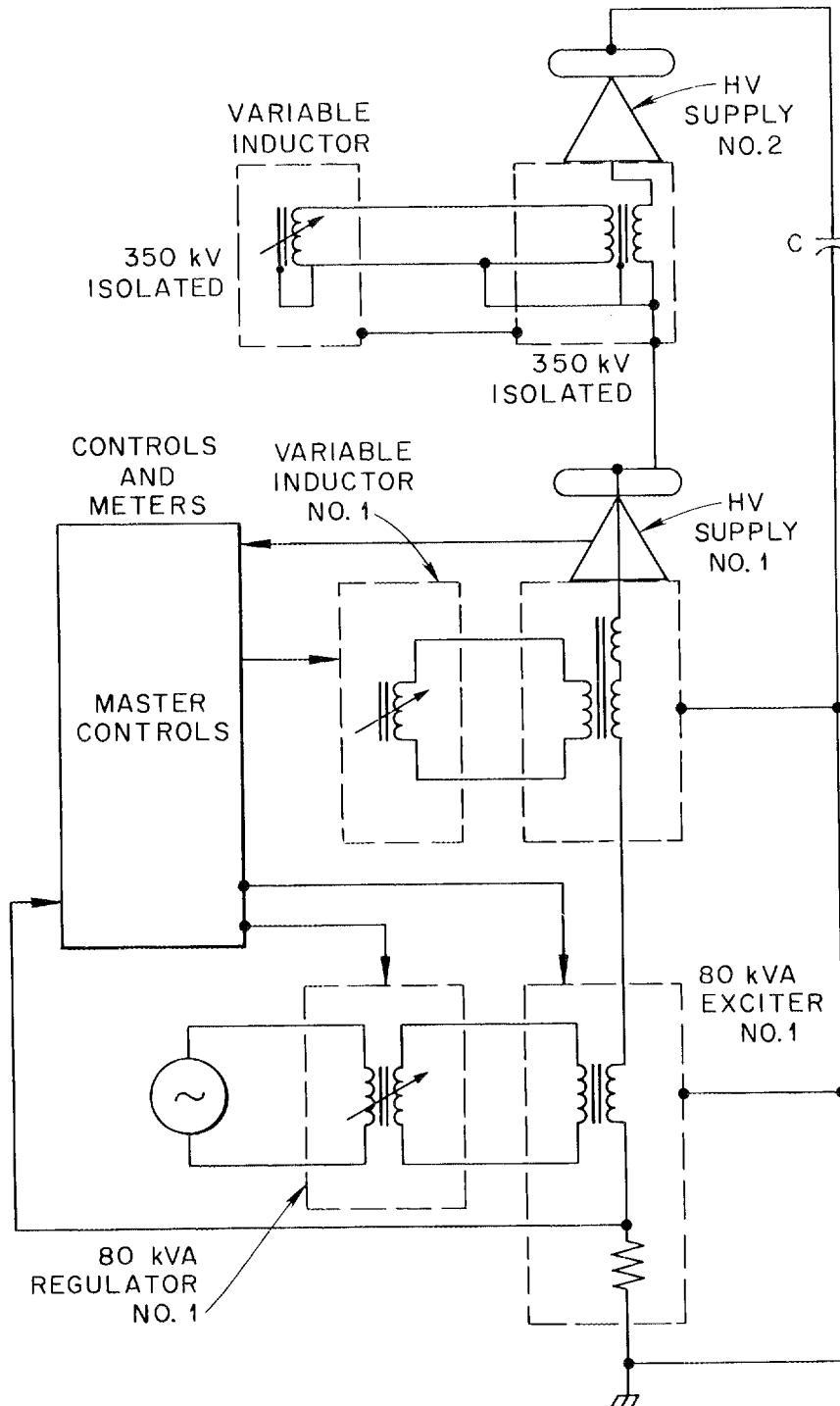


Figure 5. Series resonant units in cascade.

APPENDIX E



HEAT TRANSFER DOWN VAPOR-COOLED STRUCTURES INTO CRYOGENIC LIQUIDS

S. W. Schwenterly

If the ends of a conductor with area A , length H , and thermal conductivity $K(T)$ are maintained at temperatures T_0 and T_1 , with no additional heat exchange, the heat flow is given by the usual relation,

$$\dot{q} = \frac{A}{H} \int_{T_0}^{T_1} K(T) dT . \quad (1)$$

However, if the cold end is in a cryogenic liquid bath, the heat flow to the liquid may be reduced considerably by allowing rising vapor to exchange heat with the upper warm portions of the conductor. A calculation of this reduction was made several years ago by Sydoriak and Sommers¹ for glass helium dewars. We have carried out similar calculations for stainless steel vessels.

Sydoriak and Sommers begin by letting \dot{q}_0 be the heat flux reaching the liquid due to conduction, \dot{Q} be heat flux from all other sources, and $\dot{q}(h)$ be the heat flux through the conductor at level h . Then with complete heat exchange, the vapor and conductor are in thermal equilibrium at all levels h . Hence the total heat flux absorbed by the vapor in rising to level h is

$$\frac{\dot{Q} + \dot{q}_0}{L} \int_{T_0}^{T_h} c(T) dT = \dot{q}(h) - \dot{q}_0 , \quad (2)$$

where L is the latent heat of the liquid [$(\dot{Q} + \dot{q}_0)/L$ is then the mass of liquid vaporized per second] and $C(T)$ is the vapor specific heat. For helium, $C(T)$ is nearly temperature independent. Letting $\dot{Q} + \dot{q}_0 = D \dot{q}_0$, we have

$$\dot{q}(h) = \dot{q}_0 + C \left(\frac{D \dot{q}_0}{L} \right) (T_h - T_0) = K(T_h) A \frac{dT_h}{dh}. \quad (3)$$

D is just the ratio of the total heat leak to the conduction heat leak. Rearranging and integrating from $h = 0$ to H , we have

$$\frac{H}{A} D \dot{q}_0 = L \int_{T_0}^{T_H} \frac{K(T_h) dT_h}{C(T_h - T_0) + \frac{L}{D}}. \quad (4)$$

With no heat exchange, the specific heat term is absent and (4) reduces to (1). From the form of (4) it is apparent that for perfect heat exchange the total heat leak $D \dot{q}_0$ is nearly independent of D , since the L/D term in the denominator is negligible compared to $C(T_h - T_0)$ except for small values of T_h which contribute little to the integral. Hence \dot{q}_0 is approximately inversely proportional to D . What this means is that increasing the nonconductive heat leak \dot{Q} decreases the conductive heat leak so as to keep the total heat flux equal to what the conductive heat leak would be for $D = 1$. If we let

$$\dot{q}_0 = \frac{\alpha A/H}{D}, \quad (5)$$

where α is some constant, then

$$\frac{\dot{Q} + \dot{q}_0}{\dot{q}_0} = D = \frac{\dot{Q} + \frac{\alpha A/H}{D}}{\frac{\alpha A/H}{D}}, \quad (6)$$

and

$$D = \frac{\alpha A/H}{(\alpha A/H) - \dot{Q}}. \quad (7)$$

When \dot{Q} equals $\alpha A/H$, D becomes infinite, the conductive heat leak becomes insignificant, and the total heat leak equals \dot{Q} . On the other hand, with a given value of \dot{Q} we see that the minimum total heat leak for a given type of conductor is obtained if A/H can be chosen so that $\alpha A/H = \dot{Q}$. Smaller values of A/H cannot decrease the heat leak below \dot{Q} , and larger values will give a total heat leak of $\alpha A/H > \dot{Q}$. Of course, mechanical, electrical, or other experimental considerations may make it impossible to choose such a low value of A/H . Sydorik and Sommers evaluated the integral (4) numerically using thermal conductivity vs temperature data for Pyrex glass. For liquid helium at $T_0 = 4$ K, the values $L = 20.62$ j/gm and $C = 5.23$ j/gm-deg were used. The results of their calculations are shown in Fig. 1, which shows plots of $H/AD\dot{q}_0$ vs T_H for various values of the parameter D . Note the large reduction below the values calculated for no heat exchange.

Since the large dewar required for the cryoelectric program will be constructed of stainless steel, similar calculations for this material are of interest. Using published $K(T)$ data² for stainless steels, we have evaluated (4) numerically for D values of 1, 2, and 5. The results of these calculations are shown graphically in Fig. 2, which gives the total heat leak $D\dot{q}_0 H/A$ as a function of T_H .

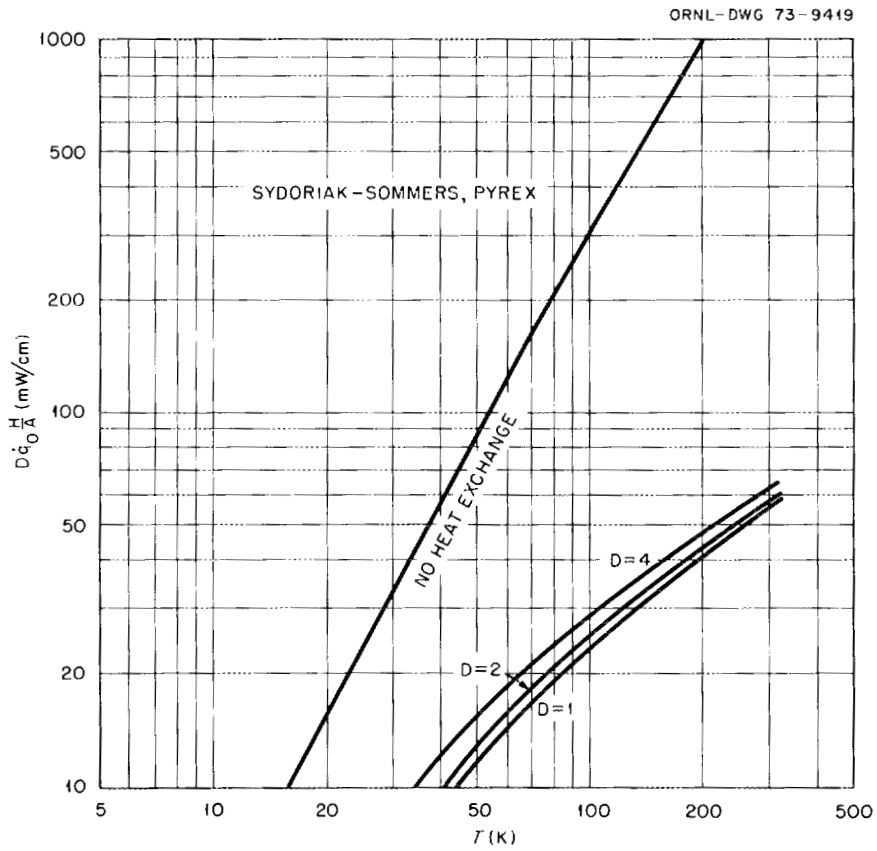


Figure 1. Effect of heat exchange between helium vapor and the walls of a Pyrex liquid helium container on the heat reaching the liquid surface (from Sydoriak and Sommers).

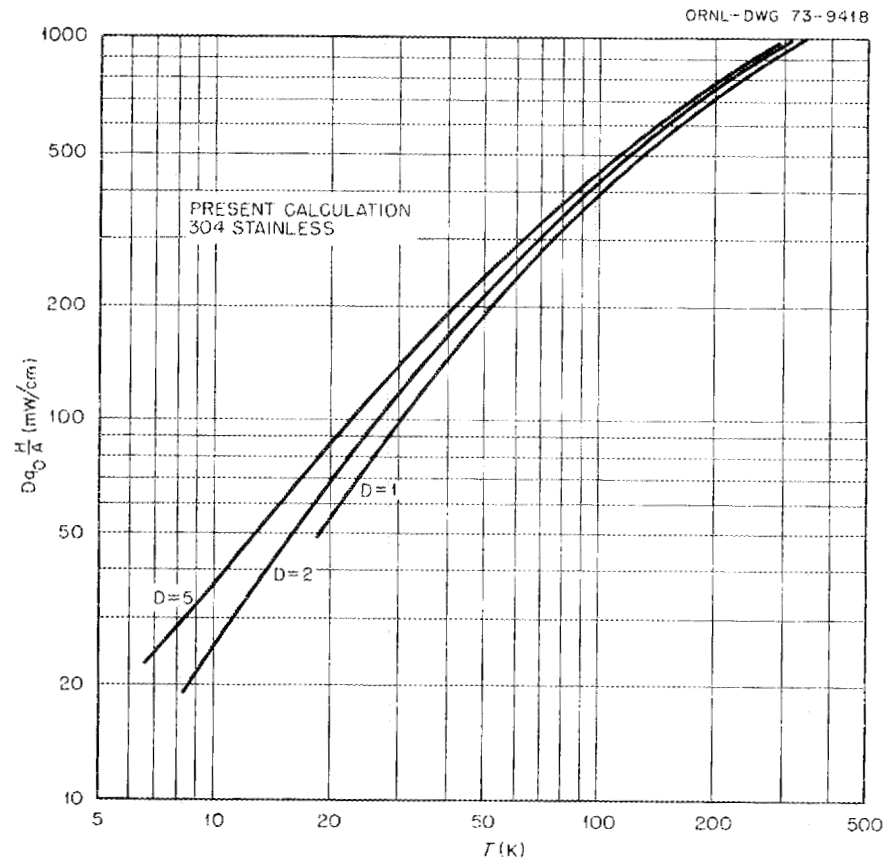


Figure 2. Total heat leak into liquid helium vs temperature, 304 stainless steel.

Referring to Fig. A-6 of this report, the heat leaks of interest are those down the ground plane tube and dewar inner vacuum tank for liquid nitrogen temperature and down the high voltage tube for room temperature. Due to the careful use of radiation shielding, all radiative heat leaks should occur from surfaces at or below liquid nitrogen temperature and can be shown to be negligible. From Fig. 2 assuming that $D = 1$, the conductive heat leaks are given by

$$\dot{Q}_{300} = A/H (958 \text{ mW/cm}) \text{ for } T_H = 300 \text{ K ,}$$

$$\dot{Q}_{77} = A/H (315 \text{ mW/cm}) \text{ for } T_H = 77 \text{ K .}$$

The ground tube and inner dewar wall have inside diameters of 40 in. and 45 5/8 in., and thicknesses of 3/8 in. and 3/16 in., respectively. The minimum distance from the nitrogen reservoir to the helium level will be about 24 in. Hence

$$\begin{aligned} \dot{Q}_{77} &= \frac{\pi [(40 \text{ in.})(3/8 \text{ in.}) + (45 \text{ } 5/8 \text{ in.})(3/16 \text{ in.})] (2.54)}{24 \text{ in.}} (315 \text{ mW/cm}) \\ &= 2.5 \text{ W .} \end{aligned}$$

The high voltage tube has an inside diameter of 7 3/4 in. and a wall thickness of 1/8 in. and reaches room temperature approximately 48 in. above the helium surface. Thus

$$\dot{Q}_{300} = \frac{\pi (7 \text{ } 3/4 \text{ in.})(1/8 \text{ in.})(2.54)}{48 \text{ in.}} (958 \text{ mW/cm}) = 0.15 \text{ W .}$$

Since the rising vapor columns of the two heat leaks are isolated from

each other by a large vacuum space, it is proper to sum the heat leaks to obtain a total of 2.7 W. Imperfect heat exchange might raise this to 3 or 4 W.

Similar calculations for the intermediate voltage cryostat shown in Fig. A-4 of this report yield a heat leak of 0.106 W, which is again almost entirely conductive.

REFERENCES TO APPENDIX E

1. S. G. Sydoriak and H. S. Sommers, *Rev. Sci. Instr.* 22, 915 (1951).
2. R. L. Powell and W. A. Blanpied, "Thermal Conductivity of Metals and Alloys at Low Temperatures," NBS Circ. 556 (1954).

APPENDIX F

PRESSURE WITHSTAND CALCULATIONS

S. W. Schwenterly

Superconducting cable designs under current consideration require helium pressures as high as 10 atm, and it is the object of this program to obtain dielectric strength data in liquid helium up to these pressures. Hence, the low temperature end of the large vacuum bushing shown in Fig. A-6 will have to withstand an external pressure difference of 10 atm on its outer perimeter without buckling. The dewar and high voltage tube must withstand a similar internal pressure. At the same time all tubes must be thin enough to keep heat leaks down to acceptable values.

I. INTERNALLY-PRESSURIZED COMPONENTS

The cryostat parts having internal pressure are the 46 in. diameter inner dewar jacket and its quartz windows, the 8 in. diameter high voltage tube, and the torispherical heads which form the dewar bottom and low temperature insulator.

Section VIII of the ASME Boiler Code (Unfired Pressure Vessels) gives several useful relations for designing vacuum and pressure equipment. For cylindrical shells, par. UA-1 gives a thickness

$$t = \frac{PR}{SE + 0.4 P} \quad (1)$$

where P is the design pressure, R is the outside radius, S is the maximum allowable stress in the material, and E is the joint efficiency. ASME

standards usually set S at one-fourth the minimum tensile strength. However, to keep down thermal leaks and total vessel weight, it was decided to design the dewar using a stress rating of one-third the tensile strength. The resulting safety factor of three should be adequate considering that all personnel will be excluded from the area by an interlocked fence while the vessel is being subjected to high voltage and pressure.

Taking $P = 150$ psi, $S = 25,000$ psi¹ for 304 stainless, and $E = 0.7$ yields

$$t = 0.196 \text{ in. for the inner dewar jacket,}$$

$$t = 0.034 \text{ in. for the high voltage tube.}$$

Consequently the inner dewar jacket was chosen to be 3/16 in. thick, while the high voltage tube thickness was set at 1/8 in. thickness for mechanical strength.

The quartz windows will be 4 in. in diameter and 5/8 in. thick, giving a theoretical breaking pressure of 570 psi and a safety factor of 3.8.²

The required thickness of a torispherical head is given in par. UG-32 of the Boiler Code by

$$t = \frac{0.885 PL}{SE - 0.1P}, \quad (2)$$

where L is the crown radius of the head. Taking $L = 46$ in., $S = 25,000$ psi, $P = 150$ psi, and $E = 1$, we have

$$t = 0.034 \text{ in. for the lower bottom.}$$

This thickness is adequate for

The proposed low temperature insulator will be a fiberglass tori-spherical head with a crown radius of 40 in. Taking one-third the tensile stress value for a similar material such as G-10 gives $S = 10,000$ psi, (2) then yields

$$t = 0.532 \text{ in. for the insulator.}$$

II. EXTERNALLY-PRESSURIZED COMPONENTS

The only part having external pressure is the 40 in. ground tube of the vacuum insulator. Externally pressurized tubes must be thicker than those under the same internal pressure due to the possibility of errors in tube roundness initiating collapse into a number of lobes. This may be prevented in some cases by the addition of stiffening rings to the shell.

Cases of this type are treated using the charts in Sect. VIII, Appendix V of the Boiler Code. From these curves, one obtains the maximum working pressure for various values of t/D and L'/D , where L' is the distance between stiffening rings. Assume that stiffening rings are placed to give $L'/D = 0.5$ and let $t = 3/8$ in. and $D = 40 \ 3/4$ in. Then Fig. UHA-28.1 for 304 stainless steel gives a value

$$B = \frac{pD}{t} = 13,000 \text{ psi .}$$

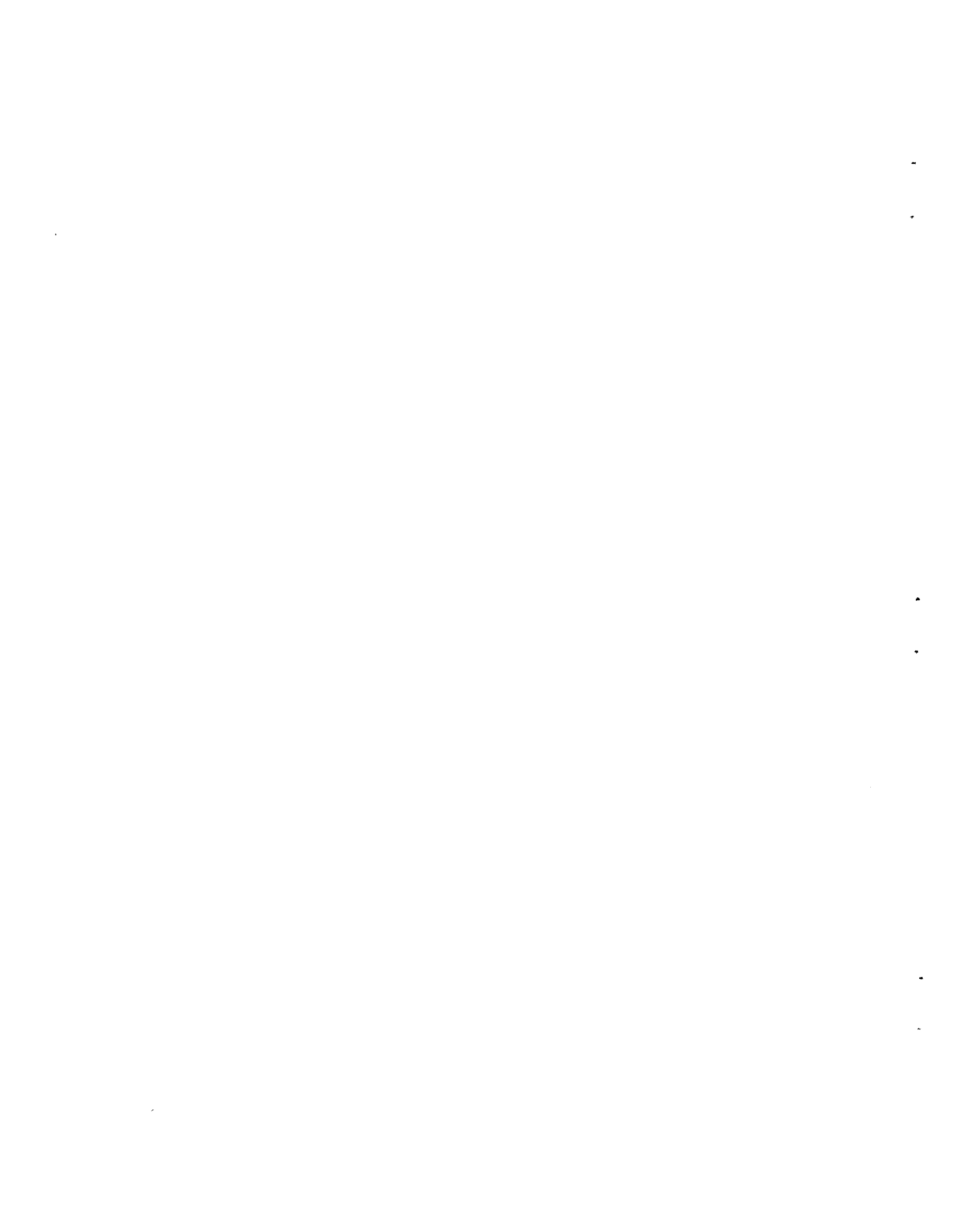
Hence, $p = 119$ psi.

However, these plots are also constructed to incorporate a safety factor of four. If this is dropped to three in conformity with the rest of the design, multiplying this pressure by $4/3$ gives 159 psi.

Further studies are underway to determine whether a composite wall will support the pressure load with a lower heat leak.

REFERENCES TO APPENDIX F

1. ASME Boiler Code, Sect. VIII, Table UHA-23.
2. Calculation by J. N. Robinson of Inspection Engineering Division,
ORNL.



APPENDIX G



COMPUTATIONAL AND EXPERIMENTAL FIELD ANALYSIS
FOR HIGH VOLTAGE ENGINEERING

W. F. Gauster, W. J. Schill, and W. C. T. Stoddart

I. INTRODUCTION

Solutions of electrostatic and electrodynamic field problems with various boundary conditions are of great practical importance as an essential part of the physics background for the design and operation of high voltage equipment. The mathematical formulation of these physics problems uses the "Laplacian," which can be expressed in rectangular coordinates as

$$\nabla^2 \varphi = \frac{\partial^2 \varphi}{\partial x^2} + \frac{\partial^2 \varphi}{\partial y^2} + \frac{\partial^2 \varphi}{\partial z^2} . \quad (1)$$

Electrostatic field problems in regions with uniform dielectric constant and without space charge lead to "Laplace's equation"

$$\nabla^2 \varphi = 0 . \quad (2)$$

When space charge must be considered, "Poisson's equation"

$$\nabla^2 \varphi = - \rho$$

is required. For transient fields, the "wave equation"

$$\nabla^2 \varphi = \frac{1}{c^2} \frac{\partial^2 \varphi}{\partial t^2} \quad (4)$$

and, finally, the "diffusion equation"

$$\nabla^2 \varphi = \frac{1}{h^2} \frac{\partial \varphi}{\partial t} \quad (5)$$

are needed for special cases.

There is a tremendous wealth of books and papers dealing with field analysis from the engineering standpoint.¹ For our purposes, we will list the following groups of field analysis:

1. Fields of simple geometries (e.g., fields produced by point and line charges, with more advanced field analysis methods, such as the "method of electric images").
2. Analytic solutions. One classical way is to use appropriate coordinate systems in order to separate the variables and to satisfy special boundary conditions. A systematic treatment of these coordinate systems is based on first and second degree surfaces and deals with 11 coordinate systems (rectangular; circular-, elliptic-, and parabolic-cylindrical coordinates; different kinds of spherical coordinates; etc.).² Many two-dimensional problems can be solved by applying the theory of complex variables (an especially powerful method is the use of conformal mapping³).
3. Computational methods. Due to the modern development of computer techniques, the computational methods are becoming increasingly important. They are replacing in many cases analytical solutions which were partly developed during the time when "higher functions" were already tabulated, however, electronic computers were not yet available.
4. Experimental field analysis.

The following Sects. II and III deal with Topics 3 and 4 listed above.

II. COMPUTATIONAL METHODS

In the absence of closed form or series analytic solutions to the applicable differential equations and boundary conditions, numerical methods are often used. Three general methods will be discussed: the finite difference, the finite element, and the quasi-charge methods.

The finite difference method is a numerical technique for solution to differential equations. The method is based on approximating the governing differential equations with ordinary algebraic equations. A simple example of application to the two-dimensional, Cartesian coordinate, differential equations follows. Given

$$\frac{\partial^2 V}{\partial X^2} + \frac{\partial^2 V}{\partial Y^2} = 0 . \quad (6)$$

Consider a point identified by indices i, j in Fig. 1 with nearest neighbors on grid lines $i-1, i+1, j-1,$ and $j+1$. The distance between points h is also indicated in the figure. One approximation to the differential equation may be written,

$$0 = \left[\frac{V_{i+1,j} - V_{i,j}}{h_1} - \frac{V_{i,j} - V_{i-1,j}}{h_3} \right] \frac{2}{h_1 + h_3} \\ + \left[\frac{V_{i,j+1} - V_{i,j}}{h_2} - \frac{V_{i,j} - V_{i,j-1}}{h_4} \right] \frac{2}{h_2 + h_4} . \quad (7)$$

Thus the potential at five adjacent points is interrelated algebraically. Upon the imposition of known boundary condition, the problem may be solved numerically. Examples of the application of the finite difference method for high voltage equipment are contained in Refs. 4 and 5. These references consider the problem of multiple dielectrics, irregular geometry, and variable boundary conditions in detail and present results for several high voltage devices. By considering the analogy between heat transfer and dielectric fields, computer codes may be used that have been developed for heat transfer. The finite difference computer code,

ORNL-DWG 73-9420

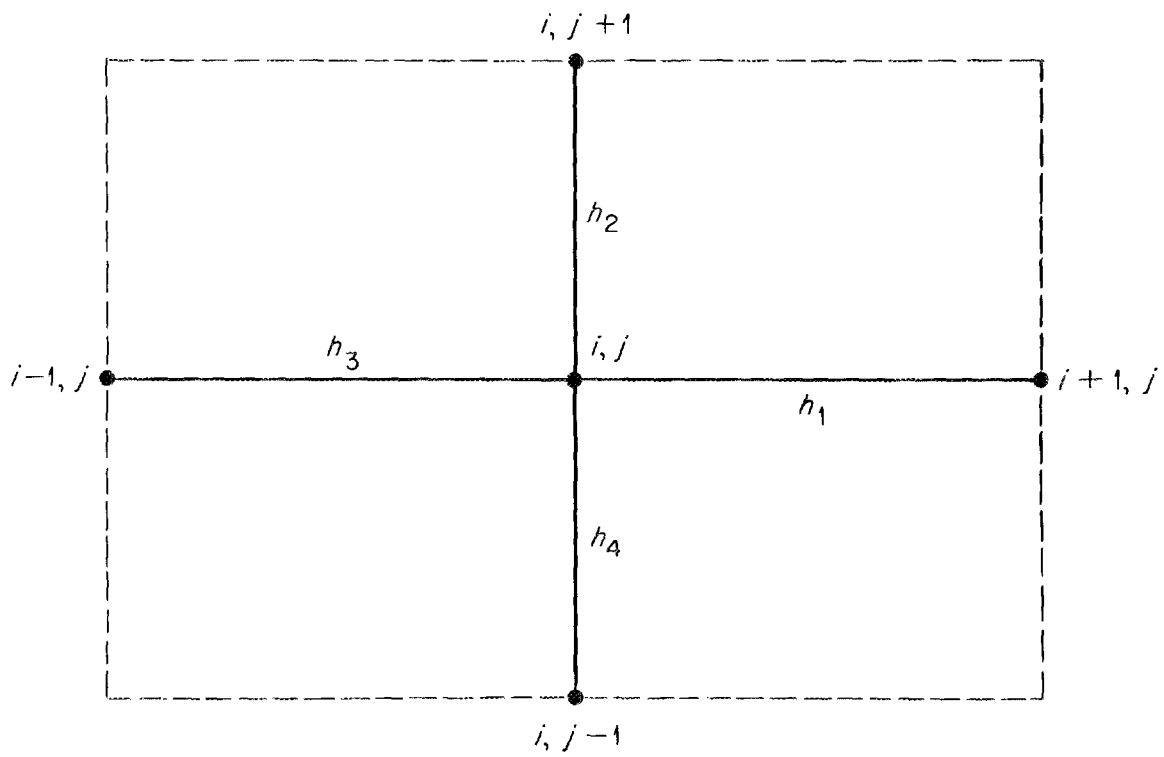


Figure 1. Finite difference grid.

HEATING IV,⁶ for solving problems in one, two, and three dimensions in Cartesian or cylindrical coordinates may be readily used for calculation of potential field problems.

For highly irregular boundaries and geometries not readily represented by combinations of small rectangles or right triangles, an alternate to the finite difference procedure is the finite element method. The finite element method transforms the problem in physics from one of finding the solution to a differential equation to that of finding the solution to an integral equation. As an example, consider Eq. (6). Define a functional **X** as

$$\mathbf{X} = \iint \frac{1}{2} \left\{ \left(\frac{\partial V}{\partial X} \right)^2 + \left(\frac{\partial V}{\partial Y} \right)^2 \right\} dx dy . \quad (8)$$

The solution which minimizes **X** is equivalent to the solution of (6) subject to the same region and boundary conditions. The finite element method proceeds by assuming an interrelationship between adjacent points surrounding a cell called an element. The potential *V* within the element is dependent only on the potential of the corner points or nodes. Since the elements adjacent to each other share nodes on their boundary, a coupling develops between nodes through the region. Mathematical details of the finite element method applied to potential field problems may be found in Ref. 7. At ORNL several programs are available for the solution of potential field problems by the finite element method. To date a program called FEATS⁸ has been used to determine several axisymmetric potential field distributions.

In the design of the 1000 kV dewar,⁹ consideration must be given to the heat leaks by radiation to the region of the test section. For

this reason, thermal radiation baffles are incorporated within the annulus between the outer 20 in. radius cylinder ground plane and the inner 4 in. radius cylinder at the test voltage potential. One criteria for the acceptance of a design is that the potential field gradient not exceed 100 kV/cm. Figures 2-6 present a typical computation mesh of finite elements used in analysis and results of equipotential contours and field gradients for four conceptual designs.

One of the classical analytical methods of potential field calculation is called the image method. In this method a certain space charge distribution may be replaced by a point or line charge with equal charge at an appropriate point in space.¹⁰ With the availability of digital computers, the foundation of the image method has been used to develop computer codes for axisymmetric and plane geometries for potential field calculation.^{11,12} The image method reduces the amount of data required for input to solve a potential field problem as compared to the finite difference and finite element methods. It should thus prove to be an excellent tool for design purposes. A digital computer code based on the image method for axisymmetric geometries is being developed.

III. EXPERIMENTAL FIELD ANALYSIS

There is very extended literature on experimental field analysis which can be applied to the special requirements of high voltage engineering. One group of these publications describes field measurements on full-size or on models of actual high voltage equipment.¹³ The other group concerns methods for solving such potential problems by means of analog computers. In contrast to solutions by digital computer methods,

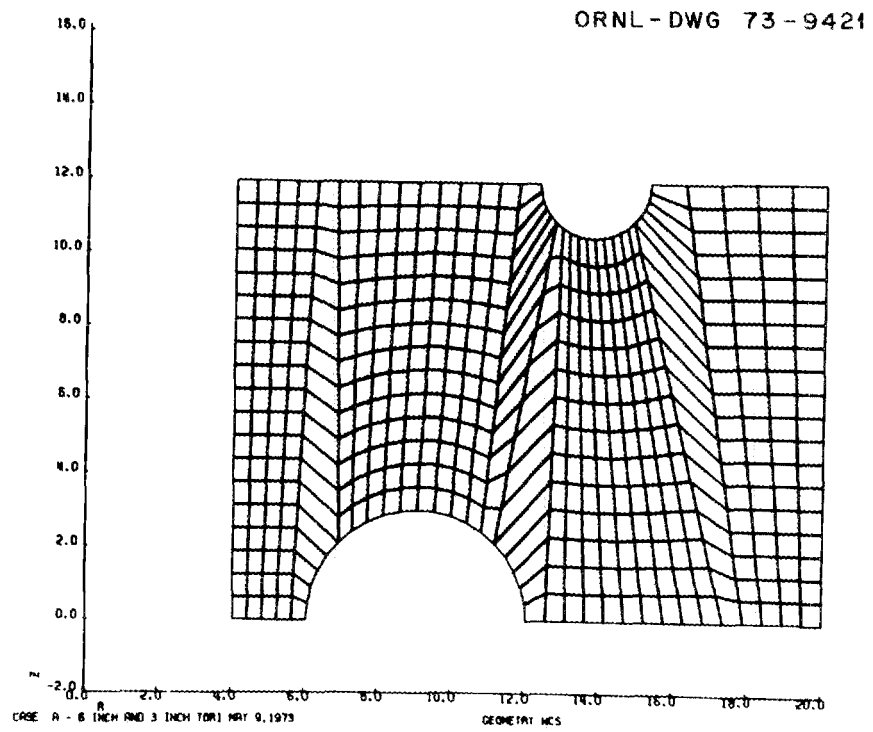
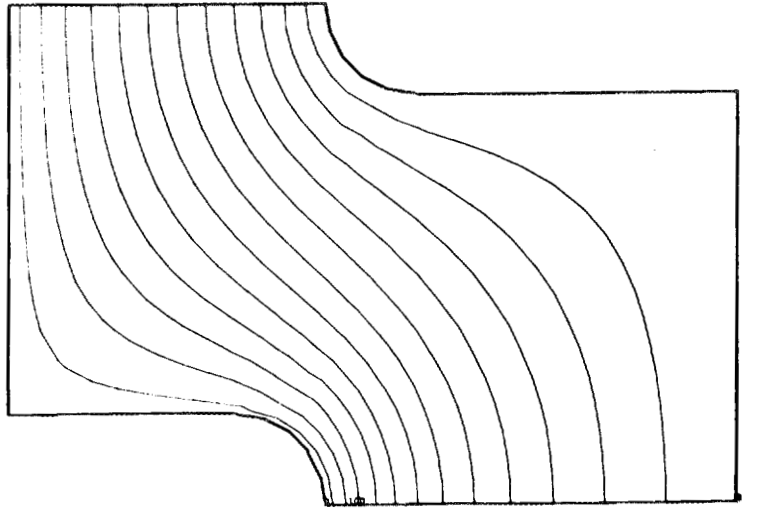


Figure 2. Finite element mesh for 6 in. and 3 in. tori.

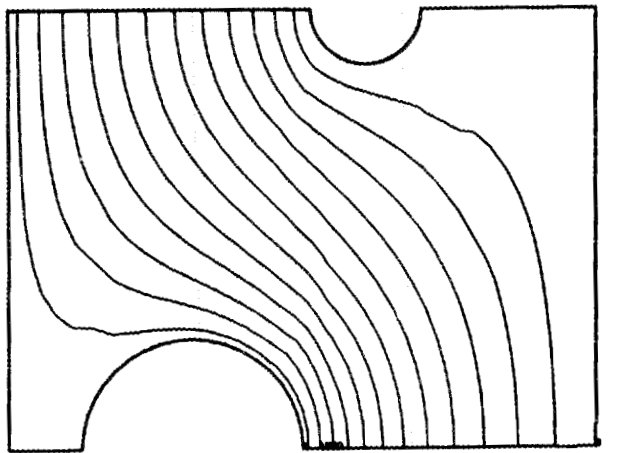
ORNL-DWG 73-9422



ELECTRIC FIELD CALCULATION W.C. STODART APRIL 18, 1973 TEMPERATURES MS

Figure 3. Results for fabricated baffles.

ORNL-DWG 73-9423

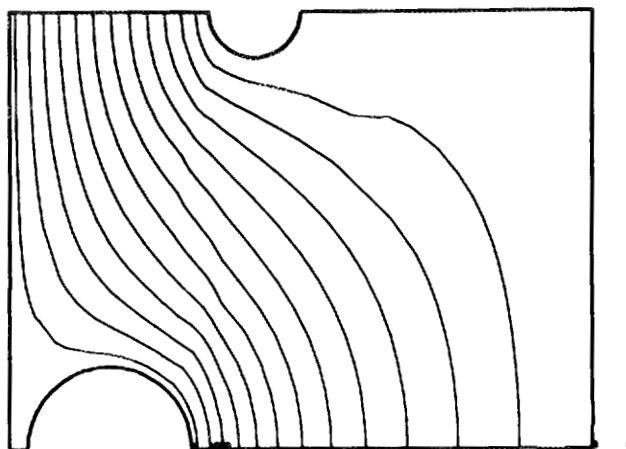


CASE A - 6 INCH AND 3 INCH TORI MAY 9, 1973

TEMPERATURES MCS

Figure 4. Results for 6 in. and 3 in. tori.

ORNL-DWG 73-9424

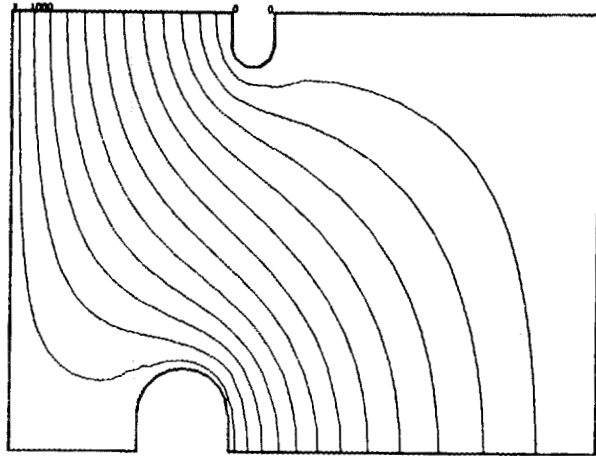


CASE 0 - 4 1/2 INCH AND 2 1/2 INCH TORI MAY 14, 1973

TEMPERATURES MCS

Figure 5. Results for 4 1/2 in. and 2 1/2 in. tori.

ORNL-DWG 73-9425



FLAT SIDED TORUS SHIELDS MAY 22, 1973

TEMPERATURES DEG C

Figure 6. Results for flat sided tori.

analog computer methods can be considered as a special kind of experimental field analysis. Of course, the analog computers can be used not only for the analysis of electrostatic field distributions but also for investigations on electrical and on hydrodynamic flow patterns, on magnetic fields, on heat flow, and for various other problems which can be reduced to the solutions of boundary problems of Laplace's equation. Ernst Weber¹⁴ makes the following summarizing statement: "Any solution for one of the field types can readily be translated into a solution for the other field types. In the experimental investigation, this permits welcome substitutions in instances where the original field is difficult, if not impossible, to explore."

For general three-dimensional potential problems with unsymmetrical arrangements of the electrodes, the electrolytic tank is the only practical version of an analog computer.¹⁵ Very early, the idea was conceived to apply the electrolytic tank also to fields with more than one dielectric.¹⁶

For axially symmetric fields, wedge-shaped electrolytic tanks can be used.¹⁷ For exact measurements, a tank with hyperbolic profile must be employed.¹⁸ However, in some cases it is more convenient to use a "three-dimensional" electrolytic tank and to insert half of the axisymmetrical test object in such a way into the electrolyte so that the plane cut of the test specimen is flush with the electrolyte surface. At the Thermonuclear Division of ORNL, such an electrolytic tank has been built for determining the electrostatic potential distribution around the model of an ion source.¹⁹

Another type of analog computer is represented by resistor networks. Selected carbon-deposited resistors with high accuracy (better than 1%)

can be employed, and between resistance steps, sufficiently accurate interpolation resistance dividers can be used so that very accurate measurement results are obtained. Another advantage of resistor networks is that boundary conditions can be changed with great ease; this is important when specified field configurations have to be achieved so that the configuration of the boundaries must be changed by trial and error.

Very extensive work on such axially symmetrical resistance network analog computers has been done by K. E. Wakefield of "Project Matterhorn," now Princeton Plasma Physics Laboratory (PPPL).²⁰ A carefully designed axially symmetrical resistance network has been built at the Thermonuclear Division of ORNL.²¹

For cases where high accuracy is not very essential and simple and fast work is more important, the "Conductive Sheet Analog Field Plotter" (AFP) is a very convenient tool. The idea of an AFP was first conceived by G. Kirchhoff in 1845.²² He considered the flow of electricity through a thin metal sheet of relatively high resistance, with the current introduced by thin metal electrodes of appropriate shape. The potential of any point at the surface of the thin metal sheet can be determined by touching it with the tip of a "tracer stylus." Equipotential lines can be easily drawn in this way. Various dielectrics with different dielectric constants ϵ_k can be represented by using for the various areas of the thin sheet different metals with corresponding resistivity ratios. An example of the field distribution in a two-conductor cable with two different dielectrics is shown in Ref. 1, p. 184. Such arrangements with thin metal sheets are, however, expensive and not conveniently handled;

and, therefore, metal sheet AFP are only used for permanent models for field plotting for educational purposes.²³

Presently, the preferred sheet material for AFP is graphitized paper, "Teledeltos, Grade L," as being used for recording instruments and for facsimile telegraphing purposes. This conductive field plotting paper is about 0.004 in. thick and has a resistance of about 2000 Ω per square. Electrodes of the desired shapes are painted with a conductive silver paint. These electrode areas have a resistance of 1 to 4 Ω per square and represent the boundaries with $V = \text{const.}$ The boundaries with $\partial V/\partial n = 0$ can be represented by cutting the rim of the field plotting paper in an appropriate shape. By using a tracer stylus, equipotential lines can be easily determined.

There is very extended literature on "conductive paper AFP." For instance, on pp. 203 and 204 of Ref. 23, 16 references are indicated. In our laboratory, we use a "conductive paper AFP" manufactured by the Sunshine Scientific Instrument Company (SSI) in Philadelphia, Pennsylvania. Details of the design of that AFP, Model 241, and instructions concerning the use of this apparatus can be found in its instruction manual.²⁴

Our extended and careful work with this type of AFP showed that for two-dimensional potential problems, we can prepare the conducting plotting paper with great accuracy (drawing electrodes with conducting silver paint, cutting the rim of the paper). Furthermore, we can trace equipotential and flow lines using the tracing stylus and the potentiometer with similar great accuracy (about $\pm 1/2\%$). Finally, no drift of the voltage source and no polarity effects of the measured voltages can be observed. However, these statements do not answer the most important question: How well

does the solution obtained with our analog computer approximate the strict mathematical solution of the potential distribution problem concerned? As we will discuss in the following, the answer depends mainly on the isotropy of the plotting paper used. Concerning the isotropy of the "Type L Teledeltos Paper," p. 10 of Instruction Manual IM24-1 contains the following statement: "Manufacturing tolerances to which the conducting paper appears to be held result in a uniformity of resistance ordinarily adequate to the needs of the field plotter. In certain cases where extreme accuracy is required, small corrections for such anisotropic variations in resistance as occur in perpendicular directions in the paper may be determined and made. In sample tested to date, the uniformity of resistance of sample areas has been found to run within from $\pm 3\%$ to $\pm 8\%$ maximum deviation from a mean value, with the paper showing the low resistance values when measured 'lengthwise of the roll' as compared with the higher values obtained when measured 'crosswise.' This anisometric [sic] property appears to be a permanent property introduced in the processing of the paper, and is always found to be oriented so that the lower resistance value occurs 'with' the length of the roll, and in quadrature to the higher value associated with 'crosswise' measurement. It can be corrected for where necessary by the use of different scale factors in perpendicular directions."

In order to test the anisotropy of the paper, the following measurements were made. From one piece of plotting paper, a sample (shown in Fig. 7) was cut. It consists of 16 "arms," Nos. 0 to 15, each 10 in. long and 1 in. wide. The direction 0-8 is "lengthwise" to the paper. In the center one electrode with about a 4 in. diameter was painted with good

ORNL-DWG 73-9426

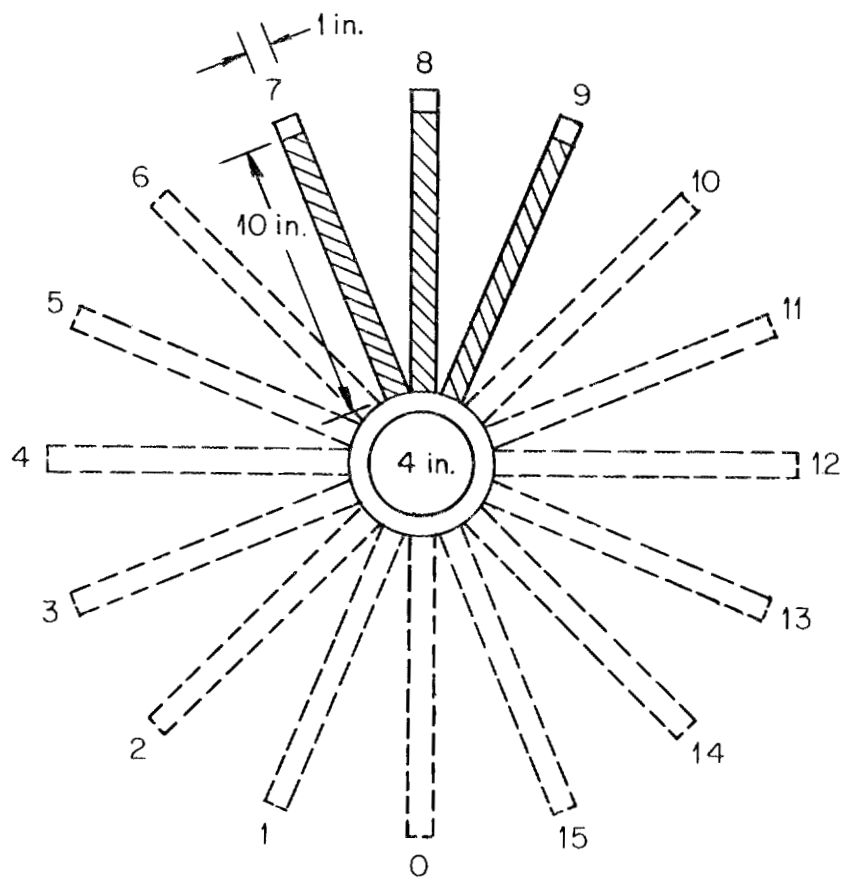


Figure 7. Arrangement for testing the isotropy of Teledeltos Paper.

conducting silver paint and a thin metal wire was arranged inside near the circumference of that electrode in order to decrease the resistance of the center part. On the outside end of each arm, 1 in. x 1 in. electrodes were painted.

First we measured the resistance of "pairs of arms," i.e., two opposite arms were switched in series. The results of these measurements are shown in Table 1.

Table 1

Pair No.	Angle ($^{\circ}$)	Deviation (%) from Average Resistance
0 - 8	0	- 6.5
1 - 9	22.5	- 4.4
2 - 10	45.	- 1.3
3 - 11	67.5	+ 3.1
4 - 12	90.	+ 5.3
5 - 13	112.5	+ 5.3
6 - 14	135.	+ 1.8
7 - 15	157.5	- 3.3
8 - 0	180.	- 6.5

Pair 0-8 is "lengthwise," and pair 4-12 is "crosswise" on the paper roll. From the comments of the instruction manual, it can be expected that pair 0-8 has the smallest resistance, which is actually the case. However, we notice that pair 4-12 does not have the highest resistance, since the resistance of pair 5-13 has the same value. The deviation of the resistances of the pairs from the mean value is somewhat smaller than the maximum tolerance of $\pm 8\%$ mentioned in the instruction manual.

Unfortunately, the results become even worse if we consider each resistance strip separately (see Table 2, next page).

The smallest resistance of any strip is 6.5% below the average resistance; the largest resistance is 9.3% above the average resistance, i.e., larger than the + 8% mentioned in the instruction manual. The strips with angles larger than 180° have appreciably higher resistance than the corresponding strips with angles smaller than 180° . The higher resistance values are the right half of the plotting paper (see last column of Table 2). From these measurement results it follows that the statement of the instruction manual, "It (the anisotropic property) can be corrected for where necessary by the use of different scale factors in perpendicular directions," does not hold at least for that roll of paper which has been used for our measurements. The high degree of anisotropy of the plotting paper is regrettable, especially since the tracing accuracy is very good. In the following we will discuss an example of finding the equipotentials of a potential field, comparing calculated values with the results of field plotting. This example will show that the practical results of field plotting are more satisfying than to be expected considering the anisotropy of the plotting paper.²⁵

Figure 3 shows the cross section of two eccentric cylindrical electrodes. The inner electrode (center O, radius r) is supposed to be on the potential V_0 , the outer electrode with the diameter $(2r + a + b)$ is on ground potential. The problem is to find the equipotential lines with $V_1 = 0.8 V_0$, $V_2 = 0.6 V_0$... $V_n = 0.2 V_0$. Analytical solutions of similar problems, e.g. by means of inversion, are well known.²⁶ For field plotting we used the following numerical data

Table 2

Strip No.	Angle($^{\circ}$)	Deviation (%) from Average Resistance	Strip No.	Angle($^{\circ}$)	Deviation (%) from Average Resistance	"180 $^{\circ}$ - Difference" (%)
0	0	- 6.5	8	180.	- 6.5	0
1	22.5	- 5.2	9	202.5	- 3.6	1.6
2	45.	- 2.7	10	225.	+ 0.1	2.8
3	67.5	-.0.4	11	247.5	+ 6.6	7.0
4	90.	+ 1.3	12	270.	+ 9.3	8.0
5	112.5	+ 1.3	13	292.5	+ 9.3	8.0
6	135.	- 1.4	14	315.	+ 5.0	6.4
7	157.5	- 5.3	15	337.5	- 1.3	4.0

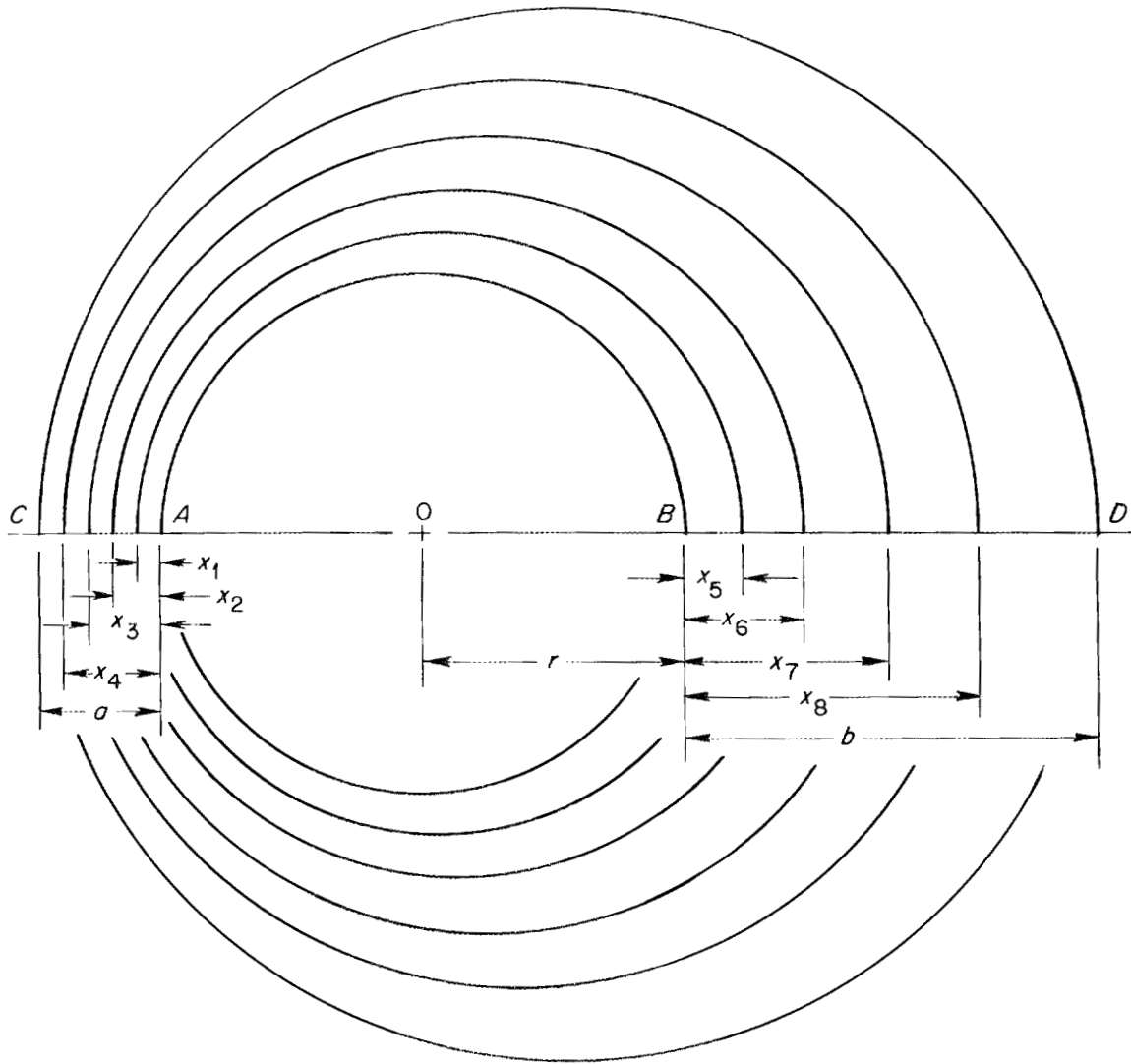


Figure 8. Example for comparison of analytical potential calculation with result of field plotting.

$$r = 6 \frac{1}{4} \text{ in.}; \quad a = 2 \frac{1}{2} \text{ in.}; \quad b = 12 \frac{7}{16} \text{ in.}$$

Table 3 shows the calculated values x_k and the values x'_k (see Fig. 8) obtained by means of conductive sheet field plotting. As shown in Table 3, the difference between calculated and measured values is smaller than 4%.

Table 3

Calculated (in.)	Measured (in.)	Error (%)
$x_1 = 0.444$	$x'_1 = 28/64 = 0.4375$	- 1.5
$x_2 = 0.916$	$x'_2 = 59/64 = 0.922$	+ 0.7
$x_3 = 1.417$	$x'_3 = 1 \frac{29}{64} = 1.453$	+ 2.5
$x_4 = 1.946$	$x'_4 = 2 \frac{1}{64} = 2.016$	+ 3.5
$x_5 = 1.428$	$x'_5 = 1 \frac{30}{64} = 1.469$	+ 2.9
$x_6 = 3.210$	$x'_6 = 3 \frac{20}{64} = 3.3125$	+ 3.2
$x_7 = 5.480$	$x'_7 = 5 \frac{42}{64} = 5.656$	+ 3.2
$x_8 = 8.411$	$x'_8 = 8 \frac{38}{64} = 8.594$	+ 2.2

Despite the fact that the AFP field plotting system does not yield as accurate results as, say, the resistor networks, it is widely and successfully used for the following reasons: It is very simple, and it is an excellent method to obtain fast and, with little effort at least, semi-quantitative information on complicated high voltage field distributions. For instance, the designs of our high voltage helium dewars are based on preliminary field studies made with our "SSI conductive paper

field plotter."²⁷ Then, exact-quantitative results have been obtained by means of digital computer calculations (see Sect. II of this appendix).

REFERENCES TO APPENDIX G

1. See for instance, Ernst Weber, Electromagnetic Fields, Vol. I, John Wiley and Sons, Inc., New York, 1950. This book is an excellent presentation of the theory as needed for engineering applications, and it gives many examples and extensive lists of references.
2. A very complete modern presentation is Field Theory Handbook by P. Moon and D. E. Spencer, Springer-Verlag, Berlin, 1961.
3. See Chap. 7 of Ref. 1 and L. V. Bewley, Two-Dimensional Fields in Electrical Engineering, The MacMillian Company, New York, 1948.
4. R. H. Galloway, H. M. Ryan, and M. F. Scott, "Calculation of Electric Fields by Digital Computer," Proc. IEE 114, No. 6, 824-829 (June, 1967).
5. H. M. Ryan, J. M. Mattingley, and M. F. Scott, "Computation of Electric Field Distributions in High-Voltage Equipment," IEEE Trans. Elec. Insul. EI-6, No. 4, 148-154 (December, 1971).
6. W. D. Turner and J. S. Crowell, "Notes on HEATING - an IBM 360 Heat Conduction Program," CTC-INF-980, Union Carbide Corporation, Nuclear Division, 1969.
7. O. C. Zienkiewicz, The Finite Element Method in Engineering Science, 2nd ed., McGraw Hill, London, 1971, Chap. 15.
8. J. A. Swanson, "FEATS, A Computer Program for Finite Element Thermal Stress Analysis of Plane and Axisymmetric Solids," WANL-TME-1888, January, 1969.
9. Cryoelectric Section, Engineering Sciences Group, Thermonuclear Division, "Cryogenic Dielectrics and Superconducting and Cryogenic

- Materials Technology for Power Transmission--Semiannual Report, March 1, 1973," ORNL-TM-4187, May, 1973, Fig. A-2, p. 27.
10. A. Nussbaum, Electromagnetic Theory for Engineers and Scientists, Prentice-Hall, 1965, Chap. 2.
 11. H. Steinbigler, "Anfangsfeldstarken Und Ausnutzungsfaktoren Rotationssymmetrischer Elektrodenanordnungen in Luft," Technische Hochschule München, Dissertation, 1969.
 12. P. Weiss, "Rotationssymmetrische Zuristoffdielektrika," Technischen Universität München, Dissertation, 1972.
 13. For field measurements on high voltage bushings, insulators, insulator strings, etc., see for instance the very detailed presentation in A. Schwaiger, Theory of Dielectrics (translated into English by R. W. Sorensen), John Wiley and Sons, New York, 1932.
 14. Reference 1, p. 183.
 15. See for example, S. Softky and J. Jungermann, "Electrolytic Tank Measurements in Three Dimensions," Rev. Sci. Instr. 23, 306 (1952).
 16. C. L. Fortescue and S. W. Farmworth, "Air as an Insulator When in the Presence of Insulating Bodies of Higher Inductive Capacity," Proc. Am. Inst. Elec. Eng. 27, 895 (1913).
 17. The first suggestion for a wedge-shaped electrolytic tank was probably made by H. Barkhausen and J. Brück, "The Shape of Electric Fields in Electron Tubes, Measured in the Electrolytic Trough," Elektrotechn. Zeitschrift 54, 175 (1933).
 18. H. K. Farr and W. R. Wilson, "Some Engineering Applications of the Electrolytic Field Analyser," Trans. AIEE 70, 1301 (1951).

19. J. P. Neal, internal ORNL report (August 25, 1959).
20. K. E. Wakefield, "A Resistance Device for Studying Axially Symmetric Magnetic Fields," PM-S23, NYO-7313, Project Matterhorn (revised November 28, 1958); and Proc. Symp. Magnetic Field Design in Thermonuclear Research, Gatlinburg, Tennessee, December 11-12, 1958, ORNL-2745 (October 7, 1959) p. 61 and other publications.
21. W. F. Gauster, ORNL-2693 (January 31, 1959) p. 104 and P. A. Thompson, ORNL-3104 (January 31, 1961) p. 116.
22. G. Kirchhoff, Annalen der Physik 64, 497 (1845).
23. An excellent presentation with a great number of references is: Field Analysis. Experimental and Computational Methods, a series of 11 lectures, edited by D. Vitkovitch, D. VanNostrand, Ltd., London and New York, 1966. This presentation has been partly used in writing this report.
24. Instruction Manual IM24-1, Sunshine Scientific Instrument Company, 1810 Grant Avenue, Philadelphia, Pennsylvania 19115.
25. The following and other examples of potential field plotting are discussed in more detail in Eng. Sci. Memos, Thermonuclear Division, ORNL (1973), "A Note on Analog Field Plotting, Parts I and II," by W. F. Gauster and W. J. Schill.
26. See for instance, Ref. 13, pp. 80-81.
27. See Fig. A-10, Sect. II.A of this report.

DISTRIBUTION

	<u>Copies</u>
U.S. Atomic Energy Commission Division of Applied Technology Washington, D.C. 20545	
B. C. Belanger	6
G. W. Johnson	6
U.S. Atomic Energy Commission Washington, D.C. 20545	
S. G. English	1
D. K. Stevens	1
U.S. Atomic Energy Commission Oak Ridge Operations Office Oak Ridge, Tennessee 37830	
D. C. Davis, Jr.	1
J. A. Lenhard	7
U.S. Atomic Energy Commission Technical Information Center P.O. Box 62 Oak Ridge, Tennessee 37830	2
Oak Ridge National Laboratory Oak Ridge, Tennessee 37830	
W. F. Gauster, 9104-2	1
R. H. Kernohan, 9104-2	1
C. C. Koch, 4500-S	1
D. M. Kroeger, 4500-S	1
R. S. Livingston, 4500-NM	1
H. M. Long, 9104-2	60
C. J. McHargue, 4500-S	1
R. A. McNees, 4500-N	1
H. Postma, 9201-2	3
S. W. Schwenterly, 9104-2	1
S. T. Sekula, 3010	1
J. M. Spicer, 4500-NM	1
D. B. Trauger, 4500-NM	1
R. A. Vandermeer, 4500-S	1
M. K. Wilkinson, 3025	1
A. Zucker, 4500-NM	2
CR Library, 4500	2
Document Reference Section, Y-12	1
Laboratory Records, 4500	2
ORNL Patent Office, 4500	1
ORNL-RC, 4500	1
Thermomuclear Division Library, 9201-2	2

	<u>Copies</u>
American Electric Power Corporation 2 Broadway New York, New York 10004 H. C. Barnes	1
Argonne National Laboratory Particle Accelerator Division 9700 South Cass Avenue Argonne, Illinois 60439 C. E. Laverick	1
Argonne National Laboratory Laboratory Program Planning Office Building 221 9700 South Cass Avenue Argonne, Illinois 60439 A. D. Tevebaugh	1
Arthur D. Little Company, Inc. 20 Acorn Park Cambridge, Massachusetts 02140 J. Nicol	1
Bonneville Power Authority P.O. Box 3621 Portland, Oregon 97208 D. G. Wohlgemuth	1
British Insulated Callenders Cables, Ltd. 38 Wood Lane London W12 7DX, England E. H. Reynolds	1
Brookhaven National Laboratory Upton, L.I., New York 11973 E. B. Forsyth	4
Central Electricity Research Laboratories Electrical Engineering Division Kelvin Avenue Leatherhead, Surrey, England J. A. Baylis	1
Commonwealth Edison Company Transmission Engineering Department 1319 South First Avenue Maywood, Illinois 60153 J. L. Williams, Jr.	1

Copies

<p>Commonwealth Edison Company Technical Center 1319 South First Avenue Maywood, Illinois 60153 A. Zanona</p>	1
<p>Consolidated Edison Company of New York, Inc. Research and Development 4 Irving Place New York, New York 10003 R. A. Bell</p>	1
<p>Consolidated Edison Company of New York, Inc. 14th Floor 4 Irving Place New York, New York 10003 H. Feibus</p>	1
<p>Consolidated Edison Company of New York, Inc. Electrical Engineering Department 4 Irving Place New York, New York 10003 J. A. Williams</p>	1
<p>Cornell University School of Electrical Engineering 204 Phillips Hall Ithaca, New York 14850 S. Linke</p>	1
<p>Edison Electric Institute 90 Park Avenue New York, New York 10016 L. O. Elsaesser</p>	1
<p>Edison Electric Institute 90 Park Avenue New York, New York 10016 R. B. Morgan</p>	1
<p>Electric Power Research Institute 90 Park Avenue New York, New York 10016 C. Starr</p>	1
<p>Electricite de France 17, Avenue du Générale de Gaulle F - 92140 Clamart, France Z. Croitoru</p>	1

Copies

Esso Research and Engineering Company P.O. Box 45 Linden, New Jersey 07036 E. O. Forster	5
General Electric Company 1 River Road Schenectady, New York 12301 G. R. Fox	1
General Electric CRD K-1 Rad. Bldg. Schenectady, New York 12305 K. N. Mathes	1
Hitachi Cable, Ltd. Research Laboratory The 1st Department 5-1, Hitaka-cho, Hitachi-shi Ibaraki-ken, Japan M. Fukasawa	1
Hydro-Québec Institute of Research Mechanical Engineering and Thermodynamics Laboratory P.O. Box 1000 Varenes, Quebec, Canada JOL 2P0 J. M. Bonneville	1
Interkantonaies Technikum Rapperswil (Ingenieurschule) 8640 Rapperswil, Switzerland H. Brechna	1
Intermagnetics General Corporation Charles Industrial Park New Karner Road Guilderland, New York 12084 C. H. Rosner	1
Kernforschungsanlage Jülich Institut für Reaktorwerkstoffe Postfach 365 5170 Jülich, Germany H. A. Ullmaier	1
Kernforschungszentrum Karlsruhe Institut für Experimentelle Kernphysik III D75 Karlsruhe, Postfach 3640 Germany P. Komarek	1

Copies

Lawrence Livermore Laboratory P.O. Box 808 Livermore, California 94550 C. E. Taylor, L-382	1
Los Alamos Scientific Laboratory University of California P.O. Box 1663 Los Alamos, New Mexico 87544 W. F. Keller	4
Magnetic Corporation of America 179 Bear Hill Road Waltham, Massachusetts 02154 Z. J. J. Stekly	1
Massachusetts Institute of Technology Mechanical Engineering Department Cambridge, Massachusetts 02139 J. L. Smith	1
National Bureau of Standards Institute for Basic Standards Cryogenic Division Boulder, Colorado 80302 R. H. Kroppschot	1
National Bureau of Standards Institute for Basic Standards Cryogenic Division, 275.00 Boulder, Colorado 80302 R. L. Powell	1
National Science Foundation Advanced Technology Applications 1800 G Street, N.W. Washington, D.C. 20550 J. R. Tudor	1
Philadelphia Electric Company 2301 Market Street, S10-1 Philadelphia, Pennsylvania 19101 L. H. Fink	1
Public Service Gas and Electric Company of New Jersey 80 Park Place Newark, New Jersey 07101 A. S. Brookes	1

Copies

Public Service Gas and Electric Company of New Jersey 80 Park Place Newark, New Jersey 07101 C. H. Hoogerhyde	1
Siemens AG Research Laboratories 852 Erlangen, Germany G. Bogner	1
Philip Sporn 74 Trinity Place, Suite 1511 New York, New York 10006	1
Stanford Linear Accelerator Center Stanford University P.O. Box 4349 Stanford, California 94305 E. Garwin	1
Stanford University Department of Applied Physics Stanford, California 94305 W. A. Phillips	
Stanford University W.W. Hansen Laboratories Stanford, California 94305 T. H. Geballe	1
Sumitomo Electric U.S.A., Inc. 345 Park Avenue New York, New York 10022 Y. Matsuda	1
Supercon, Inc. 9 Erie Drive Natick, Massachusetts 01760 J. Wong	1
Tennessee Valley Authority 202 Chattanooga Bank Building Chattanooga, Tennessee 37401 A. Z. Pfitzer	1
U.S. Department of the Interior Water and Power Department 18th and C Streets Interior Building Washington, D.C. 20240 F. F. Parry	1

Copies

U.S. Department of the Interior Water and Power Department 18th and C Streets Interior Building Washington, D.C. 20240 W. G. Smith	1
Underground Power Corporation 205 Holdenwood Road Concord, Massachusetts 01742 P. Graneau	1
Union Carbide Corporation Technical Center Linde Research Labs Tarrytown, New York 10591 D. A. Haid	1
Union Carbide Corporation Linde Division P.O. Box 44 Tonawanda, New York 14150 L. R. Niendorf	1
Westinghouse Electric Corporation 700 Braddock Avenue, 9LL3 East Pittsburgh, Pennsylvania 15112 L. A. Kilar	1
Westinghouse Research Laboratory Beulah Road, Churchill Borough Pittsburgh, Pennsylvania 15235 J. K. Hulm	1
University of Wisconsin 513 Engineering Research Building 1500 Johnson Drive Madison, Wisconsin 53706 R. Boom	1